THE

SCIENCE REPORTS

OF

ECONOMIC GEOLOGY RESEARCH PROJECT

UNIVERSITY OF CONCEPCION

No. 1

JAPAN INTERNATIONAL COOPERATION AGENCY
(1991)

THE

SCIENCE REPORTS

OF

ECONOMIC GEOLOGY RESEARCH PROJECT

UNIVERSITY OF CONCEPCION

No. 1

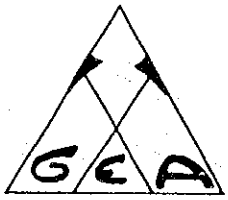

JAPAN INTERNATIONAL COOPERATION AGENCY

(1991)

PRINTED BY
EDITORA ANÍBAL PINTO S.A.
Maipú 769, Concepción, Chile

PROGRAMA DE GEOLOGIA ECONOMICA APLICADA (GEA)
Universidad de Concepción
Casilla 4107, Concepción 3, Chile

JAPAN INTERNATIONAL COOPERATION AGENCY (JICA)
P. O. Box 216, 48th Floor, Shinjuku Mitsui Building
Nishi-Shinjuku 2-1-1, Shinjuku-ku, Tokyo 163, Japan

(All announcements related with this report should be addressed to Japan International Cooperation Agency.)

Contents

KAOLIN MINERALS FROM MINA POSADA PAJONALES IN PAJONALES DISTRICT, III REGION, CHILE

Chiyoko Henmi*, Asahiko Sugaki, Nobutaka Shimada***, José Frutos**** and Eduardo Campos*****
*Faculty of Science, Okayama University, Tsushima Naka,Okayama 700, Japan. ** Kadan 4-30-503, Aoba, Sendai 980, Japan. *** Faculty of Science Kyushu University, Hakozaki 6-10-1, Fukuoka 812, Japan. **** Instituto GEA, Universidad de Concepción, Casilla 4107, Concepción 3, Chile. ***** Dept. Ciencias de la Tierra, Universidad de Concepción, Concepción 3, Chile.**

Abstract

Kaolin minerals from Mina Posada Pajonales were investigated by means of microscopy, X-ray fluorescence analysis, X-ray powder diffraction, thermogravimetric and differential thermal analyses, and scanning electron microscopy.

Kaolin ores from this mine, which were formed by hydrothermal alteration of andesitic lava and pyroclastic rocks belonging to Lower Cretaceous Bandurrias Formation, consist essentially of kaolin minerals with small amounts of quartz, alkali feldspar and goethite etc. Kaolinite as a kaolin mineral occupies most major portion of the ore and commonly associates with small amounts of halloysite (10 Å and 7 Å). Halloysite occurs as aggregate of tubular and fibrous crystals in interstices of aggregate of platy kaolinite crystals. Platy kaolinite aggregate is often surrounded with aggregate of tubular halloysite. Halloysite is thought to have been formed secondarily by hydration of kaolinite crystallized primarily as a hydrothermal alteration product.

Viseite, $Ca_{10}Al_{24}(SiO_4)_6(PO_4)_7O_{22}F_3 72H_2O$ of a rare mineral of zeolite group was found in the kaolin ore.

1. Introduction

Intensely hydrothermal alteration of the Lower Cretaceous formation consisting of andesitic lava and pyroclastic rocks is widely found in the Pajonales area which is located at about 120 km north along highway 5 from La Serena (Fig. 1). Especially,

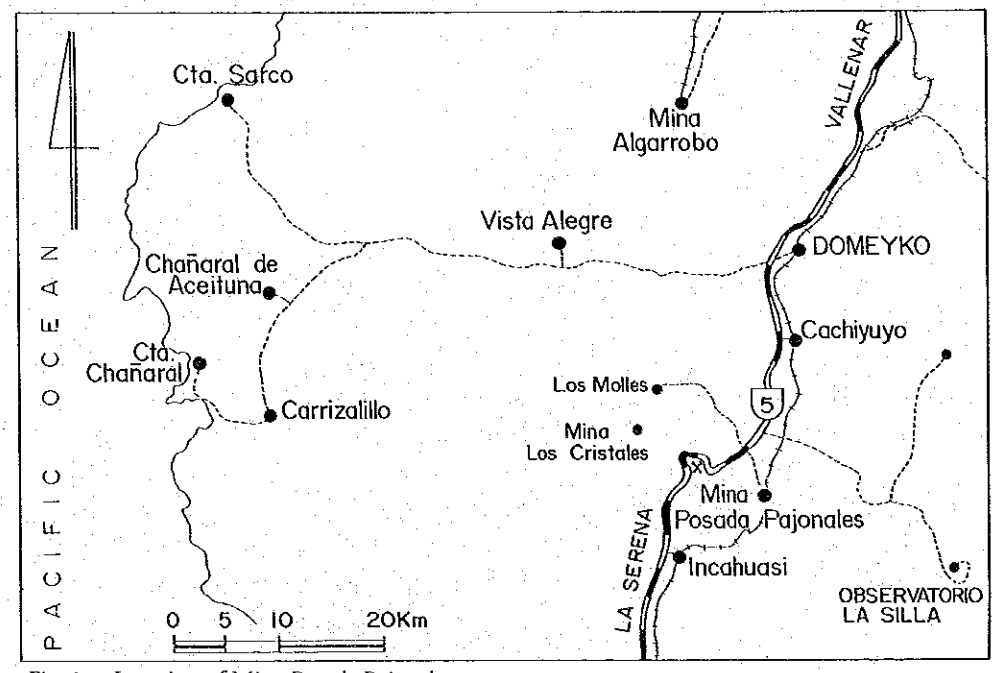

Fig. 1. Location of Mina Posada Pajonales.

kaolinization as a distinct alteration is well observed at cutting rock-wall and criff along a curved highway slope of the hill. Most intense portion of that mineralization is now working as a small kaolin mine (Mina Posada Pajonales) for a ceramic material. Mineralogical studies on the kaolin ore have been carried out be means of X-ray powder diffraction, thermogravimetric-differential thermal analyses (TG-DTA) and scanning electron microscopy. The experimental data on the kaolin ore are reported in this paper.

2. Occurrence of kaolin minerals

Aspect and feature of kaolinization can be observed at cutting cliffs along a curve slope of the highway to east hill from Pajonales and along a road to Mina Los Cristales branched to west from the highway at north the hill. Kaolin minerals occur principally as vein or dyke, and occasionally as massive and irregular forms in propylization area of the Lower Cretaceous andesitic lava and pyroclastic formation (Bandurrias Formation) accompanied with chloritization, epidotization and carbonitization (Moscoso *et al.*, 1982). Kaolin ore body of Mina Posada Pajonales shows vein or dyke-like forms in a mined trace, about 30 to 40 m long (N-S direction), 4 to 7 m wide and 10 to 15 m deep in scale. At that place, rock was completely replaced by white massive kaolin so as to unable to determine original one. However, a marginal zone of the

amounts of goethite are often found as brown colored spot, veinlet and patch-like forms in white colored kaolin ore body. Also, quartz, hematite, jarosite and alunite occur in intimate association with kaolin in the alteration area. Kaolin minerals occur as veinlet, 1 to 3 cm wide, and vein, 10 to 40 cm wide in altered andesite.

By examination under microscope on the kaolin ore, it was found that fine grained quartz and alkali-feldspar occur in intimate association with kaolin minerals as hydrothermal alteration products.

3. The bulk composition of kaolin ore

Major element analyses by XRF for kaolin ore were carried out by Fukuoka (1991) using a RIGAKU X-ray Fluorescence Spectrometer System 3070 E under conditions of 50 kV and 50 mA using a rhodium target. Twelve GSJ (Geological Survey of Japan) rock reference samples (JG-1a, JG-2, JG-3, JR-1, JR-2, JA-2, JA-3,

Table 1. The bulk compositions of kaolin ores (specimen Nos. 90062905-01-02) by XRF analysis.

	01	02	Kaolinite*1)
Wt.%			
SiO_2	51.80	54.80	46.55
TiO_2	0.59	0.76	-
Al_2O_3	29.63	36.39	39.49
Fe_2O_3*2)	2.32	1.79	-
MnO	0.00	0.00	-
MgO	0.20	0.23	-
CaO	0.07	0.18	-
Na_2O	0.14	1.48	-
K_2O	0.28	0.14	-
P_2O_5	0.19	0.32	-
H_2O^+*3)	11.76	10.26	13.96
H_2O^-*4)	2.88	3.17	-
Total	99.86	99.52	100.00
Mode*5)			
Quartz	16.1	18.2	
Kaolinite	76.0	62.5	
Alkali feldspars*6)	2.9	13.9	
Goethite	2.7	2.1	
The others	2.3	3.3	

*1) Ideal composition, $Al_2Si_2O_5(OH)_4$.
*2) Total iron as Fe_2O_3.
*3) Ignition loss after heating at 950°C for 2 hours.
*4) Loss after heating at 110°C for 2 hours.
*5) Excluding H_2O^- and normalized to 100%.
*6) All Na_2O and K_2O are assumed to be content of feldspars.

conditions of 50 kV and 50 mA using a rhodium target. Twelve GSJ (Geological Survey of Japan) rock reference samples (JG-1a, JG-2, JG-3, JR-1, JR-2, JA-2, JA-3, JB-1a, JB-2, JB-3, JGb-1 and JP-1) and one synthetic Al_2O_3 were used to obtain calibration curves for each element. A glass-disk of samples was prepared by fusing and molding a mixture of 0.5 g of powdered sample, 5 g of $Li_2B_4O_7$ as flux, and about 15 mg of LiI in a platinum crucible set on RIGAKU bead sampler. Analyses for each element were performed under conditions as follows: SiO_2 (element), PET (analyzing crystal), PC (gas-flow proportional counter), 109.12 (peak position, 2θ degree); TiO_2, LiF, PC, 86.24; Al_2O_3, PET, PC, 144.84; Fe_2O_3 (total iron), LiF, SC (scintillation counter), 57.52; MnO, LiF, SC, 62.97; MgO, TAP, PC, 45.30; CaO, LiF, PC, 113.20; Na_2O, TAP, PC, 136.74; P_2O_5, GE, PC, 141.10.

The analytical results are given in Table 1 in comparison with ideal composition of kaolinite $Al_2Si_2O_5(OH)_4$. From these analytical data, mode compositions of this kaolin ore were also calculated. Small amounts of quartz, alkali-feldspar and goethite besides kaolinite were obtained so as to have been observed under microscope.

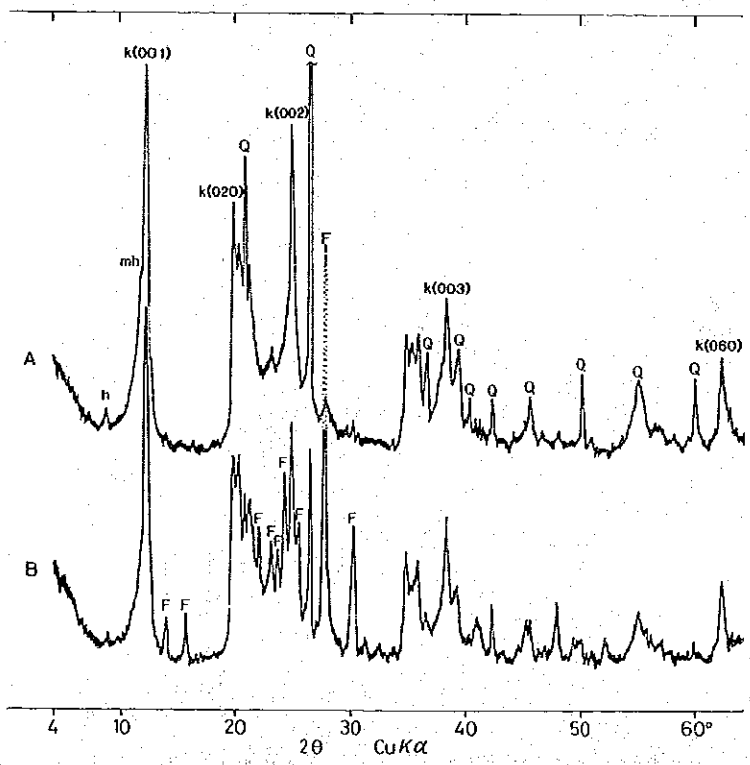

Fig. 2. X-ray powder diffraction patterns for specimens of kaolin crude ores from Mina Pasada Pajonales. (Cu-Kα, Ni-filtered, 30 kV-10 mA, 1°-0.3 mm -1°, 1,000 cps-0.5 sec, 4°/min.-20mm/min. by RIGAKU RAD-2C diffractometer).
A: specimen No. 90062905-01, B: specimen No. 90062905-02, Q: quartz, F: alkali feldspar, k: kaolinite, h: halloysite (10 Å), mh: halloysite (7 Å).

4. X-ray powder diffraction data

Two kaolin ores, specimen Nos. 90062905-01 and -02, being white colored argillaceous altered rocks were used for analysis by X-ray powder diffraction. The selection of clay fractions from the specimens was achieved by the usual elutriation method. After ultrasonic dispersion in distilled water, clay materials were fractionated to size less than 2 microns. Both the random and orientated samples of the clay fractionated were prepared. The former was filled into a aluminum holder and the later was mounted on glass slide at room temperature for X-ray diffraction. Heat treatments were performed on the orientated samples for detailed identification of clay minerals.

X-ray powder diffraction for the clay specimens was carried out by using RIGAKU D/max system or RAD-2C diffractometers under the conditions as follows: Nickel filtered Cu Kα radiation, 30 kV, 10 to 15 mA, divergence slit: 1°, receiving slit: 0.3°, scanning rate: 2° to 4° (2θ) per minute, and measuring angle range: 2° to 70°.

Specimen No. 90062905-01: X-ray powder diffraction pattern for the bulk specimen No. 90062905-01 of the kaolin crude ore is shown in Fig. 2-A. As seen in the figure, the specimen consists of quartz and kaolin minerals associated with small amounts of alkali feldspar. On the separated clay fractions, the X-ray pattern of the random orientation sample forms two groups of triplets in the range 35° to 40° (2θ) as shown in Fig. 3-A and definitely agrees with well-ordered kaolinite (Brindley &

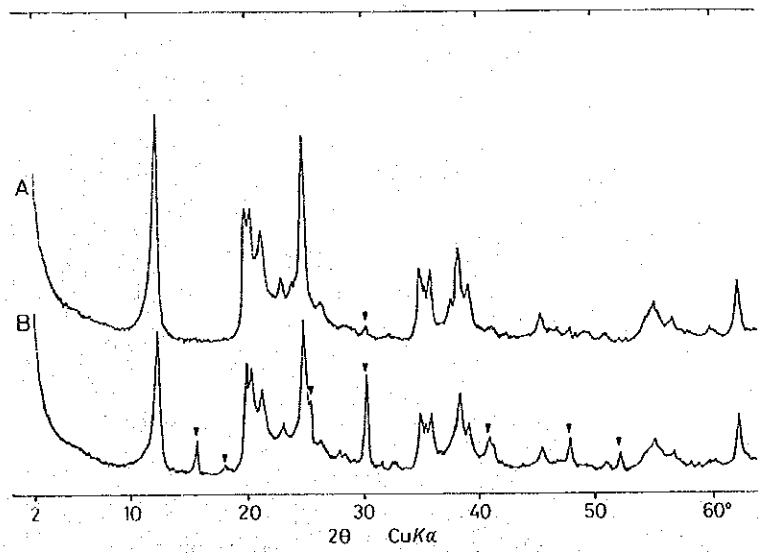

Fig. 3. X-ray powder patterns of well-ordered kaolinite in clay fractions separated from kaolin crude ore. (Cu-Kα, Ni-filtered, 30 kV-10 mA, 1°-0.3 mm -1°, 2,000 cps-1 sec, 2°/min. -10mm/min. by RIGAKU RAD-2C diffractometer).
A: specimen No. 90062905-01, B: specimen No. 90062905-02.
Solid arrows: viscite.

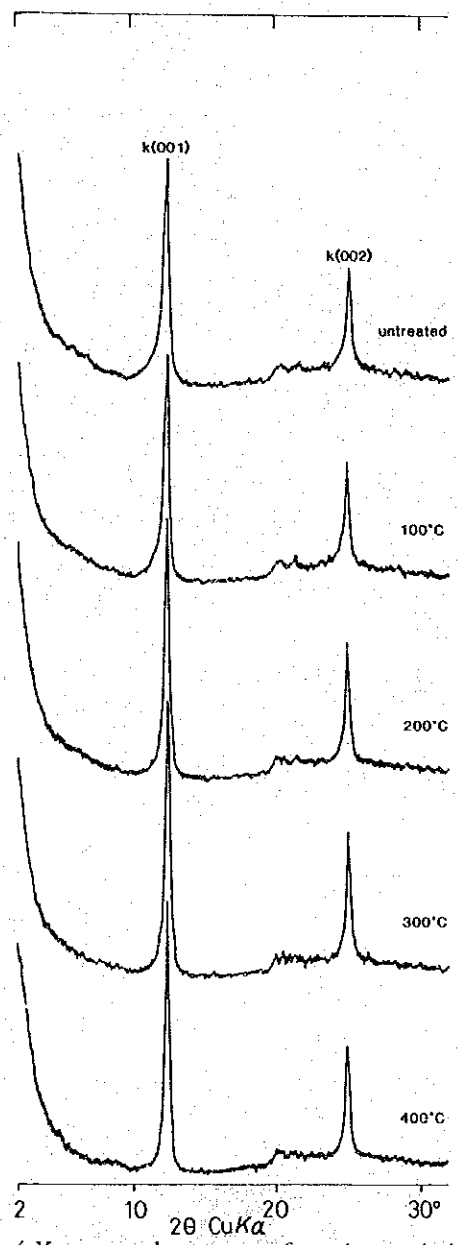

Fig. 4. X-ray powder patterns for orientated clay fractions of specimen No. 90062905-01. (Cu-K_α, Ni-filtered, 30 kV-10 mA, 1/2°-0.3 mm-1/2°, 2,000 cps-0.5 sec, 2°/min.-10mm/min.). Heating treatments are denoted. k: kaolinite.

Brown, 1980). However, the basal reflections obviously trail to the lower angle side as seen in Figs. 2-A and 3-A. With heating procedures up to 400°C, the reflection of d(001) evidently changed to a symmetrical, sharp one at 100°C or more high

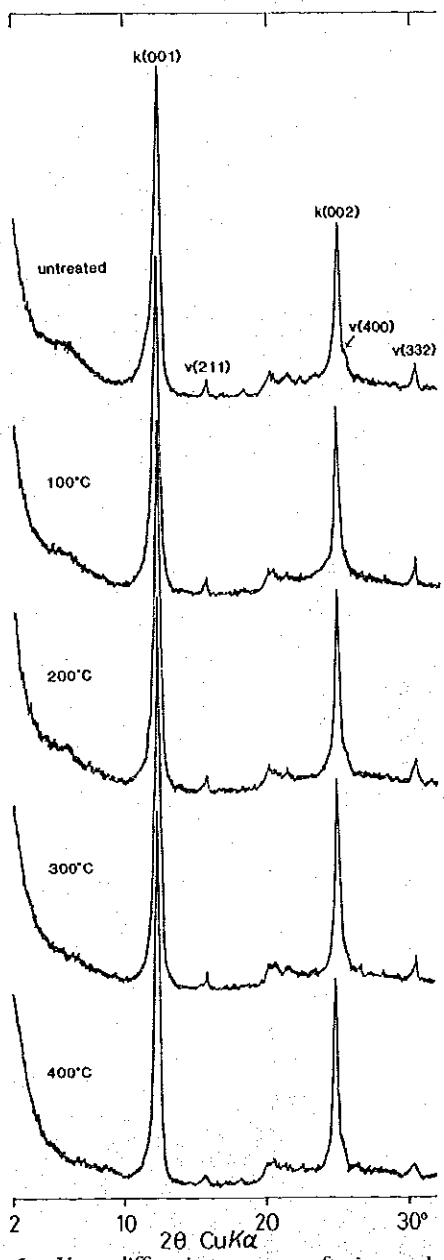

Fig. 5. X-ray diffraction patterns of orientated clay fractions from specimen No. 90062905-02. (The conditions of X-ray diffraction are the same as those in Fig. 4). Heating treatments are denoted. k: kaolinite, v: viseite.

temperature as shown in Fig. 4. From these data and also the presence of very weak 10 Å peak in the bulk specimen (Fig. 2-A), it is concluded that minor amounts of halloysite (7 Å) and halloysite (10 Å) are present in the specimen.

Specimen No. 90062905-02: The bulk specimen No. 90062905-02 of the kaolin crude ore is composed of abundant kaolin minerals and alkali feldspar with small amounts of quartz as shown in Fig. 2-B. From the diffraction data (Fig. 3-B) for the orientated sample fractionated and the result (Fig. 5) of heating treatments, the kaolin minerals in the specimen No. 90062905-02 are also identified to be a mixture of well-ordered kaolinite, halloysite (7 Å) and halloysite (10 Å). Among them, kaolinite occupies a major portion of the ore as the most essential mineral.

It is noteworthy that viseite, a rare mineral of zeolite group, was found. The predominant peaks in the diffraction patterns of Figs. 3-B and 5 agree well with those of viseite from the type locality (McConnel, 1952). The reflections of viseite were recognized up to 300°C, but began to break down at 400°C as shown in Fig. 5. This thermal behavior is in accordance with that of viseite reported by Mc Connel (1952). Dunn & Appleman (1977) proposed the chemical composition of viseite to be $Ca_{10}Al_{24}(SiO_4)_6(PO_4)_7O_{22}F_3{\cdot}72H_2O$.

5. Thermal analyses

Thermal behavior of kaolin minerals was investigated by thermogravimetric (TG) and differential thermal analysis (DTA) methods to confirm or supplement the data of kaolin minerals identified by X-ray powder diffraction. The thermal analysis was carried out by using RIGAKU high temperature type TG-DTA (8072G2) with thermal analysis station TAS100. Heating rate was 10°C per minute, and amounts of sample were 30 mg. The atmosphere was static in air.

Specimen No. 90062905-01: The TG and DTA curves for kaolin specimen No. 90062905-01 are shown in Fig. 6-A. In the DTA curve, a gently endothermic reaction at temperatures from 30°C to around 100°C presents dehydration of adsorptive water of kaolin minerals. A remarkably endothermic peak at 525°C indicated dehydration of constitution water of kaolin minerals (kaolinite, halloysite 7 Å and halloysite 10 Å). A distinctly exothermic reaction at 975°C shows recrystallization (formation of mullite and γ-alumina) from amorphous phase (metakaolin) induced by dehydration of constitution water mentioned above. The DTA curve (A) in Fig. 6 is similar to those of halloysite (10 Å), halloysite (7 Å) and kaolinite reported by Kell *et al.* (1949), Holdridge & Vaugham (1957), Sudo (1959), Nagasawa (1967) and Mackenzie (1970).

Weight decreasing of sample due to dehydrations by heating on specimen No. 90062905-01 is shown as two step reactions in the TG curve (A) of Fig. 6. The amounts decreased by dehydration of adsorptive water (and interlayer water) at low temperatures below about 100°C (and between 100° and 200°C) and constitution water at temperatures from 480° to 560°C were approximately 4.0 and 10%, respectively.

Specimen No. 90062905-02: Similarly, the DTA and TG curves for specimen No. 90062905-02 are shown in Fig. 6-B. Two endothermic and one exothermic

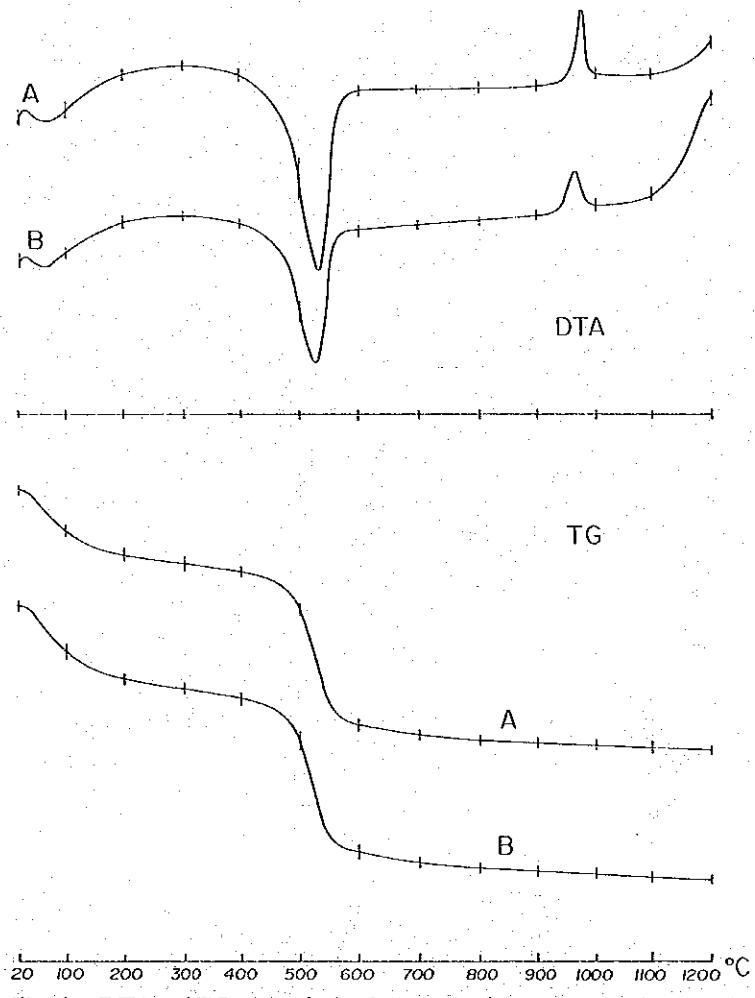

Fig. 6. DTA and TG curves for kaolin samples from Mina Posada Pajonales. A: specimen No. 90062905-01, B: specimen No. 90062905-02.

reactions of the DTA curve (B) in the figure are entirely the same as those in Fig. 6-A (specimen No. 90062905-01). The TG curve (B) in the figure also is similar to that of Fig. 6-A.

Weight decreasing of two step dehydrations at low temperatures below about 100° to 200°C and at temperatures from 485° to 550°C was approximately 4.3 and 8.7%, respectively

6. Scanning electron microscopy

The specimen No. 90062905-01 of the kaolin ore was examined by Aoki (1991) using Hitachi S550 scanning electron microscope (SEM). Its surface was coated with

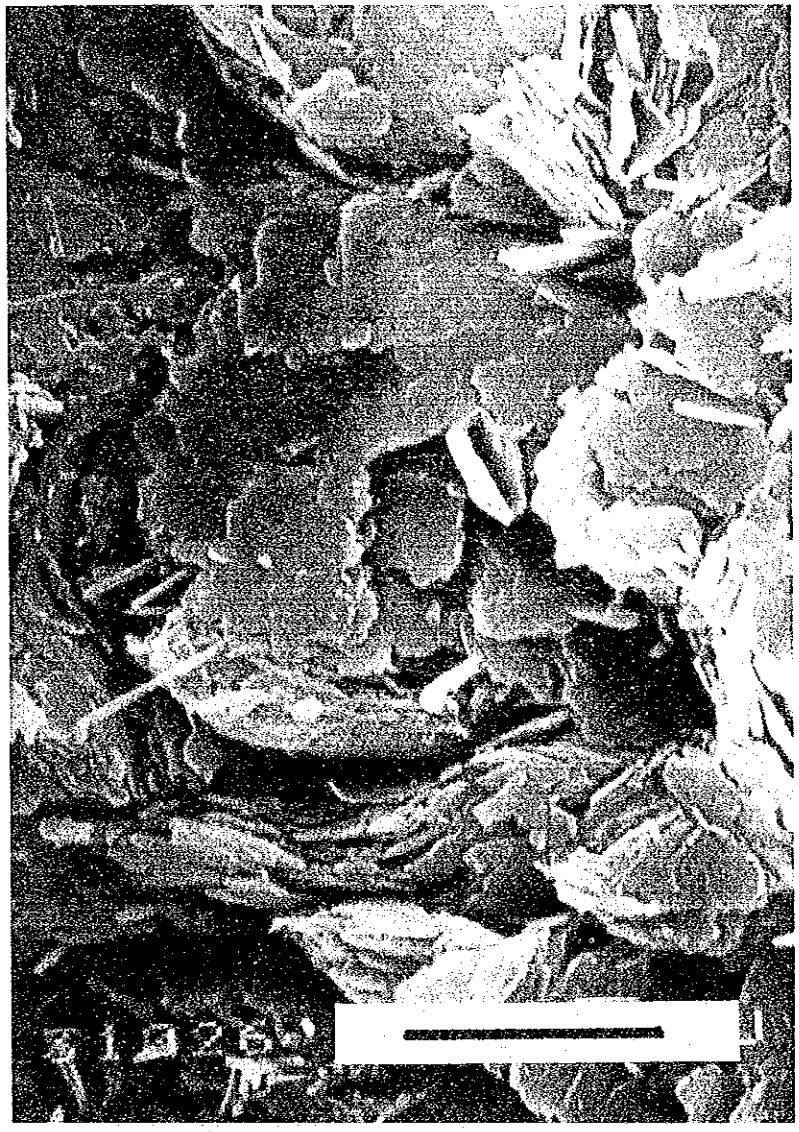

Fig. 7. SEM photomicrograph of platy kaolinite in kaolin ore.
A bar of the scale is 2 microns long. Specimen No. 90062905.
(The photomicrograph was taken by M. Aoki).

a gold film by vacuum evaporation before the examination by SEM. Observation and photomicrography were performed under such conditions as accelerating voltages: 25 kV and magnifications: 6,000 to 15,000.

As shown in Fig. 7, aggregate of platy and foliated crystals which are identified to be kaolinite occupies main portion of the sample examined. Meanwhile, aggregate of tubular and fibrous crystals with the well-known morphology of halloysite

Fig. 8. SEM photomicrograph of tubular halloysite in kaolin ore.
A bar of the scale is 5 microns long. Specimen No. 90062905.
(The photomicrograph was taken by M. Aoki).

(Takahashi, 1967; Brindley & Brown, 1980; Cairns-Smith & Hartman, 1986) was often found in the samples as seen in Figs. 8 and 9. The tubular and fibrous crystals occur in interstices of aggregate of platy kaolin crystals, and often enclose the kaolin crystals as shown in Fig. 10. They were found to be the same composition as that of the platy kaolin crystals by EDX (energy dispersive X-ray) analysis.

As described above, the kaolin ore principally consists of very fine grained aggregate of kaolinite in intimate association with small amounts of halloysite. The

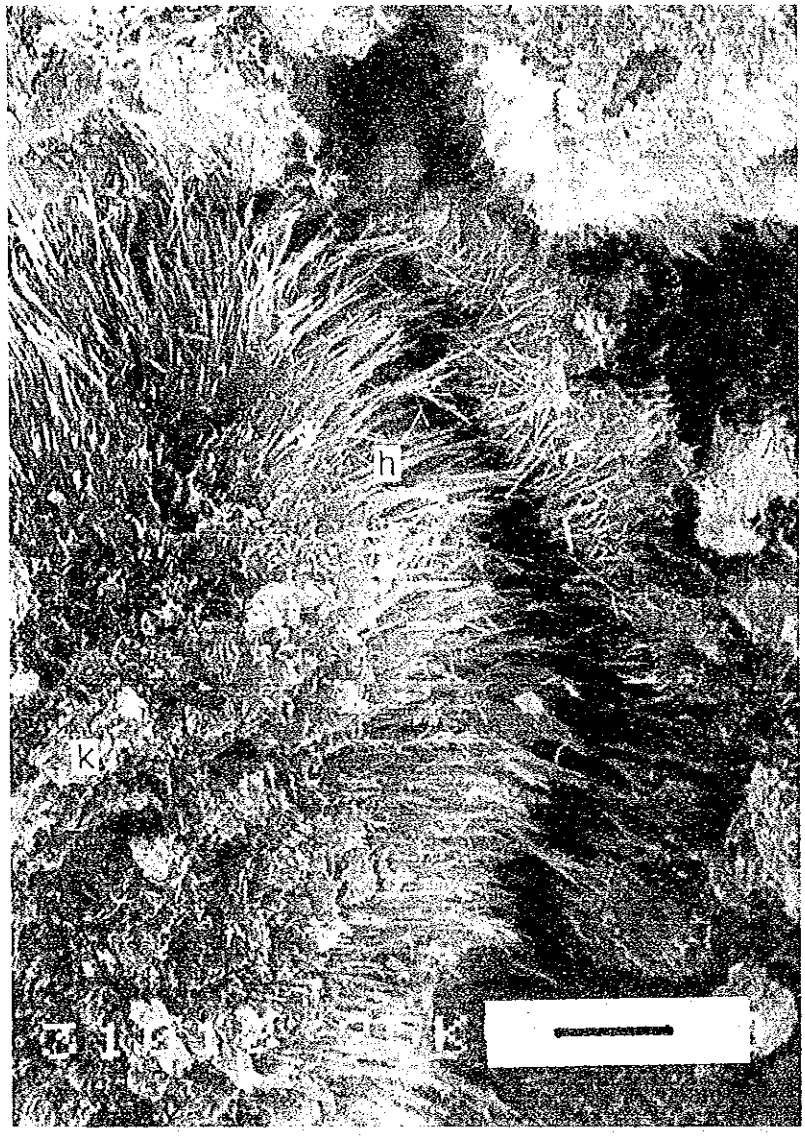

Fig. 9. SEM photomicrograph of fibrous halloysite enclosed aggregate of platy kaolinite.
h: halloysite, k: kaolinite. Bar scale is 5 microns.
(The photomicrograph was taken by M. Aoki).

result of observation by SEM well agrees with that obtained from the X-ray powder data. Occurrence of halloysite as shown in Figs. 9 and 10 suggests that halloysite is thought to have been crystallized secondarily by hydration of kaolinite produced primarily by hydrothermal alteration.

Fig. 10. SEM photomicrograph of tubular halloysite surrounding aggregate of platy kaolinite.
h: halloysite, k: kaolinite. Bar scale 5 microns. Specimen No. 90062905.
(The photomicrograph was taken by M. Aoki).

7. Summary

The kaolin ores from Mina Posada Pajonales were investigated by means of field observation, microscopy, X-ray fluorescence analysis, X-ray powder diffraction, thermogravimetric and differential thermal analyses and scanning electron microscopy. The data obtained by these examinations are summarized as follows:

1) The kaolin ore occurs generally in vein and dyke-like forms as a hydrothermal alteration product in Lower Cretaceous Bandurrias Formation consisting of altered andesitic lava and pyroclastic rocks.
2) The kaolin ore is composed essentially of kaolin minerals with small amounts of quartz, alkali feldspar and goethite, etc.
3) Kaolinite is principal mineral in the ore, but small amounts of halloysite (10 Å) and halloysite (7 Å) are present in intimate association with kaolinite.
4) Tubular and fibrous halloysite occurs in interstices of aggregate of platy kaolinite, and kaolinite crystals are often surrounded with aggregate of tubular and fibrous halloysite.
5) Kaolinite is a primary product of hydrothermal alteration, while halloysite is thought to be a secondary product by hydration of kaolinite.
6) $Ca_{10}Al_{24}(SiO_4)_6(PO_4)_7O_{22}F_3{\cdot}72H_2O$, of a rare mineral of zeolite group was found in the kaolin ore.

Acknowledgments

The authors would like to thank Prof. M. Aoki of Miyagi University of Education for his research cooperation in scanning electron microscopy and Dr. M. Fukuoka of Kyushu University for his research assistance in X-ray fluorescence analysis. The authors also wish to thank Prof. S. Higashi of Kochi University and Dr. M. Yamamoto of Kagoshima University for their instructive contribution on kaolin minerals in this paper.

References

Aoki, M. (1991): Personal communication

Brindley, G. W. & Brown, G. B (1980): *Crystal structures of clay minerals and their X-ray identification.* Monograph No. 5, Miner. Soc., London, 495.

Cairns-Smith, A. G. & Hartman, H. (1986): *Clay minerals and the origin of life.* Cambridge Univ. Press, 193.

Dunn, P. J. & Appleman, D. E. (1977): Perhamite, a new calcium aluminum silico-phosphate mineral, and a re-examination of viseite. *Am. Miner.* 41, 437-442.

Fukuoka, M. (1991): Personal communication

Holdridge, D. A. & Vaugham, F. (1957): The kaolin minerals (kandites). In R. C. Mackenzie ed., *The differential thermal investigation of clays.* Miner. Soc., London, 98-139.

Kerr, P., Kulp, J. & Hamilton, P. (1949): *Reference Clay Minerals.* Am. Petr. Inst. Research Project. 49, Columbia Univ., New York.

Mackenzie, R. C. (1970): Simple phyllosilicates based on gibbsite -and brucite-like sheets. In R. C. Mackenzie ed., *Differential thermal investigation of clays.* Vol. 1, Academic Press, London, 497-537.

Mc Connell, D. (1952): Viseite, a zeolite with the analcime structure and containing linked SiO_4, PO_4 and H_xO_4 groups. *Am. Miner.* 37, 609-617.

Moscoso, R. D., Nasi, C. P. & Salinas, P. Z. (1982): *Hoja Vallenar y Parte Norte de La Serena.* Carta Geológica de Chile No. 55, Servicio Nacional de Geología y Minería.
Nagasawa, K. (1967): Thermal properties of clay minerals. In S. Iwao ed., *Handbook of Clays.* Gihodou, Tokyo, 32-34 (In Japanese).
Sudo, T. (1959): *Mineralogical Study on Clays of Japan.* Naruzen Co. Tokyo, 88-103.
Takahashi, H. (1967): Electron microscopy of clay minerals. In S. Iwao ed., *Handbook of Clays,*. Gihodou, Tokyo, 48-63 (in Japanese).

SOME CLAY MINERALS FROM MINAS DEL PRADO, REGION DEL BIOBIO, CHILE

Chiyoko Henmi*, Asahiko Sugaki, Nobutaka Shimada*** and José Frutos******

*** Faculty of Science, Okayama University, Tsushima-Naka, Okayama 700, Japan.** Kadan 4-30-503, Aoba Sendai 980, Japan.*** Faculty of Science, Kyushu University, Hakozaki 6-10-1, Fukuoka 812, Japan.**** Instituto GEA, Universidad de Concepción, Casilla 4107, Concepción 3, Chile.**

Abstract

The clayey samples from a gold bearing vein of Minas del Prado, located at about 50 km east from Chillán, Región del Biobio, were investigated by means of X-ray powder diffraction, and thermogravimetric and differential thermal analyses. The gold veins occur in hydrothermally altered dacite and andesite lavas and pyroclastic rocks of lappilli tuff, tuff breccia and volcanic breccia belonging to the Pierna Blanca Series (Lower Miocene). They are composed of quartz and clay minerals associated with plagioclase (albite), calcite, pyrite, hematite and goethite. Clay minerals appears as a principal constituent similar to quartz in the vein. Such clay minerals colored pale yellowish brown and grayish green were identified to be a mixture of chlorite and smectite in various ratios, associated with quartz, albite and kaolin mineral. Chlorite is chamosite (IIb polytype) of iron-rich one, while smectite is a dioctahedral type, namely montmorillonite.

1. Introduction

Clay minerals occur as an essential gangue in hydrothermal ore deposits, especially porphyry copper and fissure filling deposits. They also appear as a common product in the hydrothermal alteration zones of country rocks surrounding ore deposits. Therefore, in the case making clear, the ore genesis of these deposits the investigation of clay minerals is important the same as that of other ore and gangue minerals. First of all, their study has to start from identification of clay minerals in this case. As an example, clay minerals from the gold veins of Minas del Prado, which is located at 50 km east from Chillán, Región del Biobio (Fig. 1), have been investigated and determined the kinds of clay minerals as below.

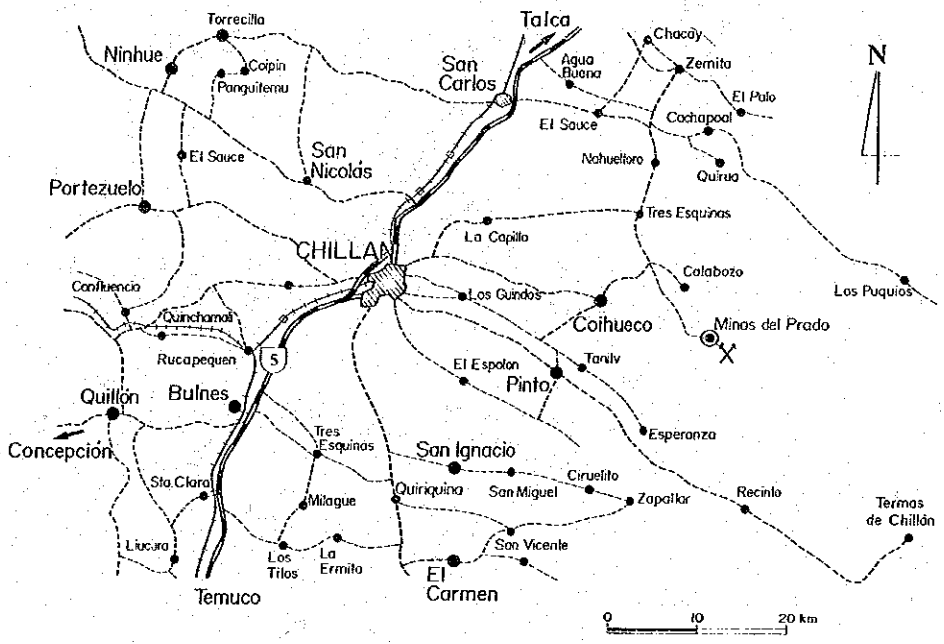

Fig. 1. Location of Minas del Prado

2. Geological outline

The area of Minas del Prado is composed of dacite and andesite laves and pyroclastic rocks such as lapilli tuff, tuff breccia, and volcanic breccia corresponding to the Pierna Blanca Series of Neogene Tertiary (Ambrus & Araya, 1981; IIG-MMAJ, 1981; Alfaro, 1984; Collao & Frutos, 1991). The K/Ar ages of two andesites are 17.05 ± 0.60 Ma and 19.72 ± 1.37 Ma in whole rocks of the Pierna Blanca Series were suffered hydrothermal alterations such as silicification, argillization and propylitization. In this area, the formation consisting of basic volcanic lavas of andesite and basalt and their pyroclastic rocks, and semiconsolidated conglomerate etc, which corresponding to the Cola de Zorro Formation (0.5 to 1.5 Ma, IIG-MMAJ, 1981) overlies on andesite lava and pyroclastic rocks of the Pierna Blanca Series mentioned above.

Gold bearing veins and stockwork of Minas del Prado occur in altered dacite and andesite and their pyroclastic rocks with sometimes sandstone and mudstone of the Pierna Blanca Series. They are quartz-clay mineral veins in association with some amounts of pyrite, calcite, plagioclase (albite), hematite and goethite. Gold, in general, appears as electrum. But no sliver minerals are found. The gold veins such as San Lorenzo, Rudemil Pérez, Pedernales, Las Mellizas, Urra and Moreno running on general to N60° to 70°E direction and dipping to 70° to 90° south, are usually 5 to 50 cm in width, rarely 120 cm including gangue rock and commonly 30 to 50 m in length, sometimes 150 m. Gold contents in the veins are normally 1 to 4 g/t, rarely 12 to 16.5 g/t (Alfaro, 1984).

3. Occurrence of clay minerals

As mentioned above, clay minerals occur as essential or accessory gangue minerals in the gold veins, and are accompanied with quartz, pyrite, plagioclase (albite) and calcite. The veins sometimes consist principally of the clay minerals. Unnamed gold bearing clay vein in lapilli tuff and tuff breccia with sandy shale and mudstone has been prospected at north-east side of the San Lorenzo vein. Its vein is about 20 m long at least and 15 cm wide, and runs to N80°W direction. Its gold contents are less than 1g/t, rarely 1 to 2g/t. The clay minerals (specimen Nos. 90062411 and 90062312) from the unnamed vein are pale yellowish brown or grayish green in color, and associates always with small amounts of very fine grained quartz and plagioclase.

To identify the clay minerals from the vein, they were investigated by methods of X-ray powder diffraction, and thermogravimetric (TG) and differential thermal analyses (DTA) as below.

4. X-ray powder diffraction data

Two specimens, Nos. 90062411 and 90062412, of clay materials showing pale yellowish brown and grayish green in color from the unnamed gold vein in Minas del Prado, were offered as samples for X-ray powder diffraction. By rough sedimentation and elutriation methods, clay-size fractions, less than 5 microns, were separated from the specimens, and the fractionated samples were used for X-ray powder diffraction. Ethylene glycol solvation was taken on the oriented sample of clay-sized fractions to examine on smectite in detail. In order to distinguish between kaolin and chlorite and also examine on smectite, the samples were boiled in 6N-hydrochloric acid solution for one hour (Oinuma & Kobayashi, 1965).

X-ray powder diffraction for the clay samples was performed by using RIGAKU D/max system or RIGAKU RAD-2C diffractometers under conditions as follows: Nickel filtered Cu-Kα radiation, 30kV, 15mA, divergence slit: 1°, receiving slit: 0.3, Scanning rate: 4° (2θ) per minute, and measuring angle range: 2° to 70° in the case using the diffractometer of RIGAKU D/max System. For iron-rich clay mineral, Co radiation was also used to obtain more intensive reflection on a low background. Pure metallic silicon was used as a external standard for exact measurements of each d-spacing.

Specimen No. 90062411: The randomly orientated sample fractionated contains abundant smectite associated with chlorite and quartz as shown in the powder pattern of Fig. 2-A. The smectite is characterized with very strong basal reflection of 15Å for air-dried sample, which was shifted to 17Å by ethylen glycol solvation and to 12.5Å by hydrochloric acid treatment as shown in Fig. 3, and the d(060) value of 1.494Å (Fig. 2-A). These facts indicate that the smectite is dioctahedral type, namely montmorillonite (Brindly, 1966).

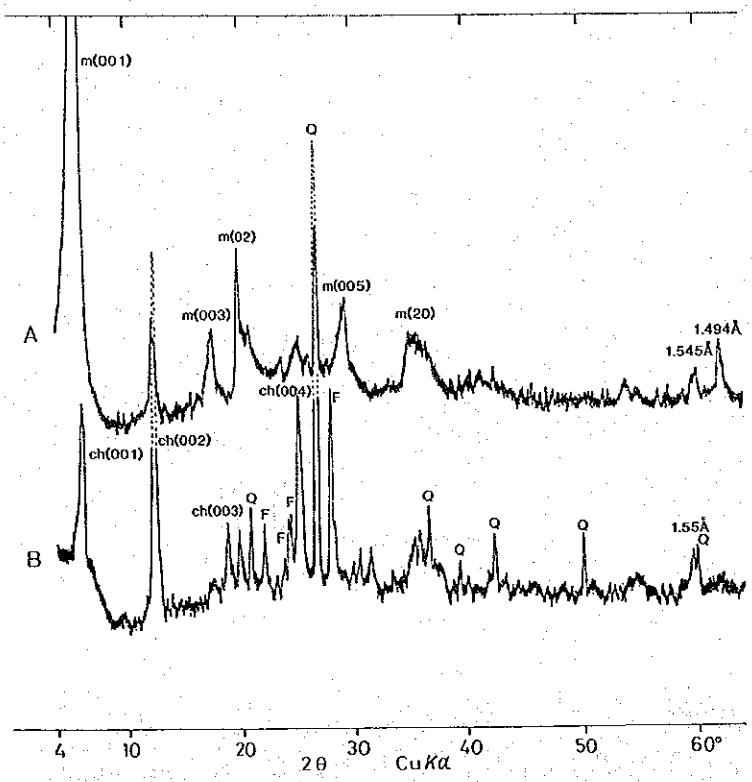

Fig. 2. X-ray powder diffraction patterns of randomly orientated clay sample from Minas del Prado. (Cu-Kα, Ni-filtered, 30kV-10mA, 1°-0.3 mm-1°, 1.000 cps-0.5 sec, 4°/min., 10 mm/min. by RIGAKU RAD-2C diffractometer) A.: specimen No. 90062411 B: specimen No. 90062412, ch: chlorite, m: montmorillonite, F: plagioclase (albite), Q: quartz.

The chlorite mineral was identified to be chamosite, which has larger occupancy of iron ions than magnesium ones in the octahedral sites of chlorite, because the d(060) value is 1.545Å and the relative intensities of first and third basal reflections are weaker than those of second and fourth ones (Shirozu, 1960, 1988) as shown in Fig. 2-A and 3. After hydrochloric acid treatment, chlorite, entirely disappeared from the powder pattern, but peaks of 7.2Å and 3.58Å remained (Fig. 3-HCl). These peaks correspond to basal reflections of kaolin mineral which super imposed on basal reflections of chloride in air-dried sample (Oinuma & Kobayashi, 1965). Thus, it is confirmed that this sample surely contains a minor amount of a kaolin mineral.

Specimen No. 90062412: The fractionated sample is composed of quartz, chlorite, plagioclase, and minor amount of smectite (Fig. 2-B). Reflections in the range 13° to 15° (2θ) may indicate that plagioclase has the composition close to albite. The chlorite mineral was identified to be chamosite, as it shows the same properties as the specimen No. 90052411. The X-ray pattern of the randomly oriented sample (Fig. 2-B) represents that chamosite has IIb polytype (Bailey and Brown, 1962). Smectite (montmorillonite) showed no clear swelling to 17Å by ethylene glycol

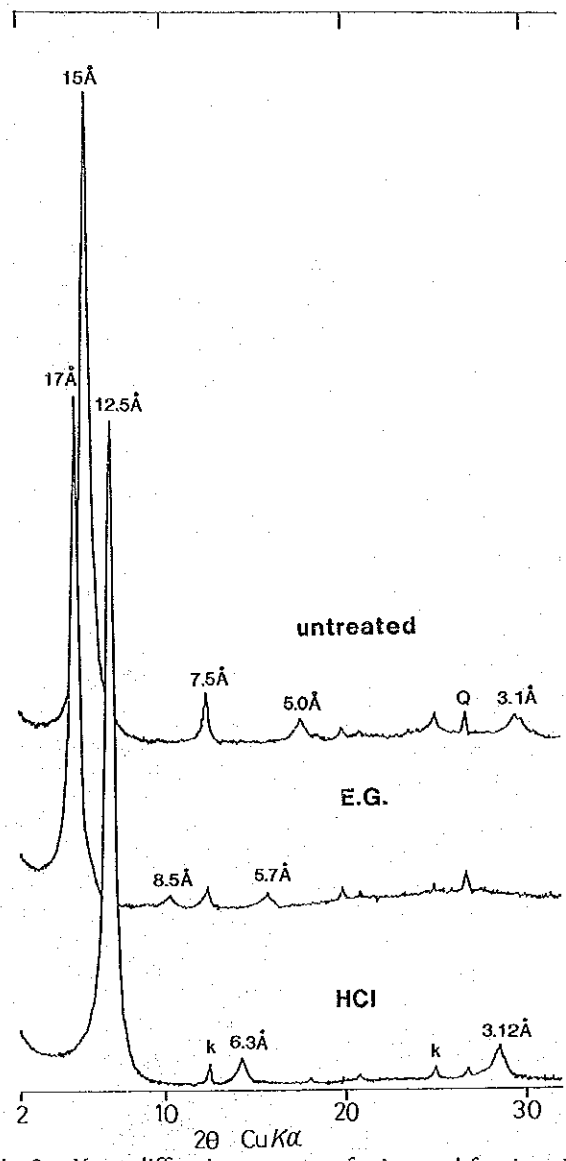

Fig. 3. X-ray diffraction patterns of orientated fractionation sample of specimen No. 90062411. (Cu-Kα, Ni-filtered, 30kV-10mA, 0.5°-0.3 mm-1°, 4.000 cps-0.5 sec, 2°/min., 10 mm/min. by RIGAKU RAD-2C diffractometer)
E.G.: means the sample treated with ethylene glycol, k: kaolin mineral, Q: quartz.

solvation due to its minor amount, but its presence is pointed out from the weak basal reflections of 001 and 003 in an air-dried, untreated sample, and also the appearance of shrunk reflections after hydrochloric acid treatment as shown in Fig. 4. While, no kaolin mineral was detected in this sample.

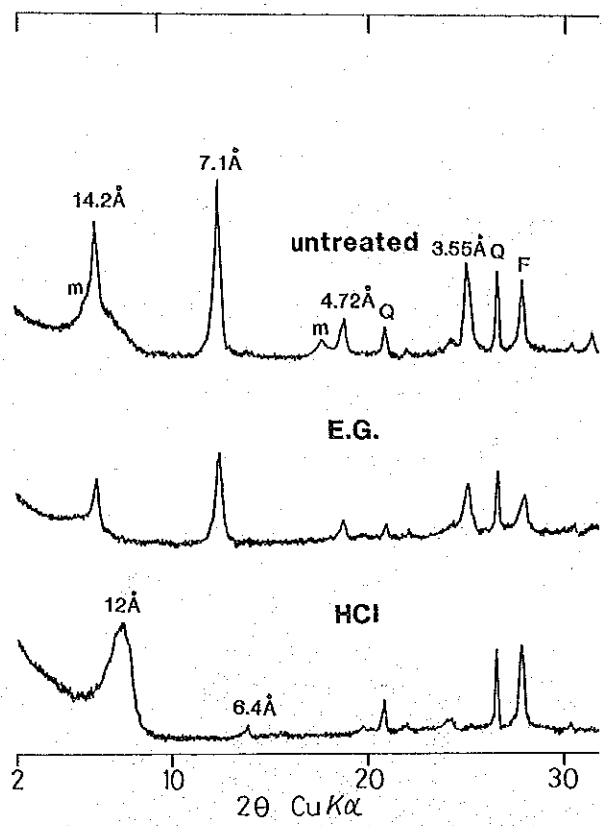

Fig. 4. X-ray powder pattern of orientated fractionation sample of specimen No. 90062412. (The X-ray conditions were the same as those of Fig. 3)
m: montmorillonite, Q: quartz, F: plagioclase (albite).

5. Thermal analysis data

To know the kinds of clay minerals by their thermal behavior, two clayey specimens (No. 90052411 and 90062412) were investigated by means of the thermogravimetric (TG) and differential thermal analyses (DTA). The thermal analyses were performed by using RIGAKU high temperature type TG-DTA (8072G2) with a thermal analysis station TSA100 and RIGAKU 8112BH thermobalance. Heating rate was 10°C per minute, and amounts of sample were 18 mg or 36 mg. The atmosphere was static in air.

Specimen No. 90062411: As shown in the DTA curve (A) of Fig. 5, the remarkable endothermic peaks at about 85° and 173°C correspond to the dehydration of absorptive and interlayer waters is smectite. The TG curve (A) in Fig. 5 indicates that the loss of this dehydration in 13 wt%. The broad endothermic reaction of the DTA curve (A) around 687°C shows the thermal features of dioctahedral-type

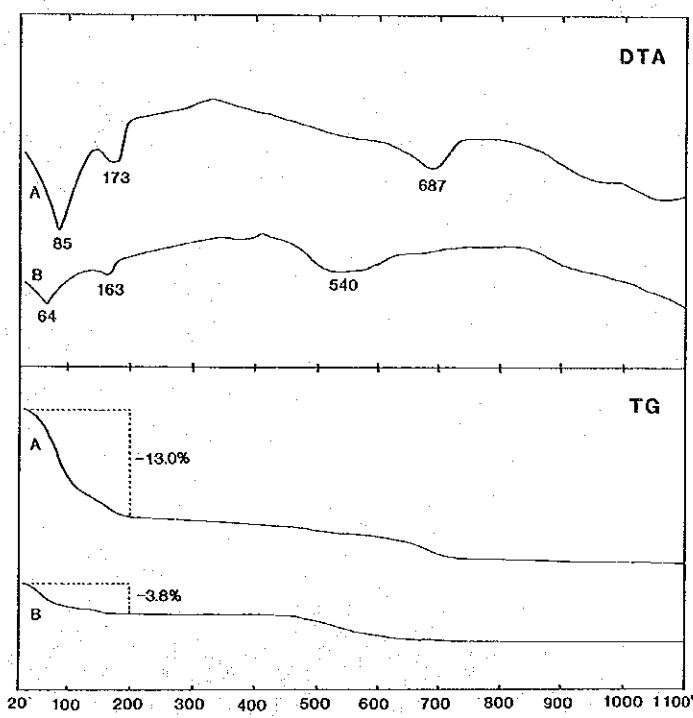

Fig. 5. DTA and TG curves for fractionated samples of specimen Nos. 90062411(A) and 90062411(B) from Minas del Prado.

smectite, namely montmorillonite (Mackenzie, 1957; Nagasawa, 1967). Its reaction is thought as the dehydration of constitution water (OH) in montmorillonite.

Specimen No. 90062412: Two small endothermic peaks at about 64° and 163°C correspond to the dehydration of absorptive and interlayer waters of montmorillonite (Nagasawa, 1967). A broad endothermic reaction around 540°C can be related to that of Fe-rich chlorite of chamosite (Shirozu, 1988). No obvious endothermic peak around 680°C appeared due to the small amounts of montmorillonite included in the sample.

6. Summary

Two clay specimens (Nos. 90062411 and 90062412) from unnamed gold bearing clayey vein in Minas del Prado were investigated by means of X-ray powder diffraction and thermal analyses of TG-DTA.

As a result, following data were obtained:

1) The gold bearing clayey vein occurs in dacite and andesite lavas and pyroclastic rocks such as lappilli tuff, tuff breccia and volcanic breccia, hydrothermally altered by silicification, argillization and propylitization, corresponding to the Pierna Blanca Series (Lower Miocene).

2) Clay minerals investigated appear as an essential constituent of the vein in association with quartz, plagioclase, calcite and pyrite.
3) The clayey sample fractionated from the specimen No. 90062411 consists of abundant smectite associated with chlorite, quartz and kaolin mineral. Smectite was identified to be dioctahedral type, namely montmorillonite from the results of the ethylen glycol solvation and hydrochloric acid treatment, and from the d(060) value of 1.494Å. This was also confirmed from the data of the DTA curve. On the other hand, chlorite was determined to be chamosite from the data of the intensities of the basal reflections and the value 1.545Å of d(060).
4) The fractionated sample from the specimen No. 90062412 is composed of essentially chlorite, quartz and plagioclase (albite) and minor amount of smectite. Chlorite is chamosite, while smectite is montmorillonite as described above (3).
These were also recognized by TG and DTA curves of this sample.
5) Conclusively, the clay minerals from a gold bearing vein in Minas del Prado are in general mixtures of chamosite and montmorillonite in various ratios, associated with quartz and sometimes small amounts of albite and kaolin minerals.

References

Alfaro, G. (1984): Study on metallic ore deposits of central south region in Chile. Ph. D. Thesis, Tohoku University, Japan. p. 268.

Ambrus, J. & Araya, M. (1981): Notes on the geology of Minas del Prado, Chile (Unpublished report).

Bailey, S. W. & Brown, B. E. (1962): Chlorite polytypism: I. Regular and semirandom one-layer structures. *Am. Mineral.*, 47, 819-850.

Brindley, G. W. (1966): Ethylene glycol and glycerol complexes of smectites and vermuculites. *Clay Minerals.* 6, 237-260.

Caillére, S. & Hénin, S. (1957): The chlorite and serpentine minerals. In R. C. Mackenzie ed., *The differential thermal investigation of clays.* Miner. Soc., London, 207-230.

Collao, S. & Frutos, J. (1991): Mineralogía, alteración hidrotermal e inclusiones fluidas del yacimiento aurífero de Mina del Prado, Región del Biobio, Sur de Chile. Congr. Geol. Chile, 1991, Actas Vol. 1, Resum. Expand., 343-346.

Greene-Kelly, R. (1957): The montmorillonite minerals (smectites). In R. C. Mackenzie ed., *The Differential Thermal Investigation of Clays.* Miner. Soc., London, 140-164.

IIG-MNAJ (1981): Informe del reconocimiento geológico de la región andina situada al este de la ciudad de Concepción.

Nagasaga, K. (1967): Thermal properties of clay minerals. In S. Iwao ed., *Handbook of Clays.* Gihodoh, Tokyo, 28-40 (In Japanese).

Oinuma, K. & Kobayashi, K. (1965): Some problems concerning clay mineralogical study on sedimentary rocks. *Progress in Clay Science,* 5, 77-84 (In Japanese with English abstract).

Shirozu, H. (1966): Determination of the chemical composition of chlorites by the X-ray and optical methods. *J. Assoc. Min. Petr. Econ. Geol.*, 44, 18-22 (In Japanese with English abstract).

Shirozu, H. (1988): *Clay Mineralogy, the Fundamentals of Clay Science.* Asakura-shoten, Tokyo, 185 (in Japanese).

SKARN MINERALS FROM MINA FORTUNA OF THE SAN ANTONIO DISTRICT, REGION DE COQUIMBO, CHILE

Masato Fukuoka*, Asahiko Sugaki and José Frutos*****
*** Faculty of General Sciences, Hiroshima University, Higashi-Senda 1-189, Hiroshima 730, Japan. ** Kadan 4-30-503, Aoba, Sendai 980, Japan. *** Instituto GEA, Universidad de Concepción, Casilla 4107, Concepción 3, Chile**

Abstract

Skarn minerals from Mina Fortuna in the San Antonio district, Region de Coquimbo, Chile were investigated by means of field observation, microscopy, X-ray powder diffraction and electron probe microanalyzer. As skarn minerals, garnet, diopside, actinolite and epidote were found in association with magnetite, pyrite, chalcopyrite, sphalerite, sphene, chlorite, quartz and calcite. Among these minerals, garnet, epidote and magnetite are most abundant minerals. Garnet belongs to grandite series with composition from grossular (andradite) 28.7 (65.7) to 66.2 (28.2) mole % as a solid solution, and crystallized at the most early stage with clinopyroxene and magnetite. While epidote has compositions from epidote (clinozoicite) 69.2 (30.8) to 91.3 (8.7) mole % as a solid solution, and produced at comparetively late stage of the skarn mineralization in association with pyrite, chalcopyrite and sphalerite. The composition of clinopyroxene is diopside 84.8 mole %, hedenbergite 13,8 mole %, johansenite 1.4 mole % as a solid solution. Also, actinolite consists of tremolite 69.0 or 54.3 mole % and ferroactinolite 31.0 or 45.7 mole % as a solid solution.

1. Introduction

It is necessary to study mineralogically in detail on skarn minerals to make clear ore genesis of the skarn-type deposits in Chile because mineralogical and geochemical data on skarn minerals from Chilean ore deposits are few. As a first step, the present authors tried investigations on skarn minerals from Mina Fortuna mine in the San Antonio district, Region de Coquimbo. The studies were carried out by means of field observation, microscopy. X-ray powder diffraction and electron probe microanalyzer, and as a result, the valuable data were obtained as be described below.

2. Geological setting

Mina Fortuna in the San Antonio district, Region de Coquimbo is situated at about 25 km northeast of La Serena (Fig. 1). In the San Antonio district, many skarn type copper (and iron) deposits such as Argentina, Florida Norte, Florida Sur, Manto Siete, Union, Poderosa, Tres Amigos And Princesa besides Fortuna are found. Geology around these mines including Mina Fortuna consists of alternated and intercalated strata of andesite lava, andesite volcanic breccia, calcareous sandstone and limestone belonging to Argueros Formation of the Hauterivian and Barremian stages (Aguirre *et al,* 1970) in Lower Cretaceous (Ardila *et al,* 1991). The strata of the Formation surrounding Mina Fortuna run to N40° to 60°W direction and dip to 20° to 35° SW. This Formation was intruded by granodiorite (or hornblende biotite granite), and a metamorphic halo (hornfels) of about 300 to 600 m in width along the contact zone in the Formation was formed. K/Ar ages of two biotites (Aguirre *et al,* 1974), and one alkali feldspars (A. Sugaki, unpublished data) of the granitic rocks are 89 and 98 Ma, and 101± 5 Ma, respectively.

Ore deposits of Mina Fortuna are skarn type replaced by metasomatic

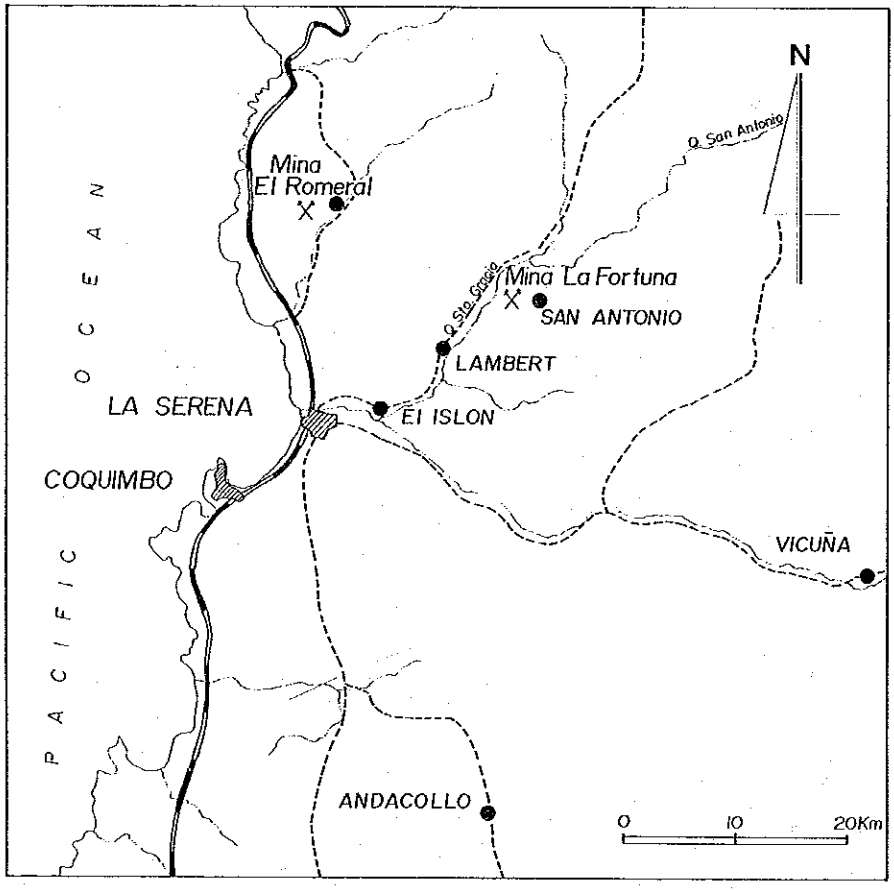

Fig. 1. Location map of Mina Fortuna in the San Antonio district, Región de Coquimbo.

mineralization limestone in the Argueros Formation, and their ore bodies have a scale of 75 to 120 m in length along the strike direction, 20 to 80 m in width (horizontal projection) along the dip side and 4 to 6 m in thickness. Ores are composed of principally magnetite, chalcopyrite, pyrite and hematite with small amounts of sphalerite in aggregate of skarn minerals such as garnet, clinopyroxene, epidote and actinolite. Quartz and calcite also occur as a product of the late stage mineralization.

Among the ore minerals, magnetite is most abundant one, and chalcopyrite and pyrite appear as disseminated spots, band-like form parallel to the stratification and irregular formed veinlets. Crude ore from the mine has generally 1.5 to 2.2% Cu with 1.0 g/t Au.

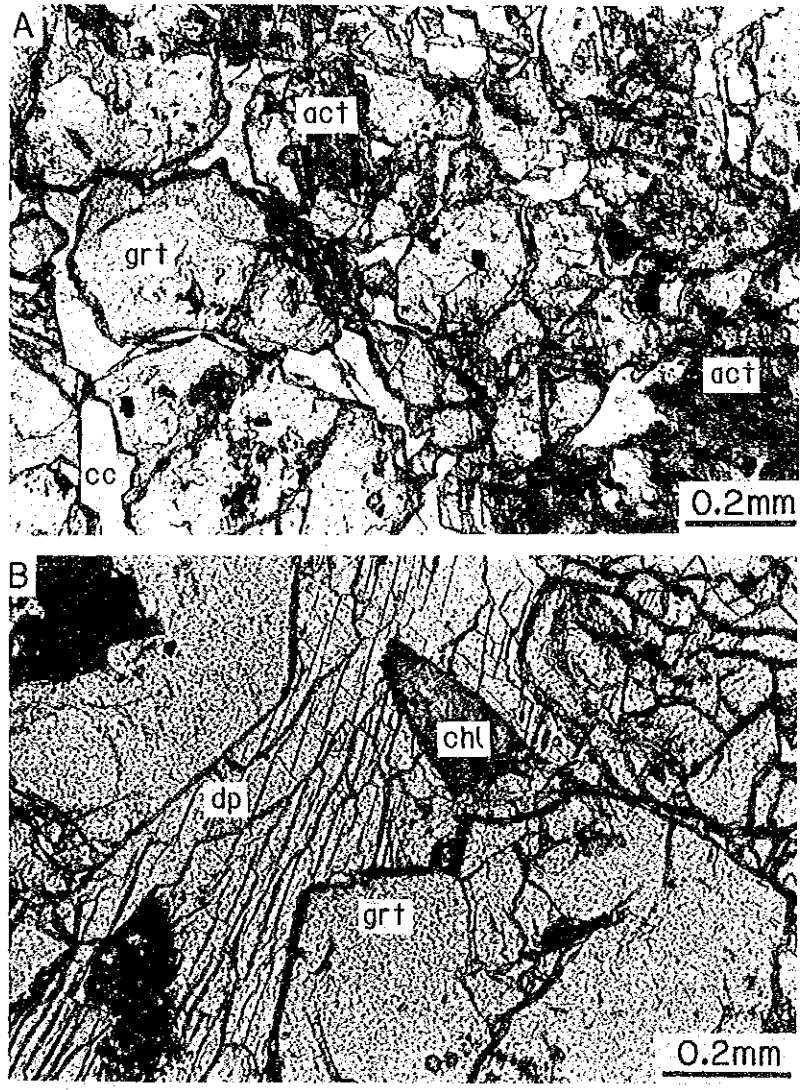

Fig. 2. Photomicrographs of skarn minerals from Mina Fortuna.
grt: garnet, act: actinolite, cc: calcite, dp: diopside, chl: chlorite.

3. Skarn minerals

As skarn minerals, garnet, clinopyroxene, actinolite and epidote occur in intimate association with each other, and are usually accompanied with ore minerals such as magnetite, pyrite and chalcopyrite, and quartz and calcite. Among the skarn minerals, garnet which is most abundant, in general, shows euhedral and hypidiomorphic granular forms, and assembles with commonly clinopyroxene (diopside), actinolite and epidote as shown in Figs. 2 and 3. Garnet is often associated with epidote and calcite. In this case, garnet of irregular forms replaced partly is enclosed in epidote and calcite, and its included crystal is usually cut by veinlet of them. Epidote, which is

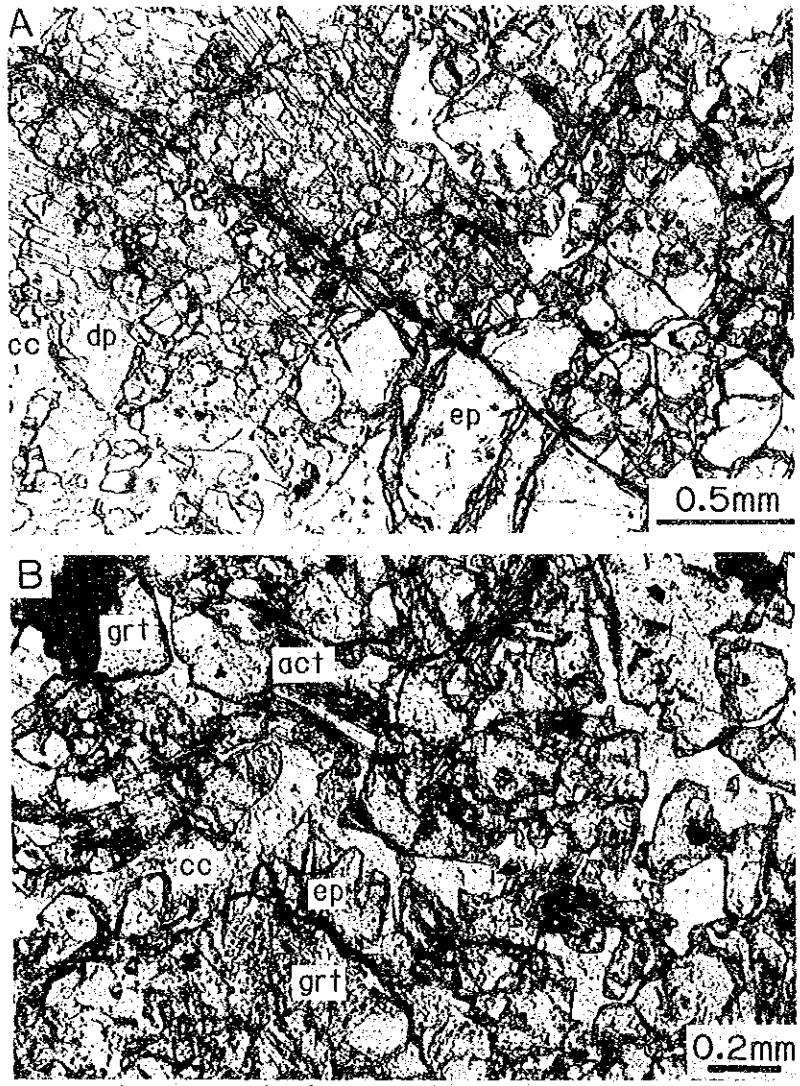

Fig. 3. Photomicrographs of skarn minerals from Mina Fortuna. dp: diopside, ep: epidote, cc: calcite, act: actinolite, grt: garnet.

second aboundant in skarn minerals, also assembles often with garnet, clinopyroxene (diopside), actinolite, chlorite, quartz, calcite and occasionally small amounts of hornblende and sphene. Epidote are granular and prismatic crystals (Figs. 2 and 3), and represents sometimes a large euhedral-prismatic crystal showing a growth zoning texture (Fig. 4). Epidote-calcite vein occasionally cuts garnet aggregate. Clinopyroxene (diopside) appears as prismatically hypidiomorphic and irregular forms as restricted with crystal faces of garnet, associating with garnet, epidote, calcite and quartz (Figs. 2 and 3). Its crystal has a distinctly developed cleaveges.

Magnetite, pyrite and chalcopyrite are principal ore minerals from this mine. Among them magnetite is most abundant, and intimately associates with garnet

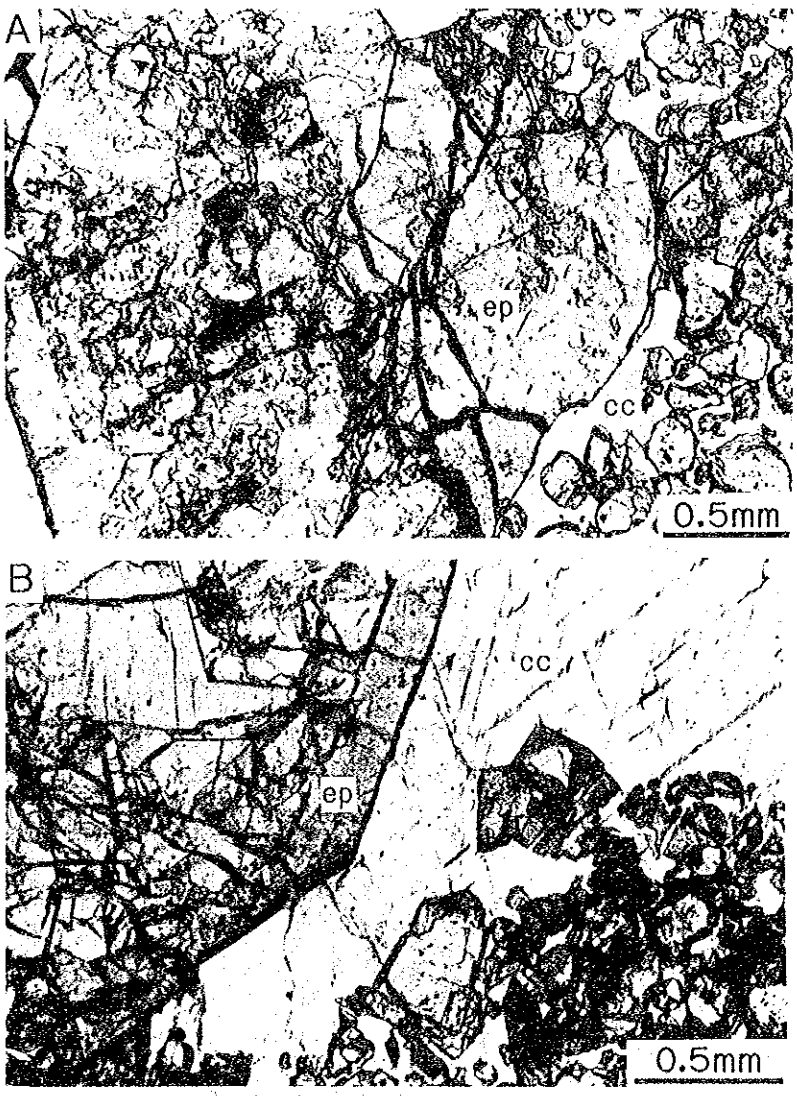

Fig. 4. Photomicrographs of skarn minerals from Mina Fortuna, ep: epidote, cc: calcite.

commonly, and frequently includes garnet grains in it. Sulfide minerals of pyrite and chalcopyrite usually occur as disseminated spots, small massive and stringer-like forms and veinlet in interstices of aggregate of garnet, clinopyroxene (diopside), epidote, actinolite and magnetite, sometimes associating quartz, calcite and chlorite. Pyrite and chalcopyrite also appear as small inclusions in such skarn minerals as above. Small amounts of sphalerite is occasionally accompanied with chalcopyrite and pyrite. Sphalerite sometimes includes fine dots of chalcopyrite. Chalcopyrite has not fine star or dendritic crystals of sphalerite.

4. X-ray powder diffraction data

The data of X-ray powder diffraction for garnet and epidote which are most essential skarn minerals from Mina Fortuna are given in Tables 1 and 2, respectively. The X-ray powder diffraction was tried by using RIGAKU D/max-C system under conditions as follows: Nickel filtered Cu-Kα radiation, 30kV, 15mA, divergence slit: 1°, receiving slit: 0.3mm, Scanning rate 2° to 4° (2θ) per minute, and measuring angle range: 10° to 70°.

The X-ray diffraction data for two type garnets of brown and dark gray to black in color are compared with each other and that of grossular from Georgetown, California, USA (JCPDS, 1986) in Table 1. Their data are in good accordance.

Table 1. X-ray powder diffraction data of brown and black colored garnets in skarn from Mina Fortuna

Brown		Black		Grossular *		
d	I	d	I	d	I	hkl
2.988	48	2.986	81	2.959	25	400
2.671	100	2.668	100	2.647	100	420
2.546	10	2.545	14	2.524	11	332
2.439	22	2.437	33	2.417	20	422
2.343	13	2.340	20	2.321	18	431
2.181	13	2.177	15	2.162	17	521
				2.093	4	440
1.937	22	1.935	21	1.921	25	611
1.890	4	1.887	9	1.872	2	620
1.724	7	1.723	11	1.710	17	444
1.656	16	1.658	23	1.643	25	640
				1.612	2	721
1.596	40	1.594	40	1.581	50	642
				1.504	2	651
1.493	8	1.493	11	1.481	10	800
a = 11.943 A		11.937 A		11.850 A		

* Georgetown, California, USA (JCPDS No. 26-292)

Calculated cell constant of garnets is given in the table. Garnets of Mina Fortuna have a little larger cell constant than that of grossular from Georgetown. Also, the cell unit of brown colored garnet from Mina Fortuna is a bit larger than that of black colored garnet. Ho vever, the cell constant values of both garnets are little smaller than that of andradite 'Deer *et al*, 1962).

Meanwh ᵉ, the X-ray powder data for epidote from Mina Fortuna are given in Table 2, in comparison with that of Dauphine, Switzerland (JCPDS, 1986). Their data are in good accordance with each other.

5. Electron probe microanalysis data

Electron probe microanalysis (EPMA) for garnet, diopside, actinolite and epidote of the skarn minerals from Mina Fortuna were carried out by using JEOL JXA8600M. The analyses were performed under conditions of accelerating voltages: 15 kV, specimen currents: 15nA, and beam diameter: 1 to 2 microns. As standard materials, pure almandin for Si, Al and Fe, rutile for Ti, olivine for Mg, diopside for Ca, jadeite for Na, and Sanidine for K of the Mineral Mount (NINM25-53) made by the Astimex Scientific Limited were used.

Table 2. The data of X-ray powder diffraction for epidote in skarn from Mina Fortuna, in the comparison with epidote from Dauphine, Switzerland (JCPDS No. 17-514)

Fortuna Mine		JCPDS No.17-514*		Fortuna Mine		JCPDS No.17-514*	
d	I	d	I	d	I	d	I
8.04	8	8.04	10	2.676	57	2.679	70
5.027	33	5.05	25	2.600	63	2.599	100
		4.79	10	2.529	39	2.531	30
4.614	15	4.59	15	2.455	16	2.460	50
4.017	56	4.02	50	2.438	17		
3.987	25	3.99	10	2.403	41	2.409	40
3.765	10	3.77	20			2.401	40
3.584	10			2.300	24	2.301	10
3.490	26	3.49	30	2.288	11	2.294	30
3.405	23	3.40	40	2.164	58	2.166	30
3.242	45					2.163	30
3.208	38	3.21	20	2.133	10	2.131	10
3.060	21	3.06	20	2.115	25	2.117	25
2.996	48	Calcite?		2.107	19	2.109	25
		2.93	10	2.072	13	2.072	15
2.920	34	2.92	25	2.046	13	2.048	20
2.899	100	2.90	100	2.029	9	2.026	10
2.816	31	2.817	40	2.008	24	2.010	15
2.688	46	2.688	15				

* Dauphine, Switzerland

The composition image of EPMA on specimen No. 9006270-2 is shown in Fig. 5. In this photomicrograph, most light gray portion indicates to be garnet, gray colored portion is epidote, and dark gray colored granular forms represent to be diopside and actionite. Most dark (black) parts show calcite. The quantitative analyses on garnet, epidote, diopside and actinolite shown in Fig. 5 were performed by EPMA. Each mineral was analyzed at number points indicated in the figure. Namely, analytical points of minerals are as follows: garnet, 1 and 2; epidote, 3 and 4; diopside, 5 and 6; actinolite, 7 and 8. As a result, the analytical data given in Table 3 were obtained. Among these data, garnets belong to grandite series (Deer *et al,* 1965), and consists of andradite 65.7 mole %, grossular 28.7 mole %, spessartine 4.7 mole %, pyrope 0.2 mole %, schorlomite 0.6 mole % and $Ca_3Mn_2Si_3O_{12}$ 0.1 mole % as a solid solution at point 1, and andradite 46.2 mole %, grossular 49.2 mole %, spessartine 2.1 mole %, pyrope 1.2 mole %, schorlomite 1.1 mole % and $Ca_3Mn_2Si_3O_{12}$ 0.2 mole % as a solid solution at point 2.

While epidote is socalled common epidote or pistacite (Ehlers, 1953; Sugaki *et al,* 1988) having epidote ($Ca_2Fe\,Al_2O\,OH\,Si_2O_7\,SiO_4$) 75.2 mole % and clinozoicite ($Ca_2Al\,Al_2O\,OH\,Si_2O_7\,SiO_4$) 24.8 mole % as a solid solution at point 3, and epidote 67.0 mole % and clinozoisite 33.0 mole % as a solid solution at point 4.

Fig. 5. EPMA composition image (back-scattered electron image) of skarn assembled with grandite garnet (1, 2), epidote (3, 4), diopside (5, 6) and actinolite (7, 8) from Mina Fortuna (specimen No. 90062701-2). Dark gray portion is calcite and others. The numbers (1 to 8) in the photograph indicate analytical points by EPMA, and also are the same as those in Table 3. The bar scale is 100 μm.

Table 3. The analytical data by EPMA for garnet, epidote, diopside and actinolite in skarn from Mina Fortuna (Specimen No. 90082701-2)

	Grandite		Epidote		Diopside		Actinolite	
	1	2	3	4	5	6	7	8
Wt.%								
SiO_2	36.18	37.04	37.89	37.68	53.75	44.05	51.38	51.32
TiO_2	0.18	0.34	0.06	0.20	0.02	0.97	0.00	0.06
Al_2O_3	7.00	11.14	23.67	24.43	0.46	9.69	0.25	2.74
Fe_2O_3*1)	21.63	15.70	11.93	10.64	-	-	-	-
FeO*1)	0.00	0.00	-	-	4.49	6.64	8.82	17.56
Mn_2O_3*1)	0.04	0.07	0.30	0.19	-	-	-	-
MnO*1)	2.26	0.96	-	-	0.45	0.14	0.67	0.82
MgO	0.06	0.30	0.00	0.03	15.52	11.92	11.88	12.26
CaO	32.26	33.72	22.64	22.99	24.76	24.85	24.12	12.22
Na_2O	0.04	0.01	0.00	0.01	0.05	0.02	0.15	0.22
K_2O	0.00	0.00	0.00	0.00	0.00	0.00	0.00	0.00
H_2O*2)	-	-	1.87	1.87	-	-	2.02	2.01
Total	99.65	99.28	98.36	98.04	99.50	98.28	99.29	99.21
	O = 12		O=12 and (OH)=1		O = 6		O=22 and (OH)=2	
Cation ratio								
Si	2.972	2.973	3.040	3.024	1.988	1.686	7.632	7.638
Ti	0.011	0.021	0.004	0.012	0.001	0.028	0.000	0.007
Al	0.678	1.054	2.238	2.311	0.020	0.437	0.044	0.481
Fe^{3+}	1.337	0.949	0.720	0.643	-	-	-	-
Fe^{2+}	0.000	0.000	-	-	0.139	0.213	1.096	2.186
Mn^{3+}	0.002	0.004	0.018	0.012	-	-	-	-
Mn^{2+}	0.157	0.065	-	-	0.014	0.005	0.084	0.103
Mg	0.007	0.036	0.000	0.004	0.856	0.680	2.631	2.720
Ca	2.840	2.900	1.946	1.977	0.981	1.019	3.839	1.949
Na	0.006	0.002	0.000	0.002	0.004	0.001	0.043	0.063
K	0.000	0.000	0.000	0.000	0.000	0.000	0.000	0.000
H	-	-	1.000	1.000	-	-	2.000	2.000
Total	8.010	8.004	8.966	8.985	4.003	4.069	17.369	17.147
Molecule percent								
Pyrope	0.2	1.2						
Almandine	0.0	0.0						
Spessartine	4.7	2.1						
Grossular	28.7	49.2						
Andradite	65.7	46.2						
Schorlomite	0.6	1.1						
$Ca_3Mn_2Si_3O_{12}$	0.1	0.2						
$Fe^{3+}/(Al+Fe^{3+})$	0.66	0.47	0.24	0.22				

*1) For garnet: calculated based on the ideal formula $[A_3B_2(SiO_4)_3]$.
For epidote: total iron and total manganese as Fe_2O_3 and Mn_2O_3, respectively.
For diopside and actinolite: total iron and total manganese as FeO and MnO, respectively.

*2) Calculated based on the ideal formula of epidote $[A_2B_3(SiO_4)_3(OH)]$ or amphibole $[A_{0-1}B_2Y_5Z_8O_{22}(OH)_2]$.

Diopside consists of compositions with diopside ($CaMgSi_2O_6$) 84.8 mole %, hedenbergite ($CaFeSi_2O_6$) 13.8 mole % and johansenite ($CaMnSi_2O_6$) 1.4 mole % as a solid solution at point 5. Actinolite has tremolite $Ca_2Mg_5Si_8O_{22}(OH,F)_2$ 69 mole % and ferroactinolite $Ca_2Fe_5Si_8O_{22}(OH,F)_2$ 31 mole % as a solid solution at point 7, and tremolite 54.3 mole % and ferroactinolite 45.7 mole % at point 8. On the other hand, the compositional image of EPMA on specimen No. 90062701-1 from Mina

Fig. 6. EPMA composition image of skarn with grandite (1 to 4) and epidote (5 to 9). The numbers (1 to 9) show the analytical points by EPMA, and correspond to those in Table 4. The dark gray portion in the photomicrograph is calcite. The bar scale is 100 μm.

Fortuna is also shown in Fig. 6. In this photograph the light gray minerals are garnet, while dark gray ones are epidote, and the analytical points from 1 to 9 are indicated. EPMA analytical values at these points are given in Table 4. Among these data, the analytical values for garnet are shown at 1 to 4 in the table. All garnets belong to grandite series. Garnet analyzed at point 1 consists of andradite 53.3 mole %, grossular 36.0 mole %, spassartin 8.8 mole %, pyrope 0.6 mole %, almandine 0.4 mole % and schorlomite 0.9 mole % as a solid solution as given in Table 4. Similarly, solid solution compositions of garnets at points 2, 3 and 4 are shown in Table 4. They consist of mostly andradite 53.3 to 43.2 mole % and grossular 36.0 to 51.9 mole % as the solid solution.

Analytical data of epidote at points 5 to 9 are given in Table 4. These analytical values indicate that epidotes are common epidote (pistacite) with clinozoicite molecule (and very small amounts piemontite molecule) as a solid solution as follows: At point 5; epidote 91.3 mole % and clinozoicete 8.7 mole %, at point 7: epidote 86.1 mole % and clinozoicite 13.9 mole %, at point 8: epidote 73.2 mole % and clinozoicite 26.8 mole %, at point 9: epidote 69.2 mole % and clinozoicite 30.8 mole %.

Garnet often occurs in a growth zoning crystal as shown in Fig. 7, as composition image of EPMA. EPMA analyses for zoned garnets at points 1 to 7 were tried, and

Table 4. EPMA analysis data of garnet and epidote from Mina Fortuna (Specimen No. 90062701-1)

	Grandite garnet				Epidote				
	1	2	3	4	5	6	7	8	9
Wt.%									
SiO_2	36.68	36.60	37.20	37.08	36.98	37.35	37.75	37.48	37.46
TiO_2	0.32	0.43	0.35	0.38	0.33	0.13	0.53	0.29	0.10
Al_2O_3	9.66	10.68	11.25	11.66	21.84	22.24	22.54	23.87	24.35
Fe_2O_3*1)	17.94	16.74	15.49	14.87	14.48	14.08	13.13	11.50	11.16
FeO *1)	0.17	0.06	0.00	0.00	-	-	-	-	-
Fe_2O_3*1)	0.00	0.00	0.22	0.45	0.12	0.17	0.01	0.08	0.16
MnO	4.34	4.30	0.90	0.54	-	-	-	-	-
MgO	0.17	0.16	0.33	0.33	0.06	0.04	0.06	0.01	0.03
CaO	30.82	31.11	33.85	34.21	23.10	23.33	23.30	23.59	23.38
Na_2O	0.01	0.00	0.00	0.02	0.02	0.01	0.00	0.03	0.00
K_2O	0.00	0.00	0.00	0.00	0.00	0.00	0.00	0.00	0.00
H_2O*2)	-	-	-	-	1.85	1.86	1.87	1.87	1.87
Total	100.11	100.08	99.59	99.54	98.78	99.21	99.19	98.72	98.51
	O = 12				O = 12 and (OH) = 1				
Cation ratio									
Si	2.969	2.950	2.974	2.961	2.994	3.005	3.024	3.003	3.002
Ti	0.019	0.026	0.021	0.023	0.020	0.008	0.032	0.017	0.006
Al	0.921	1.015	1.060	1.097	2.084	2.109	2.128	2.254	2.300
Fe^{3+}	1.092	1.015	0.932	0.894	0.882	0.852	0.792	0.693	0.673
Fe^{2+}	0.012	0.004	0.000	0.000	-	-	-	-	-
Mn^{3+}	0.000	0.000	0.013	0.027	0.007	0.010	0.001	0.005	0.010
Mn^{2+}	0.298	0.294	0.061	0.037	-	-	-	-	-
Mg	0.021	0.019	0.039	0.039	0.007	0.005	0.007	0.001	0.004
Ca	2.673	2.687	2.900	2.927	2.004	2.011	2.000	2.025	2.007
Na	0.002	0.000	0.000	0.003	0.003	0.002	0.000	0.005	0.000
K	0.000	0.000	0.000	0.000	0.000	0.000	0.000	0.000	0.000
H	-	-	-	-	1.000	1.000	1.000	1.000	1.000
Total	8.007	8.010	8.000	8.008	9.001	9.002	8.984	9.003	9.002
Molecule percent									
Pyrope	0.6	0.6	1.3	1.3					
Almandine	0.4	0.1	0.0	0.0					
Spessartine	8.8	8.9	2.0	1.2					
Grossular	36.0	40.4	49.7	51.9					
Andradite	53.3	48.7	45.4	43.2					
Schorlomite	0.9	1.3	1.0	1.1					
$Ca_3Mn_2Si_3O_{12}$	0.0	0.0	0.6	1.3					
$Fe^{3+}/(Al+Fe^{3+})$	0.54	0.50	0.47	0.45	0.30	0.29	0.27	0.24	0.23

*1) For garnet: calculated based on the ideal formula $[A_3B_2(SiO_4)_3]$.
For epidote: total iron and total manganese as Fe_2O_3 and Mn_2O_3, respectively.
*2) Calculated based on the ideal formula of epidote $[A_2B_3(SiO_4)_3(OH)]$.

the analytical values were obtained as given in Table 5. Compositions of the zoning bands and core of grandite garnet crystal change from grossular (andradite) 66.2 (28.2) to 49.9 (45.2) mole %, and from 67.7 (26.1) to 50.0 (44.4) mole %. It is found roughly a tendency that compositions of marginal bands of garnet crystal are more andradite-rich than those of its core, although the composition changes are not regularly.

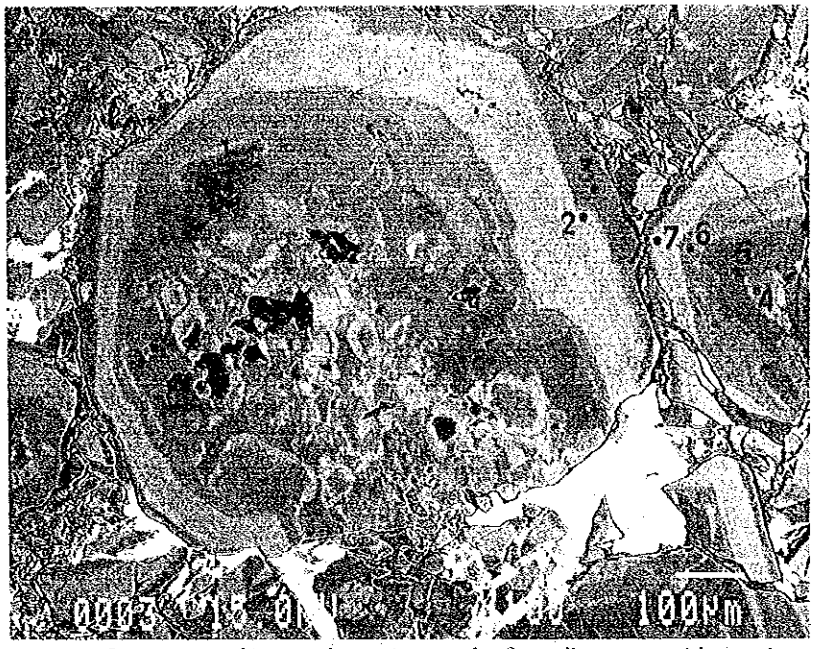

Fig. 7. Compositional image photomicrograph of grandite garnet with a zoning texture due to difference between Al and Fe concentrations. The numbers (1 to 7) are indicating the analytical points correspond to those of Table 5. The light gray portion is Mn oxide as secondary product. The bar scale is 100 μm.

6. Mineralization stages

From occurrence of Skarn, observations under microscope, EPMA composition image and analysis data, mineralization sequence of principal skarn and ore minerals from Mina Fortuna was obtained as shown in Fig. 8. As seen in the figure, crystallization of grandite garnet preceded than other skarn mineral.

Mineralization of diopside and magnetite were overlapped the middle to late mineralization stages of garnet. However, those of diopside and magnetite continued successively after finish of garnet crystallization. After formation of diopside, actinolite and epidote were crystallized. In this case, produce of actinolite preceded than that of epidote. Mineralization of sulfide minerals such as pyrite, chalcopyrite and sphalerite were carried out mainly during formations of epidote, after crystallization of actinolite. As a late stage mineralization, quartz and calcite were precipitated, although calcite sometimes was crystallized together with epidote of the late stage. Ardila *et al.*, (1991) estimated temperatures of skarn mineralization in the San Antonio district to be 550° to 230°C.

The skarn minerals with iron-copper ores from Mina Fortuna are thought to have been formed by reaction between limestone and mineralizing fluid derived from granitic magma which intruded into the Argueros Formation at Late Cretaceous (89 to 101 Ma).

Table 5. Compositional variation of zoned garnet analyzed by EPMA (Specimen No. 90062712)

	core		rim	core			rim
	1	2	3	4	5	6	7
Wt.%							
SiO_2	37.98	37.34	37.57	37.17	37.88	37.64	37.45
TiO_2	0.43	0.54	0.26	0.17	0.64	0.29	0.48
Al_2O_3	15.18	11.20	13.62	13.41	15.14	13.72	11.50
Fe_2O_3*1)	9.94	15.42	12.41	13.17	9.27	12.14	15.24
FeO *1)	0.10	0.11	0.00	0.00	0.00	0.31	0.21
Mn_2O_3*1)	0.00	0.00	0.10	0.05	0.11	0.00	0.00
MnO *1)	1.56	0.95	1.13	0.97	1.53	1.42	1.24
MgO	0.19	0.26	0.37	0.36	0.17	0.43	0.29
CaO	34.08	33.84	34.00	34.04	34.02	33.41	33.64
Na_2O	0.00	0.01	0.00	0.00	0.04	0.00	0.00
K_2O	0.00	0.00	0.00	0.00	0.00	0.00	0.00
Total	99.46	99.67	99.46	99.34	98.80	99.36	100.05
			O = 12				
Cation ratio							
Si	2.981	2.982	2.972	2.954	2.988	2.980	2.979
Ti	0.025	0.032	0.015	0.010	0.038	0.017	0.029
Al	1.404	1.054	1.270	1.255	1.408	1.280	1.078
Fe^{3+}	0.587	0.927	0.739	0.787	0.550	0.723	0.912
Fe^{2+}	0.007	0.007	0.000	0.000	0.000	0.020	0.014
Mn^{3+}	0.000	0.000	0.006	0.003	0.006	0.000	0.000
Mn^{2+}	0.104	0.064	0.076	0.065	0.102	0.095	0.084
Mg	0.022	0.031	0.044	0.043	0.020	0.051	0.034
Ca	2.866	2.896	2.882	2.897	2.876	2.834	2.867
Na	0.000	0.002	0.000	0.000	0.006	0.000	0.000
K	0.000	0.000	0.000	0.000	0.000	0.000	0.000
Total	7.996	7.995	8.004	8.014	7.994	8.000	7.997
Molecule percent							
Pyrope	0.7	1.0	1.4	1.4	0.7	1.7	1.1
Almandine	0.2	0.2	0.0	0.0	0.0	0.6	0.4
Spessartine	3.4	2.1	2.5	2.1	3.3	3.1	2.7
Grossular	66.2	49.9	59.1	57.9	67.7	58.5	50.0
Andradite	28.2	45.2	35.9	38.0	26.1	35.2	44.4
Schorlomite	1.3	1.6	0.8	0.5	1.9	0.9	1.4
$Ca_3Mn_2Si_3O_{12}$	0.0	0.0	0.3	0.1	0.3	0.0	0.0

*1) Calculated based on the ideal formula.

7. Summary

1) Mina Fortuna in the San Antonio district, Region de Coquimbo is located at about 25 km northeast of La Serena.
2) Geology around Mina Fortuna consists of andesite lava, volcanic breccia, calcareous sandstone, and limestone belonging to the Argueros Formation of Lower Cretaceous.
3) This Formation was intruded by granodiorite (or hornblende biotite granite), and

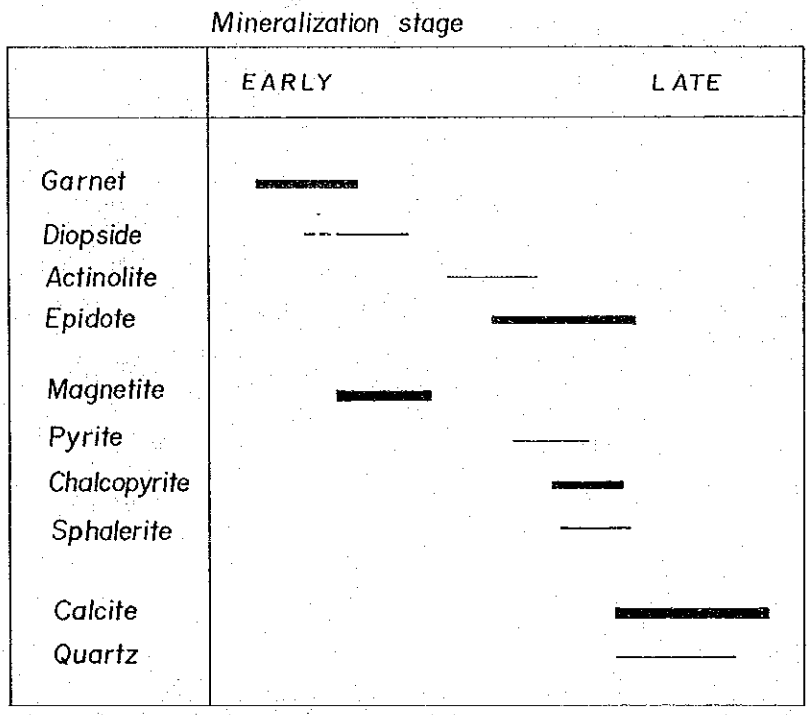

Fig. 8 Schematic diagram of the mineralization sequence of principal skarn and ore minerals from Mina Fortuna.

a metamorphic halo (hornfels) of about 300 to 600 m in width along the contact zone in the Formation was produced. K/Ar ages of two biotite and alkali feldspar separated from the granitic rocks are 89 and 98 Ma (biotites) and 101± 5 Ma (alkali feldspar).

4) Ore deposits of Mina Fortuna are a skarn type replaced by metasomatic mineralization limestone in the Arguerous Formation. As skarn and ore minerals, garnet, diopside, actinolite, epidote, magnetite, pyrite, chalcopyrite, sphalerite, chlorite, quartz and calcite occur.
5) Garnet and epidote are principal skarn minerals from Mina Fortuna, and were identified by X-ray powder diffraction. Cell constant of garnet calculated from the X-ray powder data was a=11.943 Å and 11.937 Å.
6) Garnet belongs to grandite series, and its compositions are from grossular (andradite) 28.7 (65.7) to 66.2 (28.2) mole %. Garnet shows often growth zoning texture. In this case, its marginal bands of the zoning have andradite-rich composition. Garnet crystallized at the most early stage of mineralization in association with diopside and magnetite.
7) Epidote has compositions from epidote (clinozoicite) 69.2 (30.8) to 91.3 (8.7)

mole % as a solid solution, and crystallized at late stage of the skarn mineralization in association with pyrite, chalcopyrite and sphalerite.

8) The composition of clinopyroxene is diopside 84.8 mole %, hedenbergite 13.8 mole %, johansenite 1.4 mole % as a solid solution. While actinolite consists of tremolite 69.0 or 54.3 mole % and ferroactinolite 31.0 or 45.7 mole % as a solid solution.

9) The skarn minerals with iron-copper ores from Mina Fortuna are thought to have been formed by reaction between limestone and mineralizing fluid derived from granitic magma which intruded into the Argueros Formation at Late Cretaceous (89 to 101 Ma).

References

Aguirre, L. & Egert, E. (1970): Cuadrángulo Lambert (La Serena), Provincia de Coquimbo. Inst. Invest. Geol., Chile. Carta Geol. Chile, No. 23, 28.

Aguirre, L., Charrier, L., Davidson, J., Mpodozis, A., Rivano, S., Thiele, R., Tidy, E., Vergara, M. & Vicente, J. (1974): Andean magmatism: Its paleogeographic and structural setting in the central part of the Southern Andes. Pacific Geology, No. 8, 1-38.

Ardila, R., Carrascal, E.R., Canchaya, S., Canut de Bon, C. & Collao, R. (1991a): Geología de los skarns cupríferos del Distrito de San Antonio, Región de Coquimbo, Chile. Congr. Geol. Chile., 1991, Actas Vol. 1, Resum. Expand., Viña del Mar, 253-255.

Ardila, R., Carrascal, E.R. & Oyarzún, J. (1991b): Proposición de un modelo genético para los yacimientos cupríferos tipo skarn de San Antonio y Panulcillo, Región de Coquimbo, Chile, Congr. Geol. Chile., 1991, Actas Vol. 1, Resúm. Expand., Viña del Mar, 256-260.

Deer. W.A., Howie, R.A. & Zussman, J. (1962): *Rock-forming Minerals.* Vol. 1, Ortho-and ring silicates, Longmans, London, 77-112, 193-210.

Deer. W.A., Howie. R.A. & Zussman, J. (1963): *Rock-forming Minerals.* Vol. 2. Chain silicates. Longmans. London. 42-74, 249-269.

Ehlers, E.G. (1953): An investigation of the stability relations of the Al-Fe members of the epidote group. *Jour. Geol.*, 61, 231.

JCPDS (1986): *Mineral Diffraction File, Data Book.* Int. Nat. Center for Diffraction Data, 336, 446.

Sugaki, A., Kitakaze, A. & Komatsu, R. (1988): Scheelite from the Yaguki mine and its mineralization. *Mining Geol.*, 38, 457-467. (In Japanese with English abstract and explanations of figures and Tables)

SKARN FORMATION AT FUKA, OKAYAMA, JAPAN

Chiyoko Henmi
Faculty of Science, Okayama University, Tsushima-Naka, Okayama 700, Japan.

In the Fuka area (Bicchu, Okayama, Japan), skarn minerals occur between quartz monzonite and crystalline limestone. Table 1 shows minerals which occur at Fuka. Gehlenite ($Ca_2Al_2SiO_7$) and spurrite ($Ca_5Si_2O_8(CO_3)$) are considered to be primary minerals and form each a monomineralic zone, respectively. Contaminated rocks, which mainly consist of feldspar and pyroxenes, frequently occur between the quartz monzonite and the skarn. One example of the occurrences of the skarns is shown in Fig. 1 (Kusachi, 1975). The zonal structure of the skarn is as follows: quartz monzonite, contaminated rock, gehlenite zone, spurrite zone and crystalline limestone. There are some andesite dikes cutting the skarns. Note that the skarn zones are very wide compared to the width of the igneous rock.

During the metasomatism, Si-ions moved into limestone and formed spurrite. The regions where Si and Al (and small amounts of Fe^{3+} and Mg) were added changed to gehlenite. These ions have small ionic radii in comparison with other major elements such as alkaline ions.

The chemical composition of the igneous magma was changed by the skarn formation and the resulting magma solidified as contaminated rock. In the contaminated rock, a large portion of feldspar is K-feldspar. Pyroxene sometimes shows a zonation of chemical composition from diopside ($Ca(Mg, Fe)Si_2O_6$) to aegirine ($NaFeSi_2O_6$). In the contaminated rocks, garnet sometimes has a zonal structure ranging from grandite ($Ca_3(Al, Fe)_2Si_3O_{12}$) to schorlomite ($Ca_3Fe^{2+}TiSi_3O_{12}$ and/or $Ca_3Ti_2(Fe^{3+}, Al)_2SiO_{12}$) and it contains up to 7 percent kimzeyite component ($Ca_3Zr_2(Fe^{3+}, Al)_2SiO_{12}$). The titanian -and zirconian- garnets usually occur in alkaline rocks. Baddeleyite, calzirtite and perovskite occur in the contaminated rocks. These minerals are also characteristic minerals of alkaline rocks. It can be concluded that the contaminated rock is an alkaline rock. During the metasomatism, therefore, alkaline ions have not been mobile and have remained in the igneous rock.

Table 1. Minerals from Fuka

Calcium silicates		
rankinite	$Ca_3Si_2O_7$	
kilchoanite	$Ca_3Si_2O_7$	
wollastonite-2M	$CaSiO_3$	
wollastonite-1T		
wollastonite-7T		
pectolite	$Ca_2NaH(SiO_3)_3$	
hillebrandite	$Ca_2SiO_4H_2O$	
afwillite	$Ca_3Si_2O_4(OH)_6$	
jennite	$Ca_9H_2Si_6O_{18}(OH)8.6H_2O$	
foshagite	$Ca_4Si_3O_9(OH)_2$	
xonotlite	$Ca_6Si_6O_{17}(OH)_2$	
11Å-tobermorite	$Ca_5(OH)_2Si_6O16.4H_2O$	
clinotobermortite*	$Ca_5(OH)_2Si_6O16.4H_2O$	
14Å-tobermorite	$Ca_5(OH)_2Si_6O168H_2O$	
Calcium carbonate silicates		
spurrite	$Ca_5Si_2O_8(CO_3)$	
tilleyite	$Ca_5Si_2O_7(CO_3)_2$	
fukalite*	$Ca_4Si_2O_6(OH)_2(CO_3)$	
scawtite	$Ca_7CO_3Si_6O18.2H_2O$	
Calcium aluminium silicates		
gehlenite	Ca_2AlSiO_7	
bicchulite*	$Ca_2Al_2SiO_6(OH)_2$	
grossular	$Ca_3Al_2Si_3O_{12}$	
hydroglossular	$Ca_2Al_2(Si.H_4)_3O_{12}$	
prehnite	$Ca_2Al_2Si_3O_{10}(OH)_2$	
Ti-bearing minerals		
perovskite	$CaTiO_3$	
schorlomite	$Ca_3(Fe.Ti)_2Si_3O_{12}$	
sphene	$CaTiSiO_5$	
Zr-bearing minerals		
baddeleyite	ZrO_2	
zircon	$ZrSiO_4$	
calzirtite	$CaTiZr_3O_9$	
B-bearing minerals		
oyelite*	$Ca_{10}B_2Si_8O_{29}.NH_2O$	
henmilite*	$Ca_2CuB_2O_6.6H_2O$	
pentahydroborite	$CaB_2O_4.5H_2O$	
F-bearing minerals		
apophyllite	$KFCa_4Si_8O_{20}.8H_2O$	
cuspidine	$Ca_4(F,OH)_2Si_2O_7$	
fluorite	CaF_2	
bultfonteinite	$Ca_2(SiO_3OH)F.H_2O$	
Others		
vesuvianite	pyroxene	amphibole
epidote	biotite	chlorite
diaspore	orthoclase	microcline
plagioclase	quartz	calcite
apatite	scolecite	thomsonite
hematite	magnetite	pyrrhotite
sphalerite	sillenite	

* New minerals from Fuka: clinotobermorite; Henmi and Kusachi, fukalite; Henmi et al., 1977, bicchulite; Henmi *et al.*, 1973, oyelite; Kusachi *et al.*, 1984.

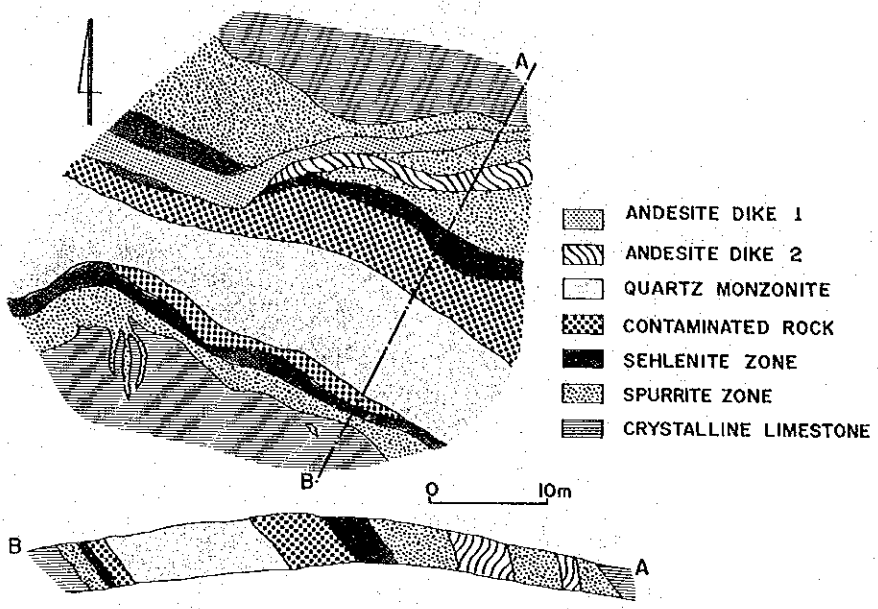

Fig. 1. Zonal structure of the skarn in the Fuka area, Okayama, Japan.

Most of skarns have been considered to be formed not by diffusion but by infiltration. During the infiltration metasomatism, alkaline ions move very easily. But at Fuka, alkaline ions remain in the igneous rock and formed the alkaline contaminated rock. On the other hand, small ions such as Si, Al and Fe^{3+} moved to limestone and formed skarns. Accordingly, the mechanism of the metasomatism at Fuka is not infiltration but diffusion.

According to the synthetic experiments by Hoscheck (1974), gehlenite is stable at temperatures above 700°C under CO_2-H_2O pressure. Under water pressure conditions, gehlenite is stable at temperatures above 630°C (Henmi *et al.*, 1973). According to the synthetic experiment by Zharikov and Shumulovich (1969), spurrite is stable at temperatures higher than 850°C at P_{CO_2} 100 kg/cm^2. At very low partial pressure of CO_2, spurrite is stable at temperatures higher than 450°C (Henmi and Henmi, 1978). At the progressive metamorphism of the skarn formation, the partial pressure of CO_2 seems to be not very low. Therefore, the occurrence of gehlenite and spurrite shows that the skarn was formed at temperatures above 800°C.

A large portion of gehlenite is decomposed to a mixture of the following hydrate minerals: bicchulite, vesuvianite and hydroglossular. The decomposition can be considered to be related to a retrogressive metamorphism subsequent to the progressive metamorphism. Synthetic experiments by Henmi (1976 and 1978) showed the decomposition products of gehlenites (gehlenite-akermanite solid

solutions) under water pressure conditions. Under 1 kb water pressure, gehlenite with the decomposition of $Ak_{20}Ge_{80}$ breaks down to the mixture of bicchulite, vesuvianite and xanthophyllite in a temperature interval between 600° and 400°C. At temperatures below 400°C bicchulite, vesuvianite and hydroglossular will form. The experimental results show conditions of the retrogressive metamorphism at Fuka.

Along one andesite dike, gehlenite and rankinite occur. This gehlenite can be considered to be formed by re-metamorphism of the andesite dike, and is thought to be a kind of annealing from the hydrated minerals. The synthetic study by Roy (1958) has shown that rankinite is stable at temperatures higher than 800°C under 1 kb water pressure. Therefore, this re-metamorphism is considered to have occurred at very high temperature. Along one of other andesite dikes, tilleyite is formed from spurrite. Tilleyite is stable at temperatures above 500°C under very low CO_2 partial pressure (Henmi and Henmi, 1978). This temperature of 500°C gives the lowest temperature of the re-metamorphism.

Most of the calcium silicate hydrates are alteration products of spurrite or are fissure-filling minerals in spurrite. For example, foshagite is the most common mineral in the alteration products of spurrite. According to Shoji (1974), foshagite is stable at temperatures between 280° and 500°C at 1 kb water pressure. The occurrence of foshagite indicated that the hydrothermal alteration of spurrite has reached a temperature between 300° and 500°C. Afwillite occurs as a fissure-filling mineral in spurrite. Afwillite is stable at temperatures below 300°C at 1 kb water pressure (Roy, 1958). Afwillite has been precipitated from the hydrothermal fluid at temperatures below 300°C.

Similar skarns are known at Kushiro, Hiroshima, Japan (K. Henmi *et al.*, 1971), at Crestmore, California, USA (Burnham, 1959), at Kilchoan, Ardnamurchan, Scotland (Agrell, 1965), at Cristmas Mountains, Texas, USA (Joesten, 1974), *etc.* At Kushiro and Crestmore, the skarns and the igneous rocks are very similar to those at Fuka but some magnesium-bearing minerals occur because the presence of limestone.

In conclusion, gehlenite and spurrite have been formed at progressive metasomatism by diffusion. During the retrogressive alteration, a large portion of gehlenite has been decomposed to hydrate minerals. Later, some parts of skarns have been re-metamorphosed by the intrusion of andesite dikes or by reactions with hydrothermal fluids of various temperatures.

References

Agrell, S. O. (1965), Polythermal metamorphism of limestone at Kilchoan, Ardnamurchan. *Mineral. Mag.*, 34, 1-15.

Burnham, C. W. (1959), Contact metamorphism of magnesian limestone at Crestmore, California. *Geol. Soc. Amer. Bull.*, 70, 879-920.

Henmi, C. (1976), Synthesis of bicchulite from gehlenite solid solutions. *Mineral. Jour.*, 8, 171-183.

Henmi, C. (1987), A hydrothermal experiment for retrograde change of gehlenite. *Mineral. Jour.*, 13, 347-367.

Henmi, C. and Henmi, K. (1978), Synthesis of spurrite and tilleyite at low CO_2 partial pressure. *Mineral. Jour.*, 9, 106-110.

Henmi, C., Kusachi, I., Kawahara, A. and Henmi, K. (1977), Fukalite, a new calcium carbonate silicate hydrate mineral. *Mineral. Jour.*, 8, 374-381.

Henmi, C., Kusachi, I., Henmi, K., Sabine, P. A. and Young, B. R. (1973), A new mineral bicchulite, the natural analogue of gehlenite hydrate from Fuka, Okayama, Japan and Carneal, County Antrim, Northern Ireland. *Mineral. Jour.*, 7, 243-251.

Henmi, K., Kusachi, I. and Numano, T. (1971), Contact minerals from Kushiro, Hiroshima Prefecture (1) gehlenite and hydroglossular. *Jour. Mineral. Soc. Japan*, 10, 160-169.

Hoschek, G. (1974), Gehlenite stability in the system CaO-Al_2O_3-SiO_2-H_2O-CO_2. *Contrib. Mineral. Petrol.*, 47, 245-254.

Joesten, R. (1974), Local equilibrium and metasomatic growth of zoned calc-silicate nodules from a contact aureole, Christmas Mountains, Big Ben Region, Texas. *Amer. Jour. Sci.*, 274, 876-901.

Kusachi, I. (1975), Occurrence of skarns at the Fuka Kita outcrop, Okayama Prefecture. Bull. *Sch. Educ. Okayama Univ.*, 43, 71-105 (in Japanese).

Kusachi, I., Henmi, C. and Henmi, K. (1984), An oyelite-bearing vein at Fuka, the Town of Bitchu, Okayama Prefecture. *Jour. Japan. Assoc. Min. Pet. Econ. Geol.* 79, 267-275.

Nakai, I., Okada, H., Masutomi, K., Koyama, E. and Nagashima, K. (1986), Henmilite, $Ca_2Cu(OH)_4\{B(OH)_4\}_2$, a new mineral from Fuka, Okayama Prefecture, Japan. *Amer. Mineral.*, 71, 1234-1239.

Roy, D. M. (1958), Studies in the system CaO-Al_2O_3-SiO_2-H_2O. IV: Phase equilibria in the high-lime portion of the system CaO-SiO_2-H_2O. *Amer. Mineral.*, 43, 1009-1028.

Shoji, T. (1974), Phase equilibria in the CaO-Al_2O_3-SiO_2-H_2O system. *Jour. Mineral. Soc. Japan*, 12, 1-15 (in Japanese).

Zharikov, V. A. and Shumolovich, K. I. (1969), High temperature mineral equilibria in the system CaO-SiO_2-CO_2. *Geochem. Intern.*, 6, 853-869.

Appendix 1. Examples of chemical composition of the skarn at Fuka

	Quartz monzonite	Contaminated rock	Gehlenite zone	Spurrite zone
SiO_2	64.26	55.55	25.31	24.73
TiO_2	0.38	0.95	1.18	0.32
Al_2O_3	14.64	15.43	22.19	1.21
Fe_2O_3	1.95	0.82	3.72	0.29
FeO	2.24	5.38	-	-
MnO	0.11	0.22	0.07	0.01
MgO	0.54	2.03	1.79	0.17
CaO	4.14	9.13	37.14	57.58
Na_2O	4.51	4.34	0.15	0.19
K_2O	4.28	3.38	0.14	0.01
$H_2O(+)$	1.85	1.78	5.99	0.86
$H_2O(-)$	0.66	0.49	0.42	0.41
P_2O_5	0.04	0.09	0.03	0.05
CO_2	-	-	1.45	13.82
Total	99.60	99.59	99.58	99.65
Q	13.96	-		
Or	25.26	19.95		
Ab	38.13	36.69		
An	7.06	12.63		
Wo	5.52	13.40		
En	1.34	2.48		
Fs	2.08	3.93		
Fo	-	1.79		
Fa	-	3.13		
Mt	2.83	1.19		
Il	0.72	1.88		
Ap	0.09	0.21		

Appendix 2. Chemical composition of representative minerals

	Gehlenite	Spurrite	Tilleyite
SiO_2	26.87	26.14	23.43
TiO_2	0.06	0.00	0.00
Al_2O_3	23.81	0.24	0.26
Fe_2O_3	2.62	0.17	0.07
FeO	0.20	-	-
MnO	0.03	0.00	0.00
MgO	3.63	0.08	0.04
CaO	39.47	61.84	56.57
Na_2O	0.18	0.12	0.08
K_2O	0.19	0.19	0.07
$H_2O(+)$	2.17	0.68	1.17
$H_2O(-)$	0.54	0.10	0.20
P_2O_5	0.01	0.01	0.00
CO_2	-	9.79	17.76
Total	99.78	99.36	99.65
	=7	=11	=13
Si	1.279	1.966	1.944
Al	1.336	0.021	0.026
Fe^{3+}	0.094	0.009	0.004
Ti	0.002	0.000	0.000
Mg	0.258	0.008	0.005
Fe^{2+}	0.008	-	-
Mn	0.001	0.000	0.000
Ca	2.013	4.984	5.029
Na	0.016	0.017	0.013
K	0.011	0.018	0.007
C	-	1.006	2.012

Apendix 3. Chemical compositions of new minerals from Fuka

	Bicchulite*	Fukalite**	Oyelite***	Henmilite****
SiO_2	28.51	29.09	35.3	-
TiO_2	0.09	0.00	0.0	-
B_2O_3	-	-	4.8	21.4
Al_2O_3	21.79	0.55	0.3	-
Fe_2O_3	2.66	0.10	0.0	-
FeO	0.25	-	-	-
MnO	0.03	0.00	0.0	-
MgO	2.72	0.14	0.0	-
CaO	35.26	54.40	41.2	31.7
CuO	-	-	-	23.7
Na_2O	0.25	0.17	0.1	-
K_2O	0.18	0.01	0.0	-
$H_2O(+)$	8.03	4.45	16.7	(23.2)
$H_2O(-)$	0.43	0.23	0.7	-
P_2O_5	0.02	0.01	0.0	-
F	-	0.32	-	-
CO_2	-	10.32	0.4	-
$-O=F_2$	-	-0.13	-	-
Total	100.22	99.66	99.5	(100.0)

* $Ca_2Al_2SiO_6(OH)_2$ C. Henmi *et al.* (1973)
** $Ca_4Si_2O_6(OH)_2CO_3$ C. Henmi *et al.* (1977)
*** $CaO\ 0.1B_2S_3\ 0.8SiO_2\ 1.25H_2O$ I. Kusachi *et al.* (1984)
**** $Ca_2Cu(OH)_4(.B(OH)_4)_2$ I. Nakai *et al.* (1986)

Appendix 4. Zirconium-containing minerals from Fuka

	Garnet	Zircon	Baddeleyite	Carzirtite
SiO_2	24.08	33.83	0.54	0.15
TiO_2	11.99	0.15	0.44	17.28
ZrO_2	7.34	63.21	94.88	67.68
HfO_2	0.16	1.22	2.16	1.00
Al_2O_3	4.32	0.03	0.07	0.16
Fe_2O_3	17.26	-	-	-
FeO	2.62	0.44	0.64	0.62
MnO	0.05	0.08	0.18	0.12
MgO	0.36	0.06	0.07	0.07
CaO	31.56	0.62	0.35	12.47
Total	99.74	99.64	99.33	99.55
	=12	=4	=2	=16
Si	2.107	1.030	0.011	0.023
Ti	0.789	0.003	0.007	1.939
Zr	0.313	0.938	0.956	4.923
Hf	0.004	0.011	0.013	0.043
Al	0.446	0.001	0.002	0.028
Fe^{3+}	1.137	-	-	-
Fe^{2+}	0.192	0.011	0.011	0.078
Mn	0.004	0.002	0.003	0.015
Mg	0.047	0.003	0.002	0.016
Ca	2.958	0.020	0.008	1.994

MINERALOGIA, ALTERACION HIDROTERMAL E INCLUSIONES FLUIDAS DEL YACIMIENTO AURIFERO DE MINAS DEL PRADO, REGION DEL BIO-BIO, SUR DE CHILE

Santiago Collao* y José Frutos**
*** Depto. Ciencias de la Tierra, Universidad de Concepción.**
**** Instituto GEA, Universidad de Concepción, Casilla 4107, Concepción 3, Chile**

Introducción

El yacimiento aurífero de Minas del Prado se caracteriza por varias vetas y cuerpos de brecha hidrotermal de baja ley de oro, emplazados en una serie de rocas volcánicas-piroclásticas del Terciario.

La alteración hidrotermal consiste en una fuerte solicificación de los cuerpos de brechas y sectores centrales de las vetas con alteración argílico-sericítica más marginal. De extensión más distal y con carácter distrital, domina una alteración propilítica compuesta por epidota, clorita, calcita y albita.

La mineralización metálica está caracterizada por una facies sulfurada en que predomina la pirita en relación a escasa y ocasional ocurrencia de arsenopirita, pirrotita, marcasita, calcopirita, tetraedrita, covelina y antimonia. La mineralización oxidada es pobre, destacándose limonita y rutilo en relación a magnetita y hematita. La mineralización de oro consiste en electrum, asociado a una segunda facies paragenética de pirita-cuarzo.

Inclusiones fluidas del tipo líquido-vapor presentes en cristales de cuarzo asociado a la mineralización de oro-pirita en las vetas, tienen un intervalo de temperatura de 182°-255°C y salinidad de 2,4-5,8% en peso de NaCl. Estos intervalos son levemente inferiores al detectado en cristales de cuarzo, como oro-pirita de un cuerpo de brecha cuyos valores de temperature oscilan entre 225-337°C y los de salinidad entre 3,0-8,5% en peso de NaCl.

En consideración de esta evidencia, el yacimiento de Minas del Prado puede considerarse como un clásici depósito epitermal de oro precipitado con minerales que reflejan una sulfidación alta en una facies silicatada, generados bajo condiciones de baja temperatura y salinidad.

El yacimiento de Minas del Prado, ubicado a 45 km al este de la ciudad de Chillán, en la Región del Biobío, ha side objeto de estudio de varios autores y compañías mineras (Ambrus y Araya1; Ambrus 2; B. R. G. M. 4; Bronkhorst 3; Ferraris *et al.*, 1987; CEDIMIN S. A., 1989, y otros), con la finalidad de evaluar fundamentalmente su potencial económico aurífero. Este potencial ha side estimado en unas 200.000 t de reservas con una ley de 2,3 g/t de Au1.

En esta investigación, el yacimiento ha sido estudiado desde el punto de vista científico-aplicado, para mejorar el conocimiento de la petrografía, minerales de alteración y metálicos y características microtermométricas que conduzcan a determinar algunas condiciones de formación del yacimiento.

El trabajo ha estado enmarcado en los Proyectos DI U. de C. No. 20.34.22 y Fondecyt No. 697/89. Este último pretende comparar las condiciones de formación de sistemas geotérmicos actuales (El Tatio, Puchultiza y Campanario), con yacimientos auríferos conocidos, dentro de los cuales figura el depósito de Minas del Prado

Metodología

El muestreo y levantamiento geológico del yacimiento se efectuó entre mayo y septiembre de 1989.

En la investigación de laboratorio se estudiaron numerosas secciones microscrópicas (35) para definir la petrografía y minerales de alteración, mineralización metálica y las características microtérmicas de las inclusiones fluidas. En la investigación fueron utilizados un microscopio Zeiss Universal (con Monocromator y microfotómetro para medidas de reflectividad), un microdurímetro Akashi, modelo D, un microscopio Nikon Optiphot-Pol y una platina calentadora-enfriadora Linkam TH-600.

Para definir algunos minerales problemas, que se presentan como pequeñas inclusiones de tamaños micrométricos (10-75m de diámetro) y conocer la composición cuantitativa del oro, se utilizó una microsonda electrónica JEOL Super Probe JXA-8600.

Las condiciones de operación de la microsonda electrónica fueron 20 kv de aceleración de voltaje y corriente de $5{,}6 \times 10^{-8}$A. Los estándares utilizados fueron oro, plata, aluminio y marcasita sintética.

Marco geológico

El yacimiento de oro de Minas del Prado está emplazado en una serie de rocas volcónico-piroclásticas (Fig. 1), constituidas principalmente por tobas de composición dacítico-andesíticas, tobas de lapilli, intercalaciones menores de flujos de andesitas y aglomerados y brechas volcánicas. Este conjunto litológico corresponde a las denominadas series Piernas Blancas (Superior e Inferior), asignadas al

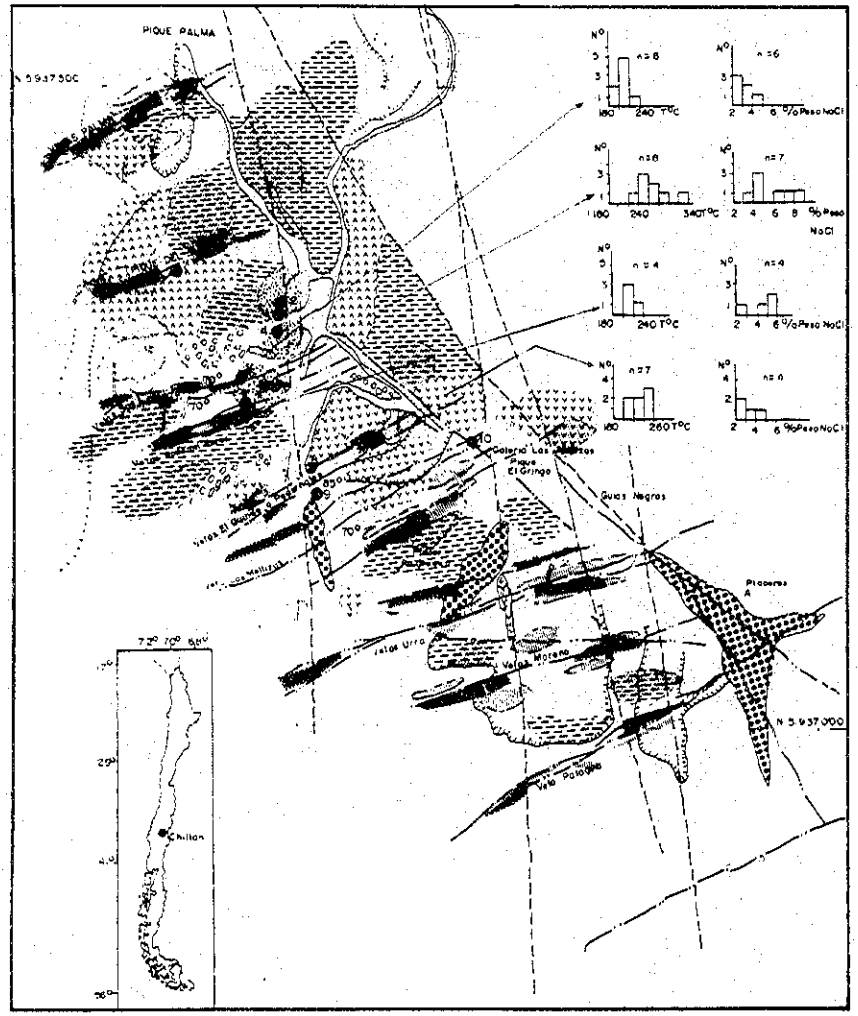

MAPA GEOLOGICO Y ESTRUCTURAL

Por Santiago Collao

0 50 100 200m

LEYENDA

- Cobertura de suelo (Cuaternario)
- Conglomerados auríferos (Au grueso y fino)
- Pórfido Andesítico
- Brechas hidrotermales
- Andesita
- Toba
- Aglomerado
- Brecha volcánicas

Serie Piedras Blancas (Terciario)

Histogramas de frecuencia (N° de inclusiones) versus Temperatura de homogeniza. (°C) o salinidad (% Peso NaCl)

- Galerías y socabones
- Canteras y trabajos a rajo abierto
- Fracturas y diaclasas
- Fallas regionales
- Vetas Au ley >5 gr/ton (espesor 75cm generalmente encajadas junto a cuerpos de brechas hidrotermales vetiformes) acompañadas de silicificación y piritización
- Vetas Au ley >5gr/ton (generalmente pequeño espesor <50cm)
- 2 Muestra

ALTERACION HIDROTERMAL

- Silicificación y Piritización. Agregados de cuarzo, calcedonia en vetas y ocasionalmente amatista en cuerpos de brecha hidrotermal. Argilización Principalmente caolín y sericita
- Propilitización Epidota, clorita, calcita, albita y ocasionalmente pirita

REFERENCIAS

Ambrus, J. y Araya, M, 1981

Brandhorst, O. 1984

Frutos, 1988

Terciario inferior a medio[1]. Cuerpos de brecha hidrotermal subvolcánica de formas irregulares (Fig. 1) y diques andesíticos se disponen discordantemente a la serie volcánico-piroclástica.

Sobreyaciendo a los conjuntos litológicos ya descritos se disponen conglomerados semiconsolidados con escaso oro de tipo placer y flujos volcánicos andesíticos y piroclásticos, correlacionables con la Formación Cola de Zorro. A esta secuencia se le ha asignado una edad cuaternaria (0,5-1,5 Ma), según datación de estudio convenido por M. M. A. J. JICA/Instituto de Investigaciónes Geológicas[6].

Control estructural y cuerpos mineralizados

La mineralización en vetas (San Lorenzo, Rudemil Pérez, Pedernales y otros (Fig. 1)) se orienta según un sistema preferente de rumbo N65°E con manto subvertical de 70°E al sureste, en tanto que algunos cuerpos de brecha mineralizados tienden a orientarse según ejes NNW. Este patrón estructural ya apreciado en estudios anteriores[3, 5], habría controlado la circulación de los fluidos responsables de la alteración hidrotermal y de la mineralización metálica. Los cuerpos de brecha en el sistema, corresponderían a una fase más temprana que la generación de las vetas, lo cual es corroborado por los resultados del estudio de inclusiones fluidas que se detalla más adelante.

Alteración hidrotermal y mineralización metálica

La alteración y mineralización metálica en el Yacimiento de Minas del Prado está relacionada con tres eventos o pulsaciones paragenéticas que se han evidenciado principalmente mediante la ocurrencia asociada de pirita-silice.

El primer evento paragenético consiste en pirita, finamente diseminada en la matriz de algunas rocas volcánicas. A este evento suele asociarse calcopirita, arsenopirita, magnetita y rutilo, los cuales están ocasionalmente diseminados o a nivel de trazas principalmente en la matriz de rocas volcánicas, del entorno de los cuerpos mineralizados.

Un segundo evento paragenético comprende venillas de agregado de cuarzo, ocasionalmente amatista (sólo en brechas hidrotermales) y cristales idiomórficos cúbicos de pirita (cristales gruesos de hasta 200 micrones de diámetro), los cuales cortan al primer evento paragenético. Esta asocianción predomina en las vetas y en los cuerpos de la brecha, y a ella pueden acoplarse arcillas (principalmente caolín) y limonita (jarosita y goetita), los cuales son más dominantes hacia las cajas de las vetas.

A este evento paragenético se asocia la mineralización de oro, la que ocurre en partículas laminares menores de 25 micrones de largo de sección, incluido en

cuarzo, ocasionalmente acompañado de tetraedrita, hematita y antimonita. El oro analizado corresponde a la variedad de "electrum" según se desprende del estudio con la microsonda electrónica, en la que se determinó una composición cuantitativa promedio de 78,5%, 18,5% y 0,15% en peso de Au, Ag y Al, respectivamente (Tabla 1).

Tabla 1. Composición cuantitativa de minerales en muestras de Minas del Prado

Electrum			
Muestras El. % peso	**SL.1**	**Br.1**	**R.P.1**
Au	78,009	78,181	79,211
Ag	18,576	18,564	18,880
Al	0,059	0,047	0,850
Total	96,645	96,792	97,850

	Pirrotita	**Marcasita**
Fe	59,825	46,094
S	89,112	58,658
Total	98,937	99,752

Inclusiones fluidas

Las inclusiones fluidas investigadas son de pequeño tamaño (5-36 micrones) y se presentan exclusivamente en cuarzo, en abundancias que no sobrepasan los 150 individuos.

La selección de inclusiones fluidas para representatividad de los resultados se restringió esencialmente a aquellas paragenéticamente ligadas a venas de cuarzo asociado a pirita con oro dentro de la vetilla y de características primarias y seudosecundarias en el cuarzo que las hospeda. Las inclusiones fluidas son bifásicas del tipo líquido-vapor, ricas en la fase líquida (80-95% en volumen), en relación a la fase vapor. Sólo excepcionalmente la relación de proporción de fase se observó invertida.

Resultados microtermales y consideraciones de la formación del yacimiento

La temperatura de homogenización de las inclusiones fluidas en cristales de cuarzo de los cuerpos mineralizados de Minas del Prado varía entre 182° y 337°C. La salinidad -calculada sobre la base de la depresión del punto de congelamiento utilizando las ecuaciones de Potter *et al.*[7]- fluctuó entre un intervalo 2,4-8,5% en peso de NaCl equivalente. De estos intervalos pueden diferenciarse subintervalos más bajos para las vetas y más altos para el cuerpo de brecha. Para el conjunto de muestras provenientes de las vetas el intervalo de temperatura de homogeneización oscila entre 182° y 255°C con variación de la salinidad entre 2,3% y 5,8% en peso de NaCl equivalente. En el cuerpo de brecha el intervalo de temperatura varía entre 225-337°C y la salinidad entre 4,2% y 8,5% en peso de NaCl equivalente. Los valores, graficados en histogramas de frecuencia (Fig. 1), expresan para las vetas, una moda entre los 200° y 220°C, en tanto que en el cuerpo de brecha la moda tiende a ubicarse entre los 240° y 280°C.

Los valores de temperatura como de salinidad aquí obtenidos, indican que el yacimiento de Minas del Prado corresponde a un típico depósito epitermal de oro, precipitado a bajas temperaturas y salinidad. Un evento térmico y de salinidad de los fluidos más alto en el cuerpo de brecha que en las vetas, estaría corroborando la idea que el emplazamiento de las soluciones en los cuerpos de brecha estaría relacionado a condiciones más tempranas y subvolcánicas que las que habrían dado lugar a las vetas.

Referencias

1. Ambrus, J.; Araya, M. 1981. Notes on the geology of Minas del Prado, Chile (Informe inédito).
2. Ambrus, J. 1981. Geoquímica de drenajes Minas del Prado. (Informe inédito).
3. Bronkhorst, D. 1981. Evaluación Geológico-Minera de Minas del Prado. Minera Phelps-Dodge. (Informe inédito).
4. B. R. G. M. 1981. La Mine de Minas del Prado. Programa de Desarrollo de Minas del Prado. (Informe inédito).
5. Frutos, J. 1989. Informe geológico-económico preliminar de Minas del Prado. (Informe inédito).
6. I. I. G. -M. M. A. J. 1981. Informe del reconocimiento geológico de la región andina situada al este de la ciudad de Concepción. (Informe inédito).
7. Potter, R. W. II; Clynne, M. A.; Brown, D. L. 1978. Freezing point depression of aqueous sodium chloride solutions. *Economic Geology*, Vol. 73, p. 284-285.

ESTUDIOS MINERALOGICOS Y MICROTERMOMETRICOS EN VETILLAS DE CUARZO, MINA MARTE

Eduardo Campos S.
Depto. Ciencias de la Tierra,
Universidad de Concepción, Concepción 3, Chile.

Introducción

El yacimiento aurífero Mina Marte, perteneciente a la Compañía Minera Anglo-American se encuentra ubicado a unos 150 km al este de la ciudad de Copiapó, más específicamente al NEE del cerro del Azufre o Copiapó, a los pies del cerro Villalobos, entre las coordenadas 27°13'50" lat. sur y 69°02' long. oeste (ver Fig. 1).

La inquietud por desarrollar la presente investigación, surgió durante la etapa de evaluación final del entonces proyecto Marte, en aquella oportunidad, mientras se realizaba una campaña de sondajes y el análisis de la información obtenida de los mismos, se observó una estrecha relación entre leyes altas de oro y presencia de vetillas de cuarzo del tipo cuarzo negro. Esta relación generó la inquietud de poder establecer diferencias a nivel de la mineralización metálica y no metálica asociada a estas vetillas por medio del estudio de cortes pulido- transparentes, y/ o a nivel de salinidades y microtemperaturas mediante el análisis de inclusiones fluidas, y poder así caracterizar los distintos tipos de vetillas, tanto como, definir algún patrón que permitiera diferenciar las distintas generaciones de vetillas presentes en Mina Marte.

Metodología

Con el propósito de definir la mineralización metálica y no metálica existente en cada una de las distintas generaciones de vetillas, se confeccionaron cortes pulidos-transparentes de modo que fuera posible el análisis de la muestra tanto a luz reflejada como a luz transmitida. El estudio de estas preparaciones se llevó a

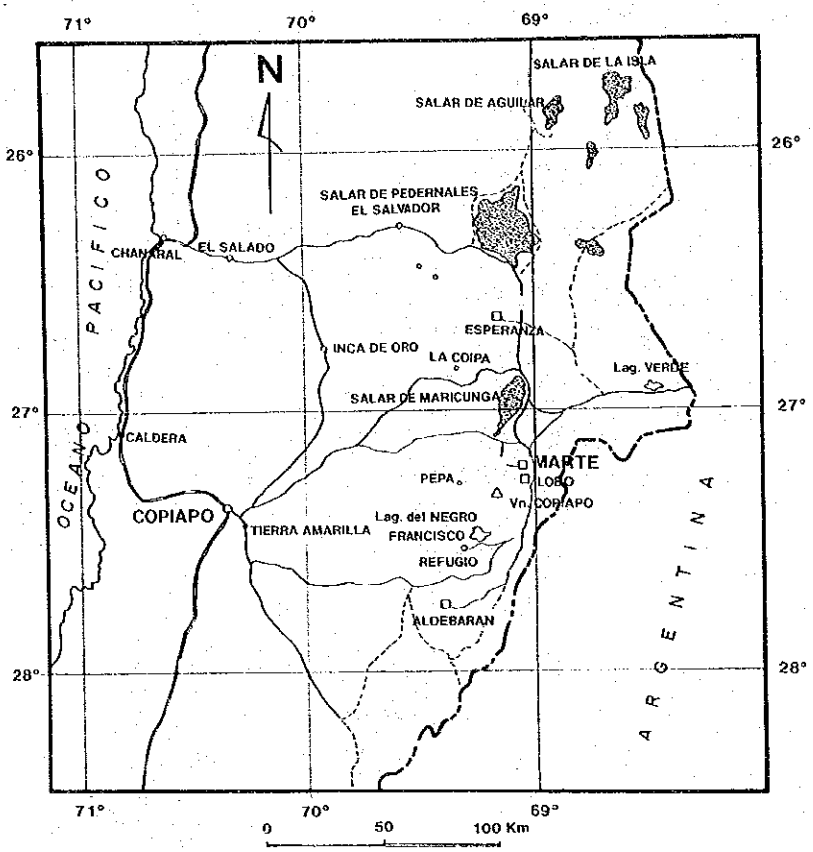

Fig. 1. Mapa de ubicación

cabo en un microscopio Nikon Optiphoto-Pol de doble óptica, con el cual fue posible lograr magnificaciones de hasta 320x. Para el estudio de inclusiones fluidas se confeccionaron secciones especulares de las preparaciones destinadas al estudio de minerales metálicos y no metálicos. En su análisis se utilizó un microscopio similar al mencionado anteriormente, acondicionado con objetivos de larga distancia de trabajo marca Zeiss (10x, 20x y 40x), con los cuales se lograron magnificaciones de hasta 400x. Para las mediciones microtermométricas se utilizó una platina calentadora-enfriadora marca Linkam Th-600 con límite superior de calentamiento de 600°C (descripción en Shepherd, 1985).

Marco geológico regional

Según ARRIETA et al., 1988, la secuencia de rocas presentes en el área estudiada es el producto de la actividad de varios centros volcánicos, probablemente sincrónicos, ubicados en ell (Volcanes Copiapó, Pastillitos y Villalobos).

Los autores mencionados, definen una sección estratiforme tipo para toda la franja, la cual consta de tres unidades discordantes entre sí.

La Unidad Basal, que aflora en el sector centro oriental del área, principalmente en las partes más profundas de las quebradas mayores, constituida por lavas porfídicas dacítico-andesíticas grises a verde oscuras, de grano fino a medio muy compactas. Esta unidad se encuentra afectada por silicificación débil a moderada de tipo pervasiva y/o vetillas de tipo stockwork. En forma subordinada en estos niveles basales se reconoce alteración propilítica débil, caracterizada por el desarrollo de clorita.

En discordancia angular y de erosión, sobreyaciendo a la Unidad Basal y ocupando probablemente una paleogeografía irregular, lo que determina espesores variables en su exposición, se presenta la Unidad Intermedia, la cual está constituida principalmente por tobas líticas y en menor grado, tobas de cristales, brechas tobáceas y areniscas tobáceas. La parte superior de la unidad es clástica y brechosa, con manifestaciones aisladas de azufre nativo. Caracterizan esta unidad, intensas coloraciones pardo-amarillentas generadas por alteración hidrotermal sílico-argílica, caracterizada por la presencia generalizada de caolín, junto al desarrollo local de limonita, jarosita, alunita y yeso.

En discordancia de erosión, sobre la unidad intermedia se dispone la Unidad Superior, la cual corresponde a dacitas y andesitas de hornblenda verdes oscuras a negras, sin rastros de alteración, a excepción de una cloritización incipiente de carácter regional.

Localmente aflora una secuencia de tobas e ignimbritas riodacíticas rosadas a blancas, sin relación de contacto directo con las unidades antes descritas. Probablemente representa el episodio volcánico más joven del área.

Además de las unidades estratificadas mencionadas, al sur del área afloran pequeños stocks subvolcánicos mostrando un probable control estructural NW-NNE en su emplazamiento. La composición varía de dioritas a dioritas cuarcíferas y presentan textura porfídicas a micorporfídicas, con matriz de grano fino, verde oscuras a grises, siendo común la presencia de magnetita diseminada y/o en vetillas hidrotermales. Localmente se desarrolla un débil vetilleo polidimensional tipo stockwork de sílice bandeada y transparente.

En relación a las estructuras presentes en el área de estudio, se observa un fallamiento inverso de gran ángulo y de rumbo general N-S, el cual aparentemente sería anterior a los complejos volcánicos estratiformes miocénicos del sector. Este fallamiento inverso originó un sistema subparalelo de horst y grabens.

Otros rasgos estructurales importantes en el área estudiada, corresponden a un fallamiento normal de rumbo variable entre N65W y N35W, el cual se evidencia en el rumbo de las quebradas, alineaciones de portezuelos, elongaciones de conjuntos de vetas y vetillas. Una tendencia subordinada se manifiesta como fallas normales menores de rumbo N-S a N40W. El fallamiento normal sería posterior al inverso.

Estudio de las vetillas de mina Marte

Consideraciones generales

La primera tarea que se llevó a cabo consistió en la definición de los distintos tipos de vetillas de cuarzo presentes en el yacimiento en cuestión, así como de su cronología relativa. Con este propósito se intentó inicialmente una clasificación paragenética basada principalmente en las observaciones macroscópicas de las muestras de testigos. Se logró distinguir claramente cinco generaciones, usando como criterio de diferenciación el color, es decir si estas eran de cuarzo gris o translúcido, y en segundo término las relaciones espaciales entre sí.

Estudio mineralógico y de alteración

Mediante el análisis macroscópico de las vetillas, no fue posible establecer diferencias composicionales entre las distintas generaciones, ya que todas ellas presentaban como constituyente no metálico principal, cristales de cuarzo anhedrales no mayores a 500 micrones. Además, resultaron ser comunes las oquedades y microfracturas, las que se presentaban total o parcialmente rellenas con minerales de alteración u opacos. Con respecto a los estudios de minerales de alteración asociados, se pudo establecer que en todas las muestras analizadad predomina la alteración de tipo argílica y en menor grado silicificación.

El estudio de la mineralización metálica presente en estas vetillas, permitió definir claramente dos formas de ocurrencia. En la primera de estas, los opacos se encuentran como inclusiones de tamaño micrométrico en los cristales de cuarzo y se ha denominado primera asociación. Para este tipo de vetillas, la mineralización está caracterizada por la presencia de abundante magnetita y calcopirita, esta última subordinada respecto a la primera, escasa pirita y trazas de hematita. Se observó además, bornita como producto de exolución de calcopirita y covelina en vetillas de generación III por reemplazo de calcopirita (ver table 1).

Tabla 1. Primera Asociación Metálica

Generación	Cpy	Py	Mg	Hm	Bn	Cv
I	++	+	+++	•	•	
II	++	+	+++	•		
III	++	+	+++		•	•
IV	+++	++	++	•	•	
V	++		++++	•		

++++ Mineral mas abundante
+++ Distintos grados de abundancia
++ Metálica con respecto al mineral
+ Mas abundante
• Trazas

El tipo de mineralización mencionado sería el responsable de la coloración característica de las vetillas de cuarzo negro. Así la aparición de dicha coloración estaría estrechamente asociada a una mayor abundancia de inclusiones metálicas en estas vetillas.

En el segundo tipo, la mineralización metálica aparece rellenando cavidades o microfracturas. En general, los minerales de esta asociación son de mayor tamaño en comparación a los de la primera, existiendo además ligeras variaciones en su abundancia relativa. Este tipo de asociación se caracteriza por presentar calcopirita como mineral principal, asociado a ella se encuentra pirita la cual, como se observó en las generaciones I y III, puede llegar a ser más abundante; en forma subordinada se detectó la presencia de magnetita y hematita, mientras que a nivel de trazas como producto de exolución de calcopirita se definió la existencia de bornita y por último, covelina producto de reemplazo de la misma (ver tabla 2).

Tabla 2. Primera Asociación Metálica

Generación	Cpy	Py	Mg	Hm	Bn	Cv
I	++	+++	+	+	•	•
II	+++	++	+	++	•	•
III	++	+++	+	•	•	•
IV	+++	++		•	•	•
V	++					

++++ Mineral mas abundante
+++ Distintos grados de abundancia
++ Metálica con respecto al mineral
+ Mas abundante
• Trazas

Análisis de inclusiones fluidas

Durante el análisis preliminar de inclusiones fluidas en las muestras de mina Marte, se pudo establecer que todas las vetillas presentaban abundantes inclusiones, sin embargo una gran cantidad de ellas resultaron ser o muy pequeñas (menores a 2,5μ), o bien del tipo monofásicas líquido o gas, a esto se sumó además la poca nitidez de la mayor parte de las inclusiones. Estas limitantes provocaron que el proceso de búsqueda de inclusiones resultara lento y engorroso, y que en un gran número de inclusiones sólo fuera posible determinar temperaturas de homogenización, no así obtener valores de salinidad. A esto obedece el hecho de que la cantidad de valores de salinidad sean considerablemente más escasos que los de homogenización.

A pesar de las limitantes mencionadas se analizó un total de 235 inclusiones del tipo primarias, todas encapsuladas en cristales de cuarzo. Las mediciones microtermométricas determinadas en estas inclusiones corresponden principalmente a la temperatura de homogenización (Th) y una cantidad menor a temperaturas de disolución de halita. Por último se determinaron temperaturas de depresión final del punto de congelamiento, siendo estos valores los más escasos.

Las características generales de las inclusiones fluidas analizadas son relativamente similares en las distintas ocurrencias paragenéticas. Desde el punto de vista morfológico, presentan principalmente formas subredondeadas y elipsoidales, estas últimas pueden ser hasta seudohexagonales, representando incluso un cristal negativo de cuarzo hexagonal. Esto último representa una forma de alto equilibrio.

La clasificación utilizada para las inclusiones corresponde a la definida por NASH (1976), la cual considera la topológica de las mismas teniendo en consideración el número de fases presentes.

Microtermometría

Los resultados microtermométricos de inclusiones primarias, obtenidos para este estudio se entregarán en forma separada para cada una de las distintas generaciones de vetillas.

Vetillas de generación I

En las vetillas de esta generación se logró analizar un total de 76 inclusiones primarias, de estas un 30.26% resultaron ser polifásicas (L+V+S), mientras que el otro 69.74% lo constituian inclusiones bifásicas (L+V). Al considerar estas inclusiones en conjunto, fue posible determinar que ellas presentaban grados de llenado variables entre 0.50 y 0.90, En relación al tamaño, la dimensión máxima observada en estas inclusiones no supera los 37.50 micrones.

Los 17 valores de salinidad obtenidos fueron determinados en inclusiones trifásicas utilizando el punto de fusión de la halita (SOURIRAJAN y KENNEDY, 1962), mediante este método se logró definir un rango entre los 25.0 y 42.0% en peso de NaCl equivalente (ver Fig. 3), con temperaturas de homogenización asociadas entre 210.0 y 350.0°C, además se obtuvieron otras 69 temperaturas de homogenización las cuales junto a las ya mencionadas definieron un rango 210.3 >350.0°C para esta generación de vetillas, en donde el 67.11% de los valores correspondieron a >350.0°C (ver Fig. 2).

TEMPERATURA DE HOMOGENIZACION EN DISTINTAS GENERACIONES DE VETILLAS EN MINA MARTE

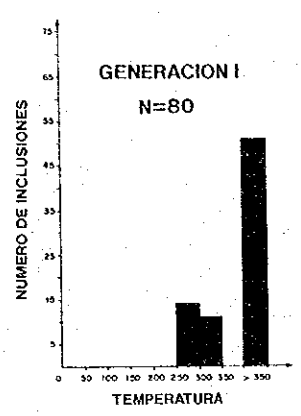

Fig.2

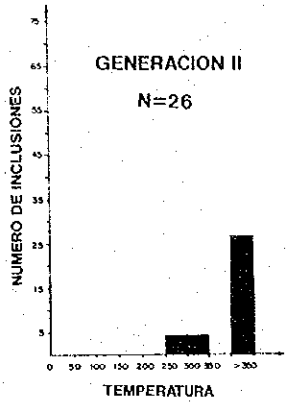

Fig.4

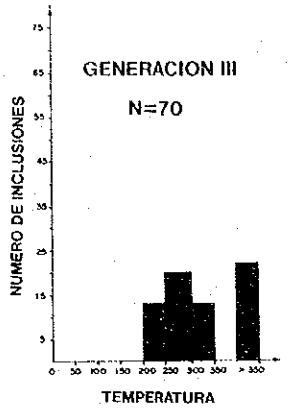

Fig.6

VALORES DE SALINIDAD EN DISTINTAS GENERACIONES DE VETILLAS DE MINA MARTE

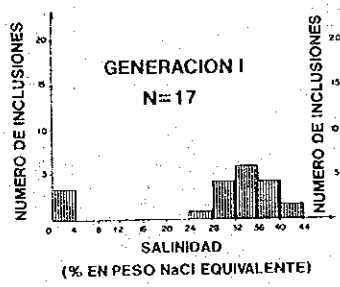

Fig.3

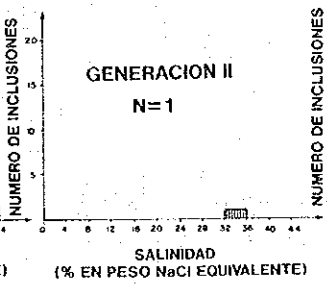

Fig.5

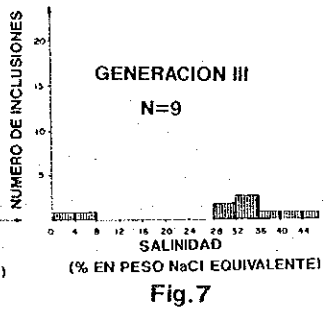

Fig.7

Vetillas de generación II

De un total de 32 inclusiones fluidas analizadas en vetillas de esta generación, 26 son primarias y de estas, 25 corresponden al tipo bifásicas y solamente una trifásica. El conjunto de las inclusiones primarias recién mencionadas presenta grados de llenado variables entre 0.50 y 0.95, pero el 42.31% de ellas mostraban valores de 0.70. El tamaño máximo observado en estas inclusiones no supera los 25.0 micrones.

Con respecto a la salinidad de las inclusiones, sólo fue posible obtener un único valor medido en la del tipo trifásica mediante el método de fusión de halida (op. cit.), el cual correspondió a 32.0% en peso de NaCl equivalente, con una Th de 296.7°C (ver Fig. 5).

De las temperaturas de homogenización obtenidas en inclusiones primarias fue posible definir un rango general de 262,7 > 350.0°C (ver Fig. 4).

Vetillas de generación III

En las vetillas de la generación III se analizaron 70 inclusiones del tipo primarias, de estas se determinó que un 20% correspondían al tipo trifásicas mientras que el 80% restante resultaron ser bifásicas. Estas inclusiones se caracterizan por presentar grados de llenados variables entre 0.50 y 0.90 además, el 54.29% de ellas mostraban valores de 0.90 y un tamaño no superior al 30.0 micrones.

Con respecto a la salinidad, se determinaron 10 valores en inclusiones trifásicas mediante el método de fusión de halita (op. cit.), estos presentan valores extremos de 31.0 y 44.0% en peso de NaCl equivalente (ver Fig. 7), con temperaturas de homogenización asociadas entre los 210.3 y > 350.0°C. Además de las inclusiones recién mencionadas, fue posible analizar otras 60 midiéndose en ellas únicamente temperaturas de homogenización. El rango general de temperatura, incluyendo las primeras mencionadas, indican valores extremos de 210.3 y > 350.0°C para esta generación de vetillas (ver Fig. 6).

Vetillas de generación IV

En estas vetillas se analizaron 14 inclusiones, todas del tipo bifásico, las cuales presentan grados de llenado variables entre 0.50 y 0.90, sin embargo, los valores predominantes resultaron ser 0.70 y 0.90 con una representatividad del 42.86% cada uno. Con respecto a la dimensión de las inclusiones, estas no superaban los 15.0 micrones.

Del total de inclusiones analizadas, sólo fue posible obtener trs valores de salinidad de 2.7, 4.65 y 1.95% en peso de NaCl equivalentes las cuales presentaban temperaturas de homogenización de 284.3 > 350,0 y 235.3°C respectivamente (ver Fig. 9). En las restantes 11 inclusiones primarias estudiadas sólo se pudeo determinar las temperaturas de homogenización para estas vetillas entre 235.4 y > 350.0°C (ver Fig. 8).

Vetillas de generación V

En vetillas de generación V se analizaron 49 inclusiones primarias, dos resultaron ser del tipo trifásicas y las restantes bifásicas. Teniendo en considera-

TEMPERATURA DE HOMOGENIZACION EN DISTINTAS GENERACIONES DE VETILLAS EN MINA MARTE

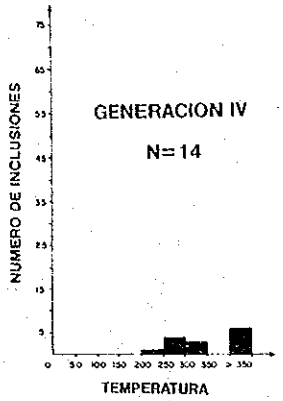

Fig.8

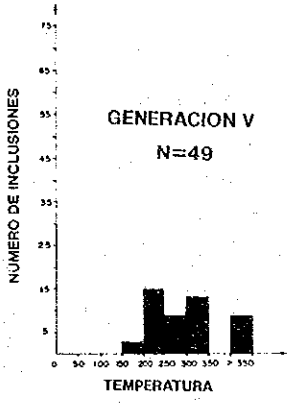

Fig.10

VALORES DE SALINIDAD EN DISTINTAS GENERACIONES DE VETILLAS DE MINA MARTE

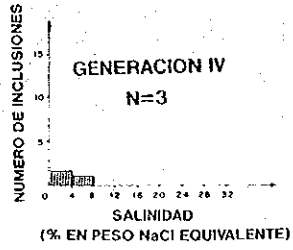

Fig.9

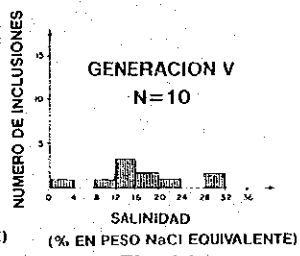

Fig.11

ción la totalidad de las inclusiones estudiadas se determinó que estas presentaban grados de llenado variables entre 0.50 y 0.95 en que un 40.10% de ellas correspondían a 0,90. El tamaño máximo observado en estas inclusiones es de 55,0 micrones.

Del total de inclusiones fluidas primarias analizadas, sólo fue posible determinar 10 valores de salinidad, los que fluctuan entre los 9.3 y 30.0% en peso de NaCl equivalentes, observándose sólo un valor de 1.96 el cual puede considerarse errático (ver Fig. 11). El rango de temperaturas de homogenización para el total de inclusiones en vetillas de la generación V fluctua entre los 177.4 y > 350°C (ver Fig. 10).

Conclusiones

En las muestras de mina Marte analizadas, fue posible diferenciar cinco generaciones de vetillas, dos del tipo cuarzo negro (II y III) y tres de cuarzo translúcido (I, IV y V). En éstas se observaron dos formas de presentación de la mineralización metálica, como finas inclusiones en cristales de cuarzo, o como relleno de microfracturas o cavidades. En ambas formas las especies mineralógicas resultaron ser similares y las diferencias se encontraron fundamentalmente en el hecho de que una de ellas resultaba más abundante en un tipo de asociación mientras que en la otra se encontraba subordinada.

La mineralización metálica contenida como inclusiones en cristales de cuarzo, es la responsable de la coloración gris en las vetillas de cuarzo negro y, aún cuando está presente en las de cuarzo translúcido, en éstas es más escasa.

En relación a algunos aspectos comunes para la totalidad de las inclusiones analizadas, se determinó que en las generaciones I, IV y V más del 90% de las inclusiones son menores a 15.0 micrones, mientras que en las generaciones II y III el 90% resultó ser mayor a 25.0. y 17.5 micrones respectivamente.

Con respecto a los grados de llenado, estos no muestran una clara diferenciación para los distintos tipos de vetillas. En general, en las generaciones I, II y III el 70% de estos variaban entre los 0.70 y 0.90, mientras que en las generaciones IV y V, el valor 0.50 es más frecuente en comparación con las antes mencionadas.

Las diferencias más claras entre las distintas generaciones de vetillas definidas en este trabajo, se observan a nivel de temperaturas de homogenización, las cuales muestran un decrecimiento desde las generaciones más tempranas hacia las más tardías. En la generación I el 80% de las temperaturas de homogenización se encuentran entre los 300.0 y > 350.0°C, mientras que en la V sólo un 34.91%. Además, la temperatura mínima medida en la generación I resultó ser 210.3°C, mientras que en la generación V alcanca los 177.4°C.

Con respecto a las salinidades obtenidas en las distintas generaciones de vetillas, estas resultaron ser muy similares en las generaciones I, II y III en donde los valores se enmarcan en el rango 25 y 44% en peso de NaCl equivalente. En la generación IV el rango definido resultó ser de 1.95-4.65 y 1.96-30% en peso de NaCl equivalentes para la generación V.

Referencias

Arrieta, M; Rodríguez, J; Vila, T. 1988. Informe de temporada *Proyecto Margeo.* Compañía Minera Anglo-American Chile Limitada. Informe Inédito.

Nash, J. T. (1976). Fluid-inclusions petrology-data from porphyry copper deposits and application to exploration. *Geol. Survey Prof. Paper*, 907 D, 16.

Shepherd, T.; Rankin, A. H.; Alderton, D. H. M.; 1985. *A Practical Guide to Fluid Inclusions Studies.* Blackie and Sons. Bishopbriggs, Glascow. Great Britain.

Sourirajan, S.; Kennedy, G. C. (1962). The system H_2O-NaCl at elevated temperatures and pressures. *Am. J. Sci.*, 260, 115-141.

THE MINERALIZATION STAGES OF TIN-BEARING MINERALS FROM BOLIVIAN POLYMETALLIC ORE DEPOSITS.

Asahiko Sugaki* and Arashi Kitakaze**
*** Kadan 4-30-503, Aoba, Sendai 980, Japan. ** Faculty of Science, Tohoku University, Aramaki-Aoba, Sendai 980, Japan.**

Introduction

The Bolivian tin belt extends from the northeast side of Lake Titicaca to the Argentinean border along the Eastern Cordillera of the Andean range. Two distinct types of tin deposits are found in the belt[8, 12, 15, 17](Clark and Farrar, 1973). The first one is deep-seated hydrothermal (mesothermal and/or hypothermal) veins which were formed by mineralization closely related to the emplacement of Mesozoic granitic magma[2, 9, 10, 15]. The other is polymetallic ore deposits which contain Sn, W, Ag, Pb and Bi[1, 2, 4, 5, 7, 12, 13, 14, 16, 17]occur and were produced by mineralization related to volcano-plutonic igneous activities in the Miocene age, such as granite, quartz porphyry and dacite[3, 6]. The latter is called as Bolivian type polymetallic ore deposits of a typical xenothermal type. Such polymetallic ore deposits occurring extensively in the Eastern cordillera are mostly vein type which fills fissures developed in quartzite, sandstone and slate of the Silurian or Ordovician formation, and dacitic tuff, tuff breccia and pyroclastics of the Miocene formation. They sometimes occur in Miocene granitic rocks, and also fill up fractures in or around stocks of Miocene quartz porphyry and dacite intensely altered hydrothermally. Tin deposits which develop as stockwork and impregnation in altered porphyry and dacite stocks are called 'porphyry tin' by Sillitoe *et al.* (1975) and Grant *et al.*[6].

Tin-bearing minerals and their mineralization

A large number of tin-bearing minerals have been reported from the Bolivian type tin deposits, and are listed in Table 1. In general, cassiterite, stannite (and kesterite) are the common constituents in tin ores and others are accessory or rare.

Table 1. Tin-bearing minerals from Bolivian type polymetallic deposits

Minerals	Chemical formula	Crystal sistem	Cell parameters a (α	b β	c γ)
Cassiterite	SnO_2	Tet	4.73	–	3.18
Herzenbergite	SnS	Orth	4.33	11.19	3.98
Ottemannite	Sn_2S_3	Orth	8.82	14.04	3.75
Berndtite	SnS_2	Hex	3.65	-	5.90
Stannite	Cu_2FeSnS_4	Tet	5.45	-	10.75
Kesterite	Cu_2ZnSnS_4	Tet	5.43	-	10.87
Rhodostannite	$Cu_2FeSn_3S_8$	Tet	7.29	-	10.31
Hocartite	Ag_2FeSnS_4	Tet	5.74	-	10.96
Canfieldite	Ag_8SnS_6	Orth	15.31	7.55	10.70
Teallite	$PbSnS_2$	Orth	4.29	11.35	4.05
Franckeite	$FePb_6Sb_2Sn_3S_{14}$	Tri	46.9	5.82	17.30
			(90.0°	94.6°	90.0°)
		Tri	11.73	5.79	5.81
Cylindrite	$FePb_3Sb_2Sn_4S_{15}$		(90.0°	92.4°	93.9°)
		Tri	11.71	3.67	6.32
			(90.0°	92.6°	90.8°)
Incaite	$FePb_4Sb_2Sn_4S_{14}$	Tri	17.29	5.79	5.83
			(90.0°	94.1°	90.0°)
Potosiite	$Fe_7Pb_8Sb_{16}Sn_{18}S_{115}$	Tri	188.06	70.10	17.28
			(90.0°	92.2°	90.0°)

Based on the data obtained by our investigation on thirty-five Bolivian polymetallic deposits in entire tin belt, the mineralization that formed the Bolivian type tin deposits can be divided into following six stages: (I) quartz-tourmaline, (II) quartz, (III) quartz-pyrite, (IV) sulfide, (V) sulfo-salt and (VI) sulfate-phosphate.

Cassiterite: Cassiterite occurs in the (I), (II), (III), (IV) and (V) stages. Among the cassiterite bearing ores, those of (I), (II) and (III) stages are principal, and of (IV) and (V) are subordinate. Its deposition extends over a long range of mineralization from stage I to stage V.

Stannite (and kesterite): Stannite occurs in the (III), (IV) and (V) stage veins. Among these veins, the sulfide (IV) vein of pyrite and/or sphalerite, is important. The zinc content in mole % Cu_2ZnSnS_4 of stannite from the (III) vein has 0.5 to 19.5 mole % Cu_2ZnSnS_4. However, stannite from (IV) stage veins contains more zinc than that from the (III) stage veins.

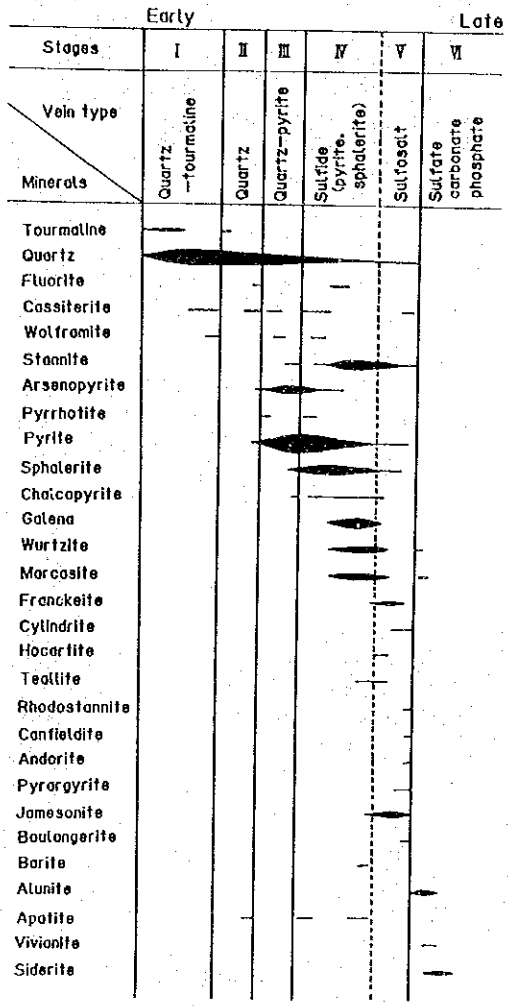

Fig. 1. Stages of mineralization on principal minerals from the Bolivian type tin deposits.

Tin-bearing sulfosalt minerals: **Franckeite** occurs in sulfosalt (V) band consisting mainly of jamesonite in pyritic sulfide (IV) veins. **Cylindrite** occurs as a band along with sphalerite at a central part of the pyritic sulfide (IV) vein. It appears as a cylindrical form associating with franckeite, jamesonite, pyrite and marcasite besides sphalerite. **Hocartite** appears in sulfosalt (V) band or veinlet consisting mainly of franckeite. It assembles with franckeite, stannite, sphalerite, pyrite, marcasite, canfieldite and quartz. **Teallite** occurs a band with gearksutite in the sulfide (IV) vein. The band is composed of franckeite, cassiterite, sphalerite, pyrite, fluorite, apatite and alunite in addition to teallite and gearksutite.

Rhodostannite appears aggregates of fine-grained crystals closely assembled with pyrite, sphalerite, stannite, stibnite, jamesonite, franckeite and wurtzite. Canfieldite occurs as microscopic mineral, closely assembling with hocartite, stannite and franckeite. Incaite occurs as a cylindrical form similar to cylindrite, associating with cylindrite, stannite, miargyrite and sphalerite.

Mineralization stages of tin minerals and its conditions

Crystallization sequences of the principal minerals are shown in Fig. 1 in relation to the mineralization stages (I) to (VI). Of these stages, the latest stage (VI) has no relation to tin mineralization. Cassiterite was crystallized at each stage of the mineralization except stage (VI). On the other hand, crystallization of stannite (and kesterite) was mainly performed at stage (IV) of sulfide mineralization, but considerable amounts of stannite were also produced at stages (III) and (V). Franckeite, hocartite, teallite, cylindrite, rhodostannite and canfieldite were mostly crystallized at stage (V) together with lead-antimony sulfosalt (jamesonite, boulangerite) and silver sulfosalt minerals (pyrargyrite, andorite). Among these minerals, teallite, franckeite and hocartite were crystallized slightly earlier in the stage than cylindrite, rhodostannite and cafieldite.

The homogenization temperature and salinity (NaCl equivalent concentration) of the fluid inclusions in quartz crystallized at an each stage from (I) stage to (V) stage were measured. These data are summarized in Table 2. There is a tendency for both the homogenization temperature and the salinity of the fluid inclusion to decrease with the progress of the mineralizations from the early (I) to the late (V) stages. Also, both the homogenization temperature and salinity of the fluid inclusions have conspicuously high values, especially at stages (I) and (II).

Table 2. Hemogenization temperature and salinity data for fluid inclusion in quartz at each stage of mineralizations

Mineralization stage	Homogenization temperature (° C)	Salinity Eq. wt% NaCl
I	260 - 510	18.5 - 55.4
II	250 - 405	23.4 - 26.0
III	250 - 400	4.4 - 19.0
IV	230 - 350	1.5 - 10.6
V	190 - 300	0.4 - 5.4

Based on the data on the homogenization temperature, iron content in sphalerite with pyrite stable field of arsenopyrite, the range of formation temperatures and sulfur fugacities at the quartz-pyrite (III), sulfide (IV) and

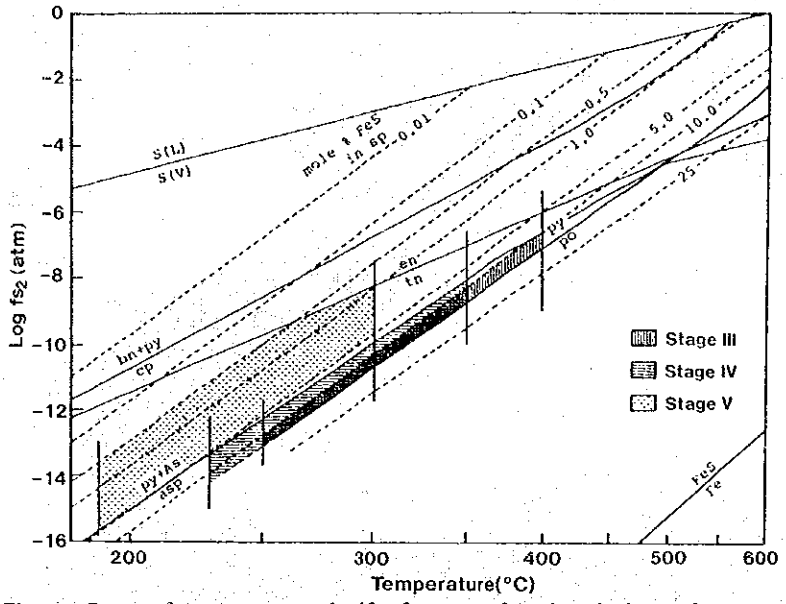

Fig. 2. Range of temperature and sulfur fugacity inferred on the basis of quartz-pyrite (III), sulfide (IV) and sulfosalt (V) stage mineralization in Bolivian tin deposits. asp: arsenopyrite, bn: bornite, cp: chalcopyrite, en: enargite, po: pyrrhotite, py: pyrite, tn: tennantite.

sulfosalt (V) stages are shown in Fig. 2. Temperature and sulfur fugacity of tin mineralizations at stages (III), (IV) and (V) are estimated as follows: stage (III), 250° to 400°C and 10^{-13} to 10^{-7} atom; stage (IV), 230° to 350°C and 10^{-15} to 10^{-9} atom; and stage (V), 190° to 300°C and 10^{-16} to 10^{-9} atom.

Reference

1. Ahlfeld, F. 1967. Metallogenic epochs and provinces of Bolivia. *Mineral Deposits,* Vol. 2, p. 291-311.
2. Ahlfeld, E.; Schneider-Scherbina, A. 1966. Los yacimientos minerales y de hidrocarburos de Bolivia. *Departamento Nacional de Geología.* La Paz.
3. Everden, J. F.; Kirz, S. J.; Cherroni, M.C. 1977. Potassium-argon ages of some Bolivian rocks. *Economic Geology.* Vol. 72, p. 1042-1061.
4. Hanus, D. 1977. Observation on Colquiri tin minerals and their intermpretation. *Neues Jahrbuch für Mineralogie Abhandlungen,* Vol. 131, p. 19-21.
5. Hanus, D. 1982. The Colquiri tin deposit: a contribution to its genesis. *In* Ore Genesis, The State of the Art (Amstutz *et al.;* Editors). *Springer-Verlag,* p. 308-318. Berlin.
6. Grant, J. N.; Hall, C.; Avila, W.; Snelling, N. J. 1979. Potassium-argon ages of igneous rocks and mineralization in part of the Bolivian tin belt. *Economic Geology.* Vol. 74, p. 838-851.

7. Grant, J. H.; Halls, C.; Sheppard, S. M. F.; Avila, W. 1980. Evolution of the porphyry tin deposits of Bolivia. *In* Granitic Magmatism and related mineralization (Ishihara, S.; Takenouchi, S.; Editors). *Mining Geology, Special Issue,* No. 8, p. 151-173.
8. Kelly, W. C.; Turneaure, F. S. 1970. Mineralogy, paragenesis and geothermometry of the tin and tungsten deposits of the Eastern Andes, Bolivia. *Economic Geology,* Vol. 65, p. 609-680.
9. Lehmann, B.; Schnieder, H. J. 1981. Strata-bound tin deposits. *In* Handbook of Strata-bound and Stratiform Ore deposits, No. 9. *Elsevier,* p. 743-771. Amsterdam.
10. Michel, H.; Reatter, K. J. 1977. Die W-Sn-Lagerstätte Chojila, Cordiller Real, Bolivien Teil 1: Nebengeisten und Tektonik. *Mineral Deposits,* Vol. 12, p. 247-262.
11. Sillitoe, R. H. 1976. Andean mineralization. A model for the metallogeny of convergent plate margins. *In* Metallogeny and Plate Tectonics (Strong, D. F.; Editor). *Geological Association of Canada, Special Paper,* No. 14, p. 59-99.
12. Sugaki, A.; Ueno, H.; Kitakaze, A.; Hayashi, K.; Shima, H.; Sanjinés, O.; Saavedra, A. 1981. Geological study on polymetallic hydrothermal deposits in the Oruro district, Bolivia. *Science Reports of the Tohoku University,* Serie 3, No. 15, p. 1-52.
13. Sugaki, A.; Ueno, H.; Shimada, N.; Kusachi, I. Kitakaze, A.; Hayashi, K.; Kojima, S. and Sanjines, O. 1983. Geological study on polymetallic hydrothermal deposits in the Potosi district, Bolivia. *Science Reports of the Tohoku University,* Series 3, No. 15, p. 409-460.
14. Sugaki, A.; Ueno, H.; Shimada, N.; Kusachi, I.; Kitakaze, A.; Hayashi, K.; Kojima, S.; Sanjinés, O.; Sánchez, A.; Velarde, O. 1984. Geologycal study onpolymetallic hydrothermal deposits in the Quechisla district, Bolivia. *Science Reports of the Tohoku University,* Series 3, No. 15. p. 1-52.
15. Sugaki, A.; Ueno, H.; Kitakaze, A.; Hayashi, K.; Shimada, N.; Kusachi, I.; Sanjinés, O. 1985. Geological study on the ore deposits in the La Paz district, Bolivia. *Science Reports of the Tohoku University,* Series 3, 16, p. 131-198.
16. Turneaure, F. S. 1960. A comparative study of major ore deposits of central Bolivia. *Economic Geology,* Vol. 55, p. 217-254, 576-606.
17. Turneaure, F. S. 1971. The Bolivian tin-silver province. *Economic Geology,* Vol. 66, 215-225.
18. Turneaure, F. S.; Welter, K. K. 1974. The ore deposits of the eastern Andes of Bolivia-The Cordillera Real. *Economic Geology,* Vol. 42, p. 595-625.

APPENDIX

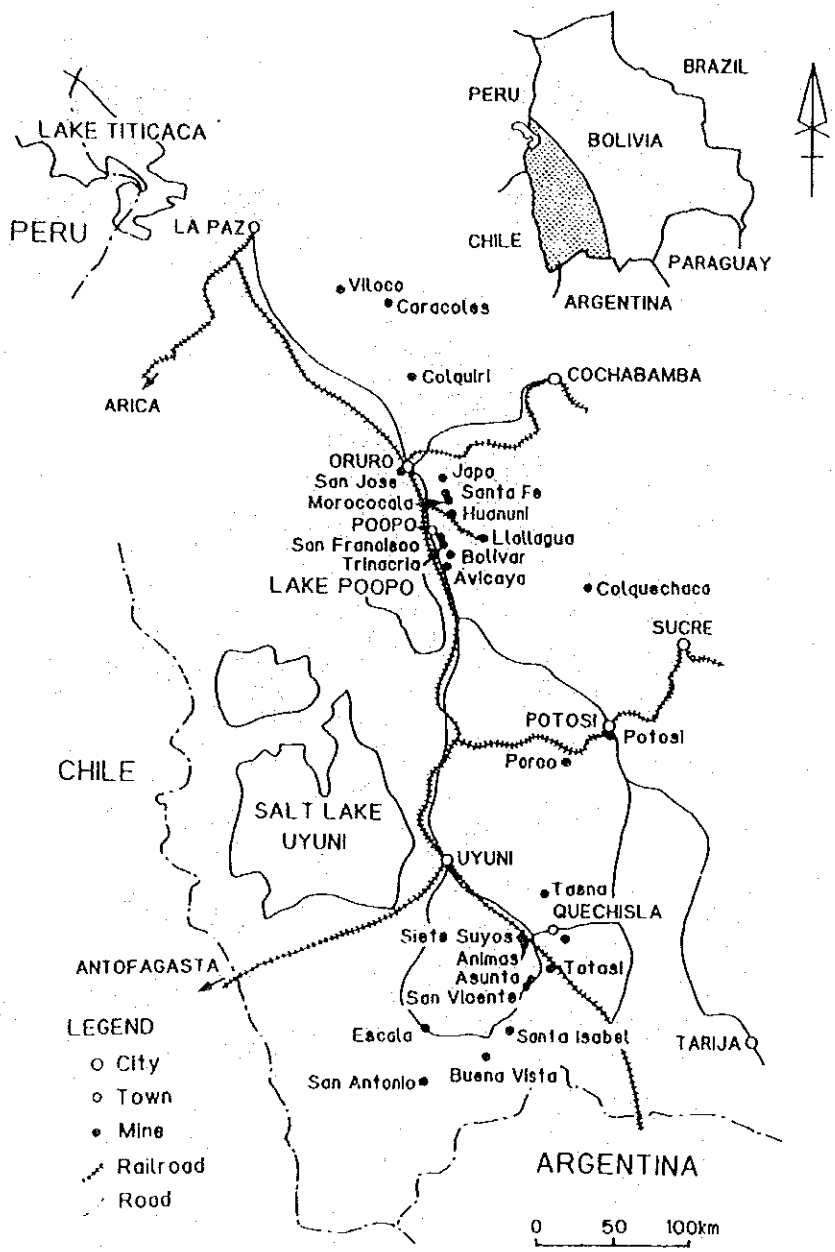

Location of Bolivian tin mines producing polymetallic ores

PHASE EQUILIBRIUM STUDIES ON THE SULFIDE SYSTEM: SYNTHESIS OF COSALITE AND EXSOLUTION OF BISMUTH BEARING BORNITE SOLID SOLUTION

Asahiko Sugaki*, Hiromi Shima and Arashi Kitakaze*****
***Kadan 4-30-503, Aoba, Sendai 980, Japan. **Faculty of Technique, Yamaguchi University, Tokiwadai 2557, Ube 755, Japan, ***Faculty of Science, Tohoku University, Aramaki-Aoba, Sendai 980, Japan.**

Introduction

A purpose of the studies on the phase equilibrium of the sulfide system is to obtain the information for forming conditions of metallic ore deposits in geological processes. From data on the phase relations obtained by experimental works of sulfide phase equilibria, temperature, pressure and sulfur activity of mineralization producing the ore deposits are estimated, and also ore textures and mineral parageneses which can be observed under microscope are interpreted realistically from the phase diagram.

The experimental data on the mineral synthesis give a definite picture of physico-chemical conditions under which the sulfide minerals are produced from the ore-forming fluid. Also, from the data on a solid solution field and its temperature relation in the phase diagram we can consider the the formations process of complicate exsolution textures with double exsolute products such as double lamellae of chalcopyrite and wittichenite (Cu_3BiS_3) in bornite.

As examples of the phase equilibrium study of the sulfide system, the phase relations in the Cu-Pb-Bi-S and Cu-Fe-Bi-S quaternary systems are reported in this paper under the following subtitles:

A) Synthesis of cosalite and its phase relations in the Cu-Pb-Bi-S system.
B) Bornite solid solution in the Cu-Fe-Bi-S system and its exsolution.

Synthesis of cosalite and its phase relations in the Cu-Pb-Bi-S system

Stoichiometric composition of cosalite is generally thought to be $Pb_2Bi_2S_5$ by

Genth (1868), and Weitz and Hellner (1960), etc. Many authors such as Van Hook (1960), Craig (1967), Shiranita et al. (1974), Chang and Hoda (1977), Sugaki and Shima (1978), Mariolacos (1979, 1980) and Bente (1980), who carried out experimental works on the phase equilibrium in the Ag(or Cu)-Pb-Bi-S system, mainly the Ag_2S(or Cu_2S)-PbS-Bi_2S_3 joins, tried a synthesis of cosalite, but it was unsuccessful. White Salanci and Moh (1969) synthesized a phase $X(2PbS_{1-x}Bi_{2x}/_3 \cdot Bi_2S_3)$, which seemed to be cosalite, during a study on the PbS-Bi_2S_3 join. However, it was verified to be principally cannizzarite by Sugaki and Shima (1978), Mariolacos (1979), and Bente (1980).

Cosalite in the natural ores usually contains small amounts of copper and silver as described by Hillebrand (1884), Berry (1939), and Palache et al. (1944). Also, Trdlicka et al. (1973), Srikrishnan and Nowacki (1974), and Shimazaki and Ozawa (1973) obtained $Cu_{0.34}Pb_{1.79}Bi_{1.80}S_5$, $(Ag_{0.07}Cu_{0.19})_{0.16}Pb_{1.75}Bi_{1.75}S_{5.24}$ and $(Ag_{0.09}Cu_{0.07})_{0.16}Pb_{1.76}Bi_{2.13}(S_{4.95}, Se_{0.01})_{4.96}$, respectively, as the composition of natural cosalite by electron microprobe.

Sugaki et al. (1982) carried out experiments on a synthesis of cosalite in the quaternary Cu-Pb-Bi-S system at 400°C by both the evacuated glass tube and hydrothermal transporting methods, and could synthesize cosalite as mentioned below. Many sulfosalt minerals belonging to the Cu-Pb-Bi-S system such as cannizzarite, lillianite, cosalite, ailinite, phase F($Cu_{12}Pb_{25}Bi_{38}S_{88+x}$) and others given in Table 1 were synthesized by an evacuated glass tube method using simple sulfides of CuS, Cu_2S, PbS, and Bi_2S_3 produced in advance from pure metals (five nine) of copper, lead and bismuth and pure sulfur element (four to five nine).

Table 1. Mineralogical data of the phases appearing in the Cu-Pb-Bi-S system

Phases	Chemical formula	Crystal system	Space group	Cell parameters a(Å)	b(Å)	c(Å)	ß
Chalcocite	Cu_2S	mon	P2/c	15.246	11.884	13.494	116.35°
Phase X	Cu_3BiS_6	hex	$P6_322$	20.42	-	6.67	-
Wittichenite	Cu_3BiS_3	orth	$P2_12_12_1$	7.694	10.393	6.710	-
Phase Y	$Cu_8Bi_8S_{19}$	orth	Pbnb	11.591	32.05	3.953	-
Cuprobismutite	$Cu_{10}Bi_{12}S_{23}$	mon	C2/m	17.513	3.909	15.255	101.09°
Phase E	$CuBi_3S_5$	mon	C2/m	13.221	4.023	14.077	115.46°
Bismuthinite	Bi_2S_3	orth	Pbnm	11.146	11.298	3.980	-
Galenobismutite	$PbBi_2S_4$	orth	Pnam	11.801	14.571	4.077	-
Cannizzarite	$Pb_{13}Bi_{14}S_{35}$	mon*	$P2_1/m$*	189.8*	4.09*	74.06*	11.9*
Lillianite	$Pb_3Bi_2S_6$	orth	Bbmm	13.546	20.611	4.117	-
Galena	PbS	cub	Fm3m	5.938	-	-	-
Phase A	$Cu_{22}Pb_4Bi_4S_{23}$	mon	A2/m	27.69	3.98	13.06	90.1°
Phase D	$Cu_{2.7}Pb_{0.9}Bi_{4.5}S_9$	mon	C2/m	13.22	4.02	14.87	99.0°
Aikinite	$CuPbBiS_3$	orth	Pbnm	11.32	11.64	4.04	-
Phase F	$Cu_{12}Pb_{25}Bi_{38}S_{88+X}$	-	-	-	-	-	-
Cosalite	$CuPb_7Bi_8S_{20}$ $(0<X<6)$	orth	Pbnm	19.134	23.804	4.059	-

*After Matzat (1979)

The phase relations in the Cu_2S-PbS-Bi_2S_3 join of the quaternary Cu-Pb-Bi-S system at 400°C are shown in Fig. 1 obtained from the data of the synthetic experiments. The phases such as galena, lillianite, cannizzarite, bismuthinite-aikinite solid solution (ss), phases A, D and E, cuprobismutite, wittichenite, phase X and chalcocite (cc) are found in this figure, but cosalite, phase F and galenobismutite do not appear. The composition $Pb_2Bi_2S_5$, which was thought to be cosalite by several

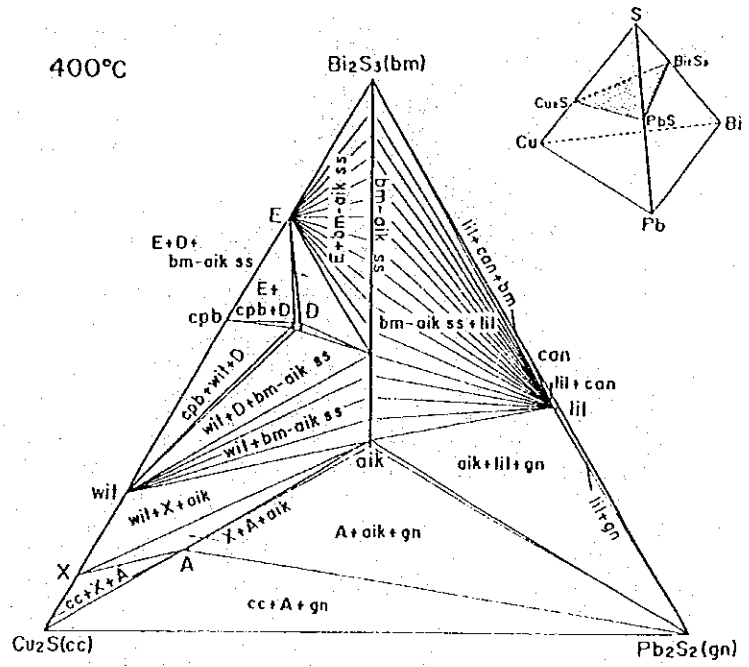

Fig. 1. Phase relations in the Cu_2S-PbS-Bi_2S_3 join of the Cu-Pb-Bi-S system at 400°C. Abbreviations are the same as those in Table 1. cc: chalcocite (Cu_2S).

authors, was not cosalite. However, it was found to be cannizzarite ($Pb_{13}Bi_{14}S_{34}$) with small amounts of lillianite from the X-ray powder data. Natural cosalite always contains small amounts of copper and silver besides lead, bismuth and sulfur. So, synthetic runs on the compositions of (Cu+Pb): Bi = 1:1 and Cu : Pb = 1:9 to 4:6 in atomic ratio were performed. However, the products of all runs were a mixture of lillianite and bismuthinite-aikinite ss. There was found no cosalite in the Cu_2S-PbS-Bi_2S_3 join of the quaternary Cu-Pb-Bi-S system.

Cosalite was synthesized as a stable phase in the CuS-PbS-Bi_2S_3 join which is more sulfur rich than the Cu_2S-PbS-Bi_2S_3 join at 400°C by the evacuated glass tube method of long runs for 50 to 200 days. To form cosalite, a condition of higher sulfur-fugacity than that of the Cu_2S-PbS-Bi_2S_3 join was necessary. Also,

grinding after heating, and reheating for long time were very important to form a nucleus of cosalite crystal. The runs forming cosalite are listed up in the Table 2. As seen in this table, a monophase of cosalite was obtained by the run No. 077 having a composition, CuS : 8.33, Pb : 58.33, and Bi_2S_3 : 33.33 in mole percent. This composition corresponds to $CuPb_7Bi_8S_{20}$.

Cosalite synthesized is an aggregate of fine grained crystals of lead gray in color with metallic luster. Under ore microscope, it has weak bireflectance of white with creamy or gray tints and shows a moderate anisotropism from brownish gray to purplish gray in color. Reflectance of synthetic cosalite is as follows: 480nm : 43.5-46.2%, 546nm : 41.8-43.7%, 589nm : 41.2-42.3%, and 657nm : 37.6-39.0%. These values are in good accordance with those of Picot and Johan (1977). X-ray powder data of synthesized cosalite show it to be orthorhombic, a:19.134(5), b:23.804(5), and c:4.062(2) Å.

On the other hand, a hydrothermal procedure on the synthesis of cosalite was performed by thermal gradient transporting method using a welded gold tube. In this case, a mixture of cosalite, lillianite and phase F produced by the evacuated glass tube (dry) method was employed as a nutrient (starting) material, and 5m NH_4Cl aqueous solution or 5m NH_4Cl-7.5m NH_4OH mixed aqueous solution (pH 7.1) were used as solvents. The runs were carried out at 400°C under 500kg/cm2 during 7 to 10 days. In the case using 5m NH_4Cl aqueous solution as solvent, aggregate of lillianite, cannizzarite and bismuthinite-aikinite ss were crystallized. But cosalite did not occur.

Table 2. Experimental data on the runs produced cosalite in the CuS-PbS-Bi_2S_3 join at 400°C

Run No.	Composition (mole %) CuS	PbS	$BiS_{1.5}$	Heating time (days)	Products
036	3.00	47.00	50.00	181	lil+cos+(can)
037	3.50	46.50	50.00	181	lil+cos+(can)
038	4.00	46.00	50.00	180	lil+cos+(can)
039	4.50	45.50	50.00	180	cos+lil+(can)
098	5.00	45.00	50.00	190	cos+lil+(can)
040	5.50	44.50	50.00	188	cos+lil+(can)
041	6.00	44.00	50.00	188	cos+lil+(can)
077	6.25	43.75	50.00	80	cos
085	6.50	43.50	50.00	199	cos+lil+F+S(1)
113	7.00	43.00	50.00	192	cos+lil+F+S(1)
082	7.50	42.50	50.00	198	F+cos+lil+S(1)
114	8.00	42.00	50.00	190	cos+F+lil+S(1)
205	6.75	43.49	49.76	78	cos+F+lil+S(1)
207	4.48	41.87	53.33	57	cos+can+bm-aik ss+S(1)
208	1.87	43.02	55.11	57	cos+can+bm-aik ss+S(1)
209	7.85	37.05	55.10	52	cos+bm-aik ss+S(1)
210	11.96	33.02	55.02	52	F+bm-aik ss+cos+S(1)

aik: aikinite, cos: cosalite, bm: bismuthinite, can: cannizzarite, lil: lilianite, S(1): sulfur liquid, F: phase F.

When employed 5m NH_4Cl 7.5m NH_4OH mixed aqueous solution (pH 7.1) as solvent, cosalite was formed as aggregate of needle-shaped crystals in intimate assemblage with lillianite and cannizzarite. Its crystal data obtained by Guinier camera and automatic four-circle diffractometer are the same as those of cosalite synthesized by dry method as follows: orthorhombic, space group Pbnm, a:19.134(2), b:23.804(2), c:4.059(1)Å. A relatively large crystal of cosalite synthesized hydrothermally was analyzed by electron microprobe, and the following analytical data were obtained: Cu1.5, Pb37.6, Bi43.3 and S16.6 in weight percent ($Cu_{2.5}$, $Pb_{19.5}$, $Bi_{22.3}$ and $S_{55.7}$ in atomic percent). Its composition is represented as $Cu_{0.91}Pb_{7.02}Bi_{8.02}S_{20.04}$ which shows to be in good accordance with $CuPb_7Bi_8S_{20}$ of cosalite synthesized by the evacuated glass tube method.

The phase relations in the CuS-PbS-Bi_2S_3 join are shown in Fig. 2. As seen in this figure, there are newly found cosalite and phase F. Phase F corresponds to phase AG ($Cu_{12}Pb_{25}Bi_{38}S_{88}$) by Mariolacos (1979, 1980). From the fact that both cosalite and phase F are not produced in the Cu_2S-PbS-Bi_2S_3 join, but appear in the CuS-PbS-BiS join, it is thought that they are formed under higher sulfur fugacities than those in the Cu_2S-PbS-Bi_2S_3 join. Indeed, they are often accompanied by sulfur (liquid). The phase relations around cosalite are also shown in Fig. 3. As seen in figure, cosalite assembles with cannizzarite, lillianite, bismuthinite-aikinite ss, phase F and sulfur (liquid), meanwhile phase F coexists with bismuthinite-aikinite ss, cosalite, lillianite

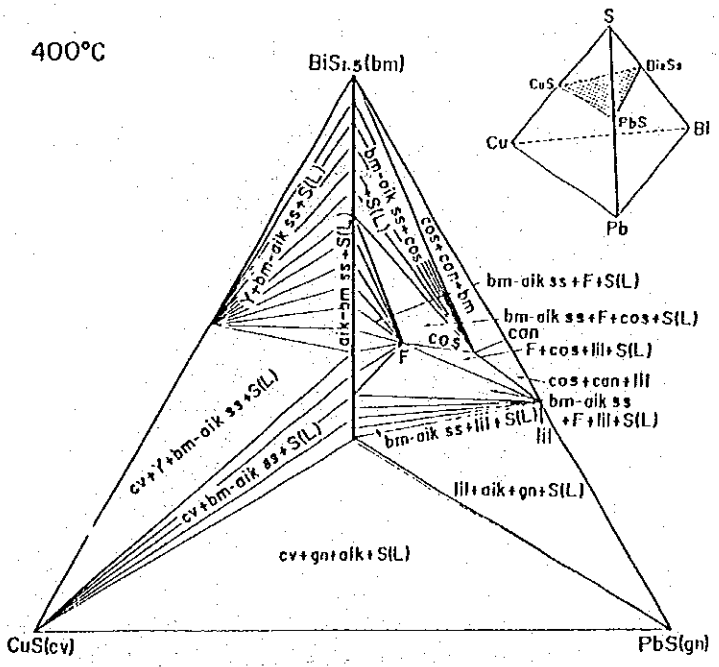

Fig. 2. Phase relations in the CuS-PbS-Bi_2S_3 join of the Cu-Pb-Bi-S system at 400°C. cv: covellite (CuS).

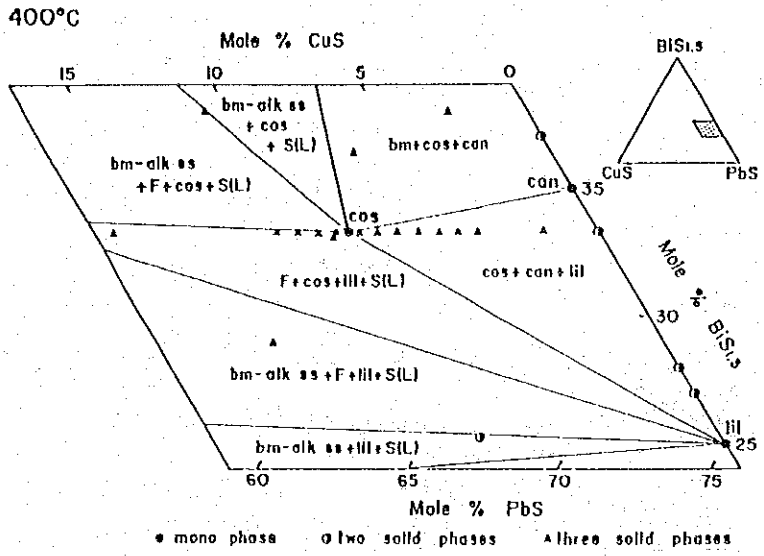

Fig. 3. Phase assemblages around cosalite in the CuS-PbS-Bi_2S_3 join at 400°C.

and sulfur (liquid). There are found five univariant assemblages with cosalite and/or phase F in the figure as follows:

1) bismuthinite + cosalite + cannizzarite (+ sulfur (liquid))
2) cosalite + cannizzarite + lillianite (+ sulfur (liquid))
3) bismuthinite-aikinite ss + phase F + cosalite + sulfur (liquid)
4) phase F + cosalite + lillianite + sulfur (liquid)
5) bismuthinite-aikinite ss + phase F + lillianite + sulfur (liquid)

Sinthesized cosalite is stable below 480°C, but it decomposed into a mixture of lillianite and galenobismutite at 490°C of above as shown in DTA curve (Fig. 4).

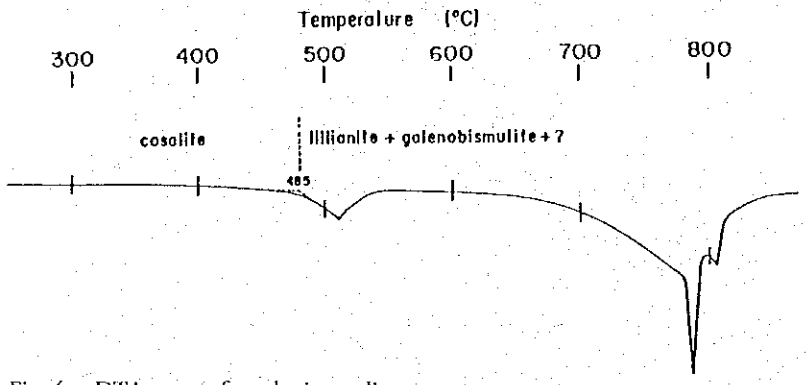

Fig. 4. DTA curve of synthetic cosalite.

Bornite solid solution in the Cu-Fe-Bi-S system and its exsolution

Many minerals and synthetic phases are present in the quaternary Cu-Fe-Bi-S system as given in Table 3. Studies on the phase relations of the Cu-Fe-Bi-S system have been carried out by Sugaki *et al.* (1981, 1984). Based on their experimental data, the isothermal phase diagram obtained by projection to the Cu_2S (chalcosite, cc)-Bi_2S_3 (bismuthinite, bm)-$Fe_{0.9}S$ (pyrrhotite, po) plane from the sulfur corner in the Cu-Fe-Bi-S tetrahedron (Fig. 5) at 420°C is shown in Fig. 6. Bornite which has a considerable solid solution field in the Cu-Fe-S face of the quaternary system, even more extends within the quaternary tetrahedron as noticeable volume of the solid solution as seen in the figure. The bornite solid solution at 420°C coexists with chalcopyrite, wittichenite (Cu_3BiS_3), cuprobismutite ($Cu_{10}Bi_{12}S_{23}$), phase Z ($Cu_{8.4}Fe_{1.2}Bi_{10.8}S_{22}$) and nukundamite ($Cu_{3.39}Fe_{0.61}S_4$) or bismuth. However, because the assemblage of chalcopyrite and wittichenite becomes stable below 395°C, the bornite solid solution cannot coexist with cuprobismutite or emplectite ($CuBiS_2$) and phase Z below that temperature mentioned above.

On cooling, the bornite solid solution reduces its field as shown in Figs. 7 and 8, and finally reaches to the stoichiometric composition Cu_5FeS_4 at 25°C (Fig. 9). This compositional change of the bornite solid solution on cooling means an exsolution process of the solid solution to segregate chalcopyrite and wittichenite from the bornite solid solution. In fact, bornite under microscope observation often has chalcopyrite and/or wittichenite lamellae as the exsolution product.

Table 3. Crystallographic data on the phases appearing in the Cu-Fe-Bi-S system

Phases	Abb.	Chemical formula	Crystal system	Space group	Cell parameters a(Å)	b(Å)	c(Å)	ß
Phase X	X	Cu_3BiS_6	hex	$P6_322$	20.42	-	6.67	-
Wittichenite	wit	Cu_3BiS_3	orth	$P2_12_12_1$	7.694	10.393	6.710	-
Emplectite	emp	$CuBiS_2$	orth	Pnam	6.144	14.525	3.925	-
Cuprobismutite	cpb	$Cu_{10}Bi_{12}S_{23}$	mon	C2/m	17.513	3.909	15.255	101.09°
Phase D	D	$Cu_3Bi_5S_3$	mon	C2/m	13.08	4.00	14.70	99.4°
Phase E	E	$CuBi_3S_3$	mon	C2/m	13.221	4.023	14.077	115.46°
Bismuthinite	bm	Bi_2S_3	orth	Pbnm	11.146	11.298	3.980	-
Phase Y	Y	$Cu_8Bi_8S_{19}$	orth	Pbnb	11.591	32.05	3.953	-
Phase Z	Z	$Cu_{8.4}Fe_{1.2}Bi_{10.8}S_{22}$	mon	C2/m	17.483	3.902	12.869	108.11°
Bornite (high form)	bn	Cu_5FeS_4	cub	Fd3m	5.50	-	-	-
Nudundamite	nk	$Cu_{3.39}Fe_{0.61}S_4$	hex	P3ml	3.7830	-	11.1950	-
Chalcopyrite	cp	$CuFeS_2$	tet	I42d	5.278	-	10.430	-
Intermediate solid solution	iss	$CuFe_2S_3$	cub	F43m	(5.272	-	-	-)
Pyrrhotite	po	$Fe_{1-X}S$ ($Fe_{0.9}S$)	hex	P6/mmc	(3.441	-	5.738	-)

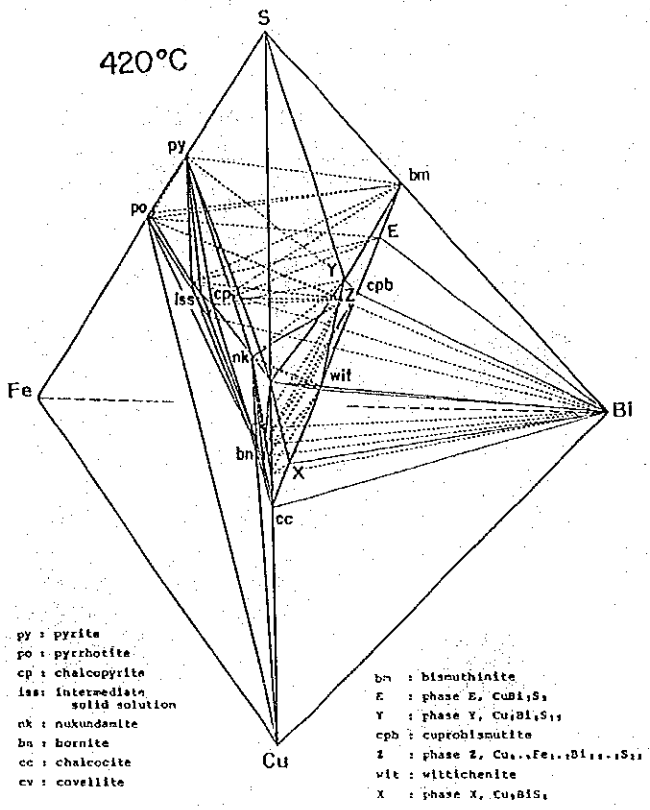

Fig. 5. Phase relations in the quaternary Cu-Fe-Bi-S system at 420°C.

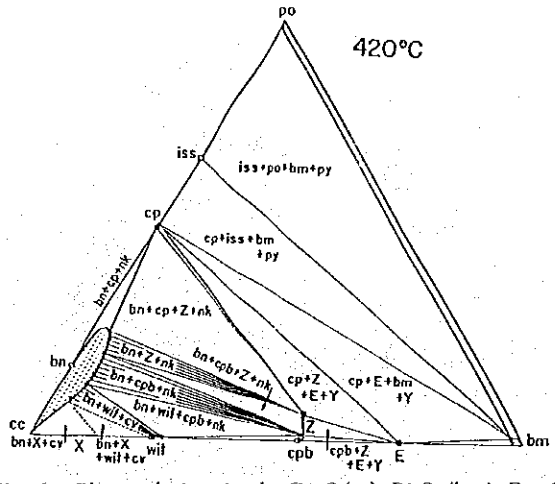

Fig. 6. Phase relations in the Cu_2S (cc) -Bi_2S_3 (bm) -$Fe_{0.9}S$ (po) join of the Cu-Fe-Bi-S system (Fig. 5) at 420°C. Abbreviations are the same as those in Fig. 5 and Table 3.

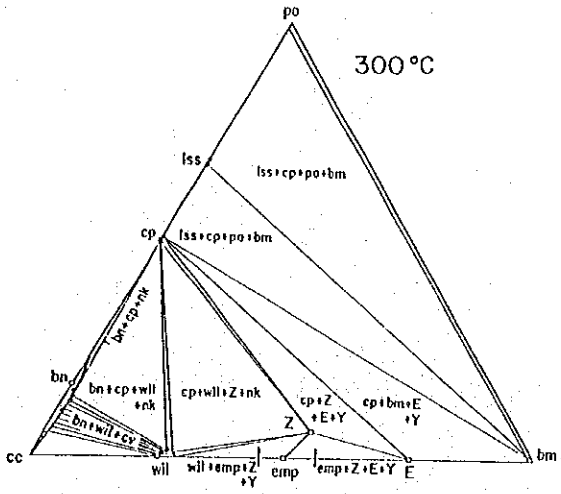

Fig. 7. Phase relations in the Cu_2S (cc) -Bi_2S_3 (bm) -$Fe_{0.9}S$ (po) join of the Cu-Fe-Bi-S system at 300°C.

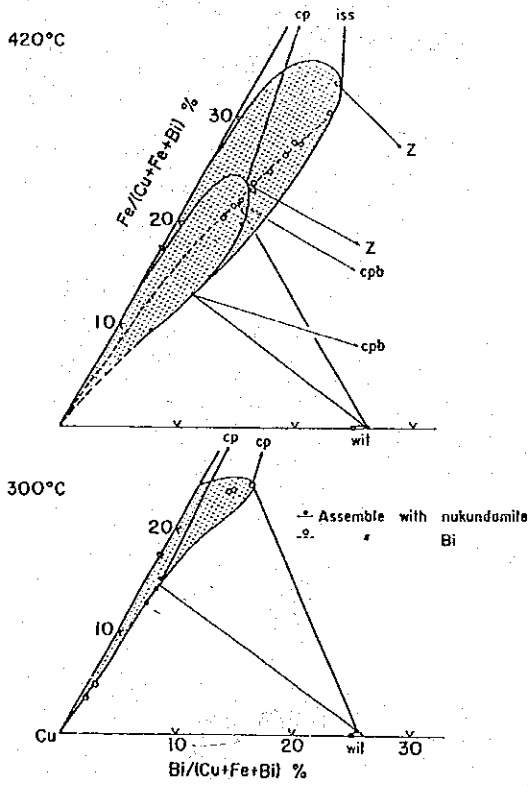

Fig. 8. Bornite solid solution fields projected on the Cu Bi Fe metal plan from sulfur corner of the quaternary tetrahedron at 420° and 300°C.

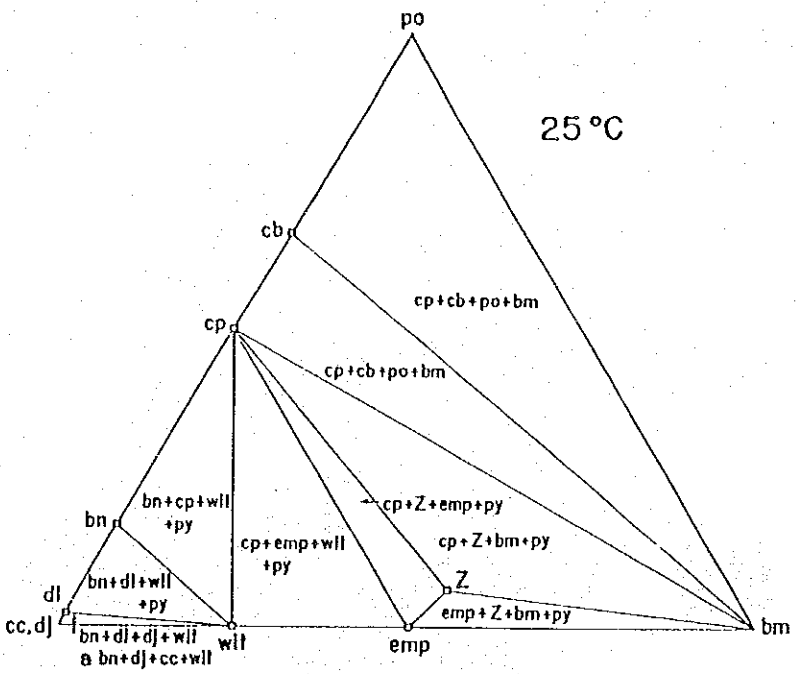

Fig. 9. Phase relations in the Cu_2S-Bi_2S_3-$Fe_{0.9}S$ join at 25°C.

Table 4. Chemical composition of the original bornite solid solutions which have exsolution lamellae of wittichenite and/or chalcopyrite at room temperature

Volume percent		Weight percent Cu	Fe	Bi	S	Total	Atomic percent Cu	Fe	Bi	S
Obari mine										
bn	73.1%									
wit	15.6%	56.0	10.8	7.9	25.3	100.0	46.3	10.2	2.0	41.5*
cp	11.2%									
		59.2	10.8	5.5	25.1	100.6	48.2	9.9	1.3	40.5**
Sannotake-Yokozuru mine										
bn	91.8%									
wit	6.9%	60.9	10.5	3.5	25.1	100.0	49.2	9.6	0.9	40.3*
cp	1.3%									

* Modal analysis by automatic image analyzer
** By EPMA (Homogenized at 475°C)

For example, double lattice exsolution texture of chalcopyrite and wittichenite lamellae in bornite from the Obari mine, Japan is observed. Also, bornite from the Sannotake-Yokozuri mine, Japan has fine wittichenite as exsolution product. These exsolution lamellae disappear to form the solid solution with bornite by heating to 400°C or above (Sugaki, 1951). To know the chemical composition of the original

bornite solid solution crystallized primarily from ore solution, the area of exsolved wittichenite and/or chalcopyrite, and host bornite from both the Obari and Sannotake-Yokozuru mines were measured under microscope using automatic image analyzer. The values measured and calculated are given in Table 4. The composition of the original bornite solid solution from the Obari mine obtained by EPMA after homogenization by diffusion by heating to 475°C the exsolution products, chalcopyrite and wittichenite lamellae, into host bornite is also represented in the table.

The compositions of two bornite solid solutions obtained above are situated on the boundaries of the bornite solid solution field at 380°C (Obari) and 300°C (Sannotake-Yokozuru) as shown in Figs. 10 and 11. In the case of the Obari bornite solid solution, the exsolution of chalcopyrite from the bornite solid solution begins at 380°C, and on cooling the solid solution changes its composition along a straight line from point a to point b, extending the direction of the tie line between point a and chalcopyrite (Fig. 10), thus separating continuously chalcopyrite as exsolution lamella. At point b on the solid solution boundary at 320°C, the exsolution of wittichenite is started together with that of chalcopyrite. Then, the bornite solid solution changes its composition continually along a curve from point b to point c (Cu_5FeS_4) decreasing temperatures from 320°C to 25°C, separating both wittichenite and chalcopyrite. Finally, the bornite solid solution reaches to stoichiometric composition Cu_5FeS_4 at room temperature.

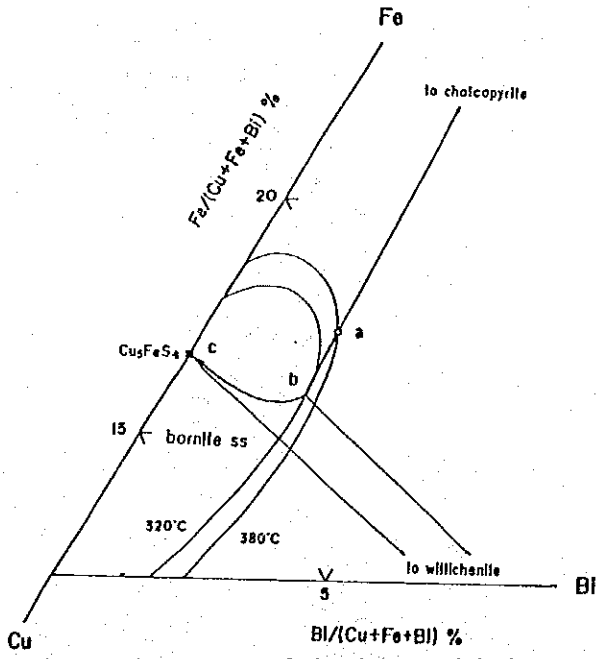

Fig. 10. Exsolution course of Obari bornite solid solution with $Cu_{46.3}Fe_{10.2}Bi_{2.0}S_{41.5}$ on cooling.

On the other hand, the bornite solid solution of the Sannotake-Yokozuru mine changes its composition straightly along a line from point a to point b (Cu_5FeS_4), corresponding to an extension of the tie line between point a and wittichenite, by cooling from 300°C to room temperature, exsolving wittichenite only as shown in Fig. 11.

As mentioned above, the exsolution process of the bornite solid solution can definitely be understood by using the phase diagram of the sulfide system. The data on the phase assemblages in the diagram are thought to act as an important role on the interpretation of the mineral paragenesis and its texture in the ores.

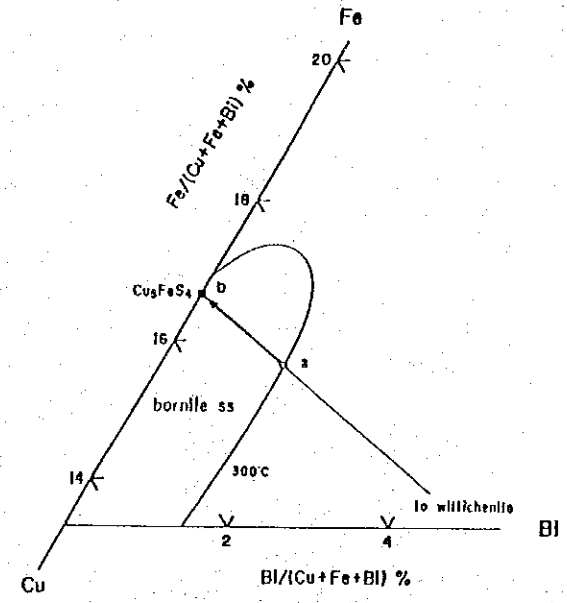

Fig. 11 Exsolution course of Sannotake-Yokosuru bornite solid solution with $Cu_{49.2}Fe_{9.6}Bi_{0.9}S_{40.3}$ on the cooling.

References

Bente, K. (1980): Experimentelle Untersuchungen en Cu-Pb-Bi-Sulfosalzen in System CuS-Cu_2S-PbS-Bi_2S_3. *N. Jb. Miner. Mh.*, 385-395.

Berry, L. G. (1939): Studies of mineral sulfosalts. 1. Cosalite from Canada and Sweden. Univ. Toronto Studies, Geol. Ser., 42, 23-30.

Chang, H. L. & Hoda, S. H. (1977): Phase relations in the system PbS-Cu_2S-Bi_2S_3 and the stability of galenobismutite. *Am. Miner.* 62, 346-350.

Craig, J. R. (1967): Phase relations and mineral assemblages in the Ag-Bi-Pb-S system. *Miner. Deposita,* 1, 278-306.

Genth, F. A. (1868): Contribution to mineralogy. *Am. Jour. Sci,* Ser. 2, 45, 305-321.

Hillebrand, W. F. (1884): On an interesting variety of lollingite and other minerals. *Am. Jour. Sci.,* Ser. 3, 27, 349-358.

Mariolacos, K. (1979): Phase relations in the system Bi_2S_3-PbS-$CuPbBiS_3$ at 450°C and its exension in the system Bi_2S_3-PbS-Cu_2S. *N. Jb. Miner. Mh.*, 73-80.

Mariolacos, K. (1980): Phasenbeziehungen in System Bi_2S_3-PbS-Cu_2S bei 440°C. *N. Jb. Miner. Mh.*, 396-400.

Matzat, E. (1979): Cannizzarite. *Acta Crystallogr.*, B. 35, 133-136.

Palache, Ch., Berman, H. & Frondel, G. (1944): Dana's System of Mineralogy. Willey, New York, 1, 445-447.

Picot, P. & Johan, Z. (1977): Atlas des mineraux metallique. Mémoires du Bureau de recherches géologique et mineres, 131.

Salanci, B. & Moh, G. (1969): Die experimentelle Untersuchung des pseudobinaren Schnittes PbS-Bi_2S_3 innerhalb des Pb-Bi-S Systems in Beziehung zu naturlichen Blei-Wismut-Sulfosalzen. *N. Jb. Miner. Abh.*, 112, 63-95.

Shimazaki, H. & Ozawa, T. (1978): Tsumoite, BiTe, a new mineral from the Tsumo mine, Japan. *Am. Miner.*, 63, 1162-1165.

Shiranita, A., Sugaki, A., Shima, H. & Kitakaze, A. (1974): Phase equilibrium study in the Pb-Bi-S, especially PbS-Bi_2S_3 system (abstr.). Abstr. Joint Symposium Ube, 43 (in Japanese).

Srikrishnan, T. & Nowacki, W. (1974): A redermination of the crystal structure of cosalite $Pb_2Bi_2S_5$. *Z. Kristallogr.*, 140, 114-136.

Sugaki, A. (1951): Thermal experiments on the lattice intergrowth of chalcopyrite and klaprothite in bornite from the Obari mine, Japan. *Sci. Rept. Tohoku Univ., Ser.* 3, 4, 11-17.

Sugaki, A., Kitakaze, A. & Hayashi, K. (1981): Synthesis of minerals in the Cu-Fe-Bi-S system under hydrothermal condition and their phase relations. *Bull. Miner.*, 104, 484-495.

Sugaki, A., Kitakaze, A. & Shima, H. (1982): Synthesis of cosalite and its phase relations in the Cu-Pb-Bi-S quaternary system. Proc. 13th IMA, Cryst. Chem. Miner., Varna, 291-298.

Sugaki, A., Kitakaze, A. & Hayashi, K. (1984): Hydrothermal synthesis and phase relations of the polymetallic system, especially on the Cu-Fe-Bi-S system in Sunagawa, I., ed., Material Science of the Earth's Interior: Toky, Terrapub. 543-583.

Sugaki, A. & Shima, H. (1978): Synthesis of sulfides and sulfur-bearing system. Recent Prog. Natural Sci. Japan, 3, 267-277.

Trdlicka, z., & Kropácek J. & Hoffman, v. (1973): Cosalite from Zlate Hory (Silesis, Czechoslavakia). Acta Univ. Carolinae. Geol. Rost 1-2, 47-50.

Van Hook, H.J. (1960): The ternary system Ag_2S-Bi_2S_3-PbS. *Econ. Geol.*, 55, 759-788.

Weitz G. & Hellner, E. (1960): Über komplex zusammengesetzte sulfidische Erza. VII. Zur Kristalstructur des Cosa lite, $Pb_2Bi_2SA_5$. *Z. Kistallogr.*, 113, 385-402.

BEHAVIOR OF HALOGEN ELEMENTS IN HYDROTHERMAL MINERALIZATION AND RELATED MAGMATISM IN THE ISLAND ARC SYSTEM

Munetomo Nedachi
Faculty of General Educación, Kagoshima University, Koorimoto 1-21-30, Kagoshima 890, Japan.

Introduction

In the island arc area, the genetic relationship between hydrothermal mineralization and magmatism are recognized by almost all investigators. Magma had been believed as an ore bringer, and it had been considered that the ore solution emanated from the magma. This classic hypothesis had not been reinforced by further precise and quantitative data.

In this twenty years, the researches on geothermal fields has developed, and contributed to understand the roles of magmatism and meteoric water on hydrothermal mineralization. A magma plays a role as a heat source for the convection of the meteoric water which leached various metals from rocks, transported the metals and precipitated the ore minerals in a limited place; ore deposits. The isotope geochemistry and others justified the sea water convection model on the submarine type ore deposits. In this case, also a magma plays as a heat source. However, the classic theory looks to have still remained to explain numerous data. We cannot abandon the role of magma as an ore bringer. We have obtained the knowledge that there are many origins of ore solution; meteoric water, sea water, metamorphic water, magmatic water and others. We will be able to discuss on the proportion of roles of various waters, quantitatively, in near future.

In this report, the behavior of halogen elements in mineralization and the related magmatism is summarized mainly based on the author's works, to show that we should not abandon the classic theory.

Halogen bearing mineral as a chemical fossil

Stolley *et al.* (1971) published high Cl content of biotite in the intrusive rocks related to mineralization. Many researchers had excited in this paper. Because Helgeson and his families had published many physico-chemical data which emphasized the important role of chlor-complex and/or thiocomplex for transportation of metals (*e.g.*, Helgeson, 1969), and Holland (1972) simulated the emanation model of metals from melt to vapor phases as a function of Cl content in the granitic system. Various chemical fossil of Cl (like as fluid inclusion) had been desired. Unfortunately, however, any data to show the universality of their work had not been obtained from other district in 1970's. Stolley *et al.* (1976) themselves denied the confidence as a chemical fossil, although Muñoz and Ludington (1974) showed that biotite and apatite had remained unchanged their F content. Nedachi (1980) published the halogen content of biotite and apatite in granitic rocks. He showed that the partitioning of Cl between these hydrous minerals depended on the chemistry of octahedral and tetrahedral site of biotite. From the synthetic experiments, Muñoz and Swenson (1981) got the similar but more applicable conclusions. Hence, it became acceptable that some rock-forming hydrous minerals have remained unchanged their halogen contents, and also that the halogen behavior could be discussed using the whole rock compositions.

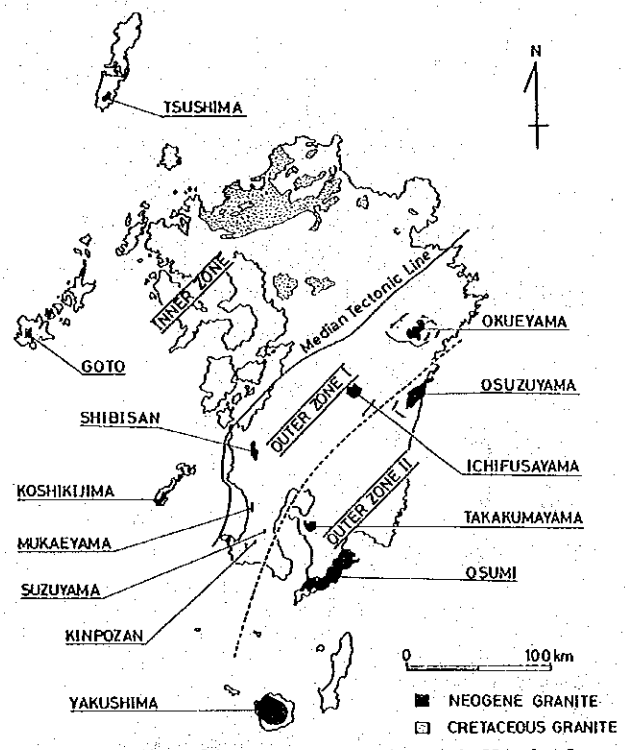

Fig. 1. Locality of the Neogene granitic mass in Kyushu, Japan (Nedachi *et al.*, 1984).

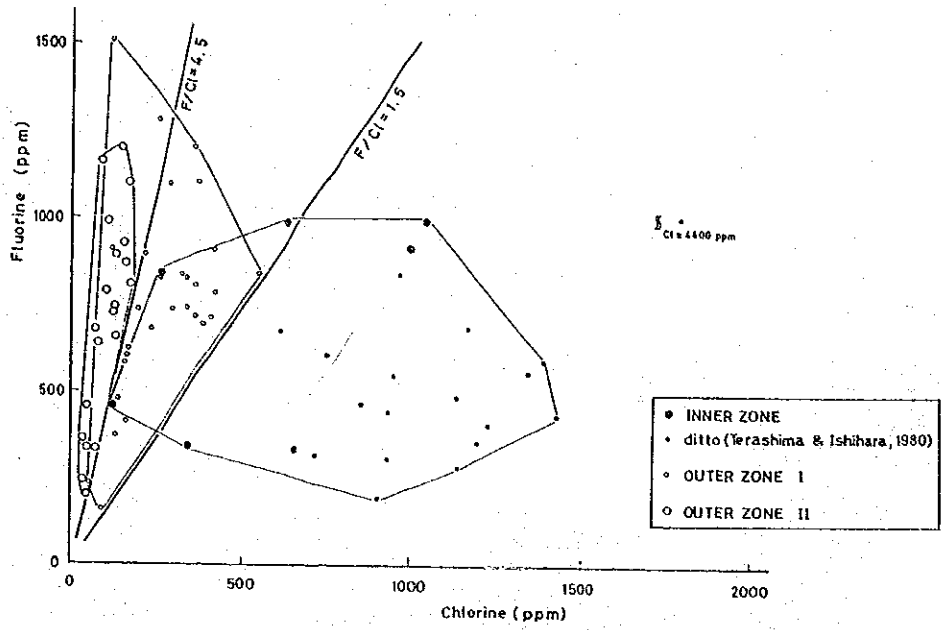

Fig. 2. Cl and F contents of the granitic rocks in Kyushu, Japan (Nedachi *et al.*, 1984).

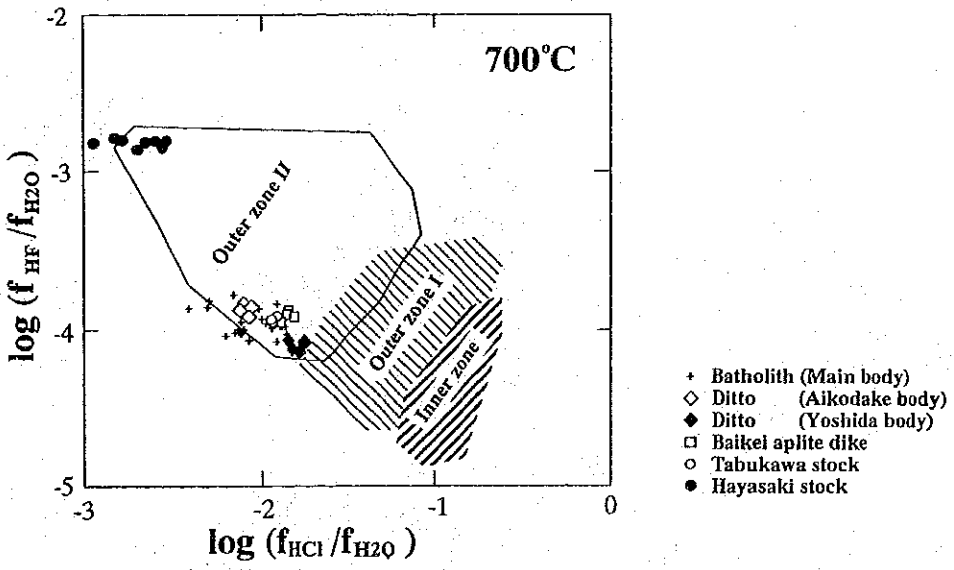

Fig. 3. f_{HCl}/f_{H_2O} and f_{HF}/f_{H_2O} values estimated using the chemical compositions of biotite (Nedachi, 1980; Nedachi, unpublished).
The symbols are of the Yakushima W(-Sn) mining district in the Outer zone II.

Zoning of halogen contents in the island arc system

The halogen contents of rocks and ores, however, do not provide so simple interpretation for the relationship between magmatism and hydrothermal mineralization. Their behaviors depend basically on each geological sequence. We discuss at first on the halogen behavior in the granitic magma along the island arc region. Fig. 1 shows the locality of the Neogene granitic mass in Kyushu of Japan to Ryukyu island arcs. As shown, this area is divided into the following three zones from the Asian Continent side to the Pacific Ocean side, based on the petrography;

Inner zone: low Sr initial isotope ratio
- I-type
- Magnetite series
- Zn-Pb-Cu metallogenic province

Outer zone I: intermediate petrology
- Sn province

Outer zone II: high Sr initial isotope ratio
- Cordierite-bearing S-type
- Ilmenite series
- W province

Fig. 2 shows that the Cl and F contents of the granitic rocks in this area strongly coincide with the asymmetrical zoning (Nedachi *et al.*, 1984). The rock-forming minerals of these rocks show more distinguish tendency. Fig. 3 shows the f_{HCl}/f_{H2O} and f_{HF}/f_{H2O} values estimated using the chemical compositions of biotite (Nedachi, 1980; Nedachi, unpublished). These data indicate that the source materials and the mode of emplacement of granitic rocks strongly affect the behavior of halogen elements. Asymmetrical zoning of granitic rocks are well recognized in the whole area of the circum-Pacific rim regions, and their asymmetric patterns are sometimes different. However it is said that petrologic and metallogenic provinces well corresponds to the halogen behavior, according to the author's experiences; the Cretaceous granitic mass in the Inner zone of Southwest Japan (Ishihara and Terashima, 1977; Tusue *et al*, 1981), Kitakami Mountains in the Northeast Japan (Nedachi and Ueno, 1985), Highland area in Papua New Guinea (Nedachi *et al.*, unpublished), and Andes Cordillera (Nedachi *et al.*, unpublished).

Halogen behavior in the magma related to mineralization

Generally, there are many intrusive units in the mining district. Among those intrusives, the mineralization is related to the limited intrusive rock. To choice

the closest intrusive unit spatially and temporary related to mineralization seems meaningful to consider the role of magma to mineralization. We determined those intrusive units using various methods (*e.g.*, Nedachi, 1974).

Figs. 3 and 4 are examples. Fig. 3 shows the calculated f_{HCl}/f_{H2O} and f_{HF}/f_{H2O} of magma of the Yakushima W(-Sn) mining district (Nedachi and Yamamoto, unpublished). The closest granitic unit related to the mineralization is the Hayasaki stock of which the magma shows extremely high f_{HF}/f_{H2O} and extremely low f_{HCl}/f_{H2O}. On the other hand, Fig. 4 shows the Cl/OH versus Mg/Fe of biotite in the granitic rocks in the Akagane Cu-Fe-Au mining district, Northeast Japan. The closest rocks related to mineralization is granite porphyry of which the f_{HCl}/f_{H2O} are higher than those not related to mineralization in the same mining district. Including the features from other mining districts mainly in the western Pacific island arc system, it is said that the magmas related to Cu, Zn, Pb, Ag and Au mineralization show high f_{HCl}/f_{H2O}, that those to W mineralization show the high f_{HF}/f_{H2O} and low f_{HCl}/f_{H2O}, and that those to Sn mineralization show high f_{HCl}/f_{H2O} or high f_{HF}/f_{H2O}. These phenomena well coincide with the physico-chemical features of predominant complexes of each metals published previously. Also these data suggest the existence of strong relationship between magmatism and mineralization. Various metals have been concentrated either in the residual magma or at the top of the magma chamber under water-undersaturated conditions and removed as the complex with halogen elements from the magma after the magma has saturated in water. However, the absolute values of f_{HCl}/f_{H2O} and $f_{HF}/$

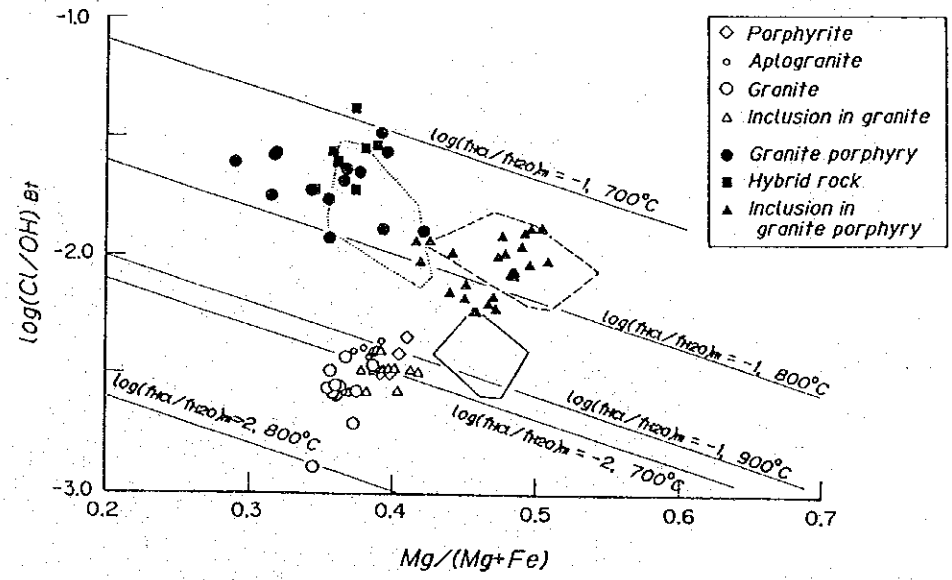

Fig. 4. Cl/OH versus Mg/Fe of biotite in the granitic rocks in the Akagane Cu-Fe-Au mining district, NE Japan (Nedachi *et al.*, 1987).

f_{H2O} can be defined as those for the intrusive rocks related to mineralization, even if on the comparison between the same metal mineralization.

Of course, the ore solution emanated from the water-saturated magma has an ability to leach various metals from surrounding rocks. Cl and F contents in the sedimentary rocks are lower than those in igneous rocks. The hydrous minerals in the hornfels is slightly rich in Cl along the grain margin. This evidence suggests either addition of Cl from surrounding solution or leaching of water during contact metamorphism. At least the leaching of halogen is not in the process. It means that meteoric water of low salinity never increase halogen content to get an ability to dissolve metals. The ore solution should be derived from magma or others (*e.g.*, heated sea water).

The mineralization mentioned above are mainly from plutonic or subvolcanic sequences. Same phenomena are observed in the epithermal mineralization districts as mentioned later.

Behavior in mineralization

Hydrous minerals often occur in the ore deposits. We discuss on the halogen behavior in mineralization stage, using the hydrous minerals formed hydrothermally in the ore deposits.

Large crystals up to 15mm in diameter occur in the Panguna porphyry copper deposit, Papua New Guinea. The apatite occurs in the boundary between the surrounding potassic zone and the central phyllic zone, and chalcopyrites of main mineralization stage grow on the surface of the apatite crystals. The X-ray images of P and Cl of the apatite are shown in Fig. 5 (Nedachi et al, 1988). As shown,

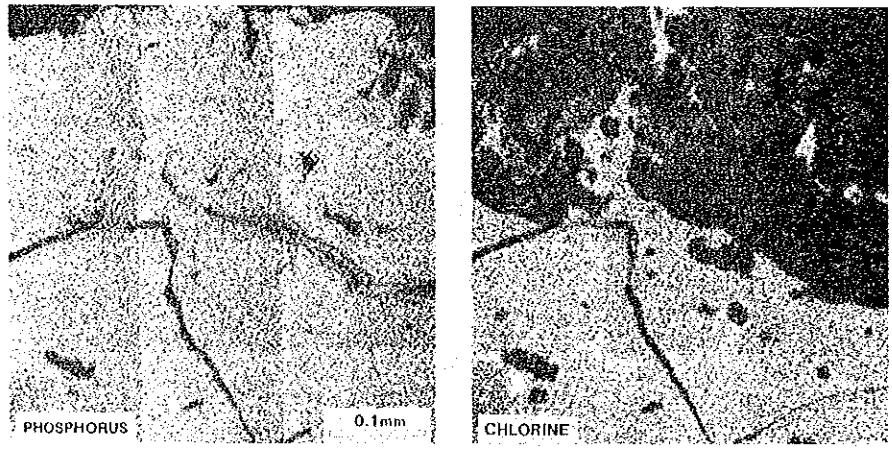

Fig. 5. X-ray images of P and Cl of apatite from the Panguna mine, Papua New Guinea (Nedachi, 1988).

the crystal is divided into two domains with relic texture; Cl-rich and Cl-poor parts. This evidence suggests that Cl-rich apatite was initially precipitated from high salinity solution, and that the solution of low salinity leached Cl from the apatite, at the later stage. The high salinity magmatic solution mixed with low salinity meteoric water seem to decrease the ability to dissolve metals, and induce the precipitation of ore minerals by the decomposition of chloro-complexes.

On the other hand, apatite also occurs in the central argillic zone of the last hydrothermal stage. The apatite is characterized by rather high F and extremely low Cl content. From these phenomena and some stable isotopic data (Ford and Green, 1977), the evolution of ore solution might be drawn as follows: 1) The fluid rich in Cl has been emanated from the Cl rich magma. Cl rich hydrous minerals have been precipitated from the fluid. 2) Dilution of Cl rich magmatic fluid by meteoritic pure water have been emplaced in the outer potassic zone to decompose chloride complex and to induce precipitation of ore minerals. 3) With decreasing the temperature, the meteoritic water might have infiltrated into the roof of the residual magma. However the meteoritic water lost the ability to precipitate base metals, because of mixing with the magmatic fluid and of the reaction with the Cl rich hydrous minerals. The role of the altered meteoritic water in the phyllic zone might be same with that of the magmatic fluid which has transported base metals to the outer potassic zone. Hence, the cylinder like distribution of high Cu concentrated zone has been formed. 4) Fluorine has increased in the later magmatic fluid and fixed in the later hydrous minerals in the central phyllic zone. Similar evidences are often observed in other ore deposits (*e.g.*, the Kano Sn-Cu ore deposit in Kyushu; Nedachi, 1987).

Role of halogen in epithermal gold mineralization

Nedachi and Ueno (1989) measured the halogen contents of the volcanic rocks around the Hishikari epithermal gold deposits, Kyushu, Japan. In this district, the volcanic rocks are bimodal in composition from basaltic andesite to rhyoritic dacite, and are of magnetite series.

Halogen content of whole rocks, rock-forming hydrous minerals are very high in the island arc system. Data suggest the following mechanism of the gold mineralization. Slightly ore solution rich in Cl and SO_2 separated under rather high oxidation condition from hydrous dacite magma and gold formed chloro-complex, such as $AuCl^{2-}$. The ore solution emanated into the sediments which should be under reduced condition because of the enrichment of organic carbon. The temperature decreased and the solution reduced in the sediments. (Porphyry type gold deposits might formed at the roof of the magma). With decreasing the magmatic activity, the reduced meteoric water became to circulate into the residual magma (or mineralized zone). The reduced meteoric water changed the

$AuCl^{2-}$ + SO_2 to $Au(HS)^{2-}$. This meteoric water ascended into the oxidized volcanic rocks, and precipitated the gold minerals by decomposition of thio-complex under oxidation condition and by decreasing the temperature. The controlling factor is only cooling and the change of redox condition.

Conclusions

Halogen contents in the igneous rocks along the island arc show the following features.

1) Asymmetric zoning of halogen contents of minerals and rocks is recognized along the island arc system. The features suggest that halogen elements are indicators of the source materials of the magma along the island arc system.
2) F content increases and Cl decreases with the increasing differentiation index of each magma.
3) The Cl/OH ratios of minerals decreases generally with the increasing of the differentiation index, in each intrusive unit.
4) High f_{HCl}/f_{H2O} is the character of the magma related to Cu, Zn, Pb, Au, Ag mineralization in a mining district.
5) High f_{HF}/f_{H2O} is the character of the magma related to W mineralization.
6) Cl content of the pre-ore silicate minerals is higher than that of post-ore silicate minerals.

The following hypothesis can be drawn from the described evidences.

7) Fluid rich in Cl, is derived from granitic magma. The solution has an ability to carry base metals from granitic magma, and sometimes from the country rocks.
8) Dilution of magmatic water by meteoritic water would decompose Cl complex and induce precipitation of metal ore deposits.
9) Fluorine remained in hydrous minerals during dilution.

Finally, it is concluded that the classic theory; magma as an ore bringer, is still available in some hydrothermal mineralization in the island arc system, although meteoric water and/or other water also might play an important role for mineralization. Recently we could trace the evolutions of three kinds of water; magmatic water, sea water, and meteoric water in the small epithermal gold deposits in Papua New Guinea, using halogen geochemistry and isotope geochemistry of O, H and S. The proportion of the contribution by these water should be dissolved in future.

References

Helgeson, H.C. (1969): Thermodynamics of hydrothermal system at elevated temperatures and pressures. *Am. J. Sci.*, 267, 729-804.

Holland, H.D. (1972): Granite, solutions, and base metal deposits. *Econ. Geol.*, 67, 281-301.

Ishihara,S. and Terashima, S. (1977): Chlorine and fluorine contents of granitoids as indicators for base metal and tin mineralization. *Mining Geol.*, 27, 191-199.

Muñoz, J.L. and Ludington, S.D. (1974): Fluorine-hydroxyl exchange in biotite. *Am. J. Sci.*, 274, 396-413.

Muñoz, J.L. and Swenson, J.L. (1981): Chlorine-hydroxyl exchange in biotite and estimation of relative HCl/HF activities in hydrothermal fluids. *Econ. Geol.*, 83, 1236-1245.

Nedachi, M. (1980): Chlorine and fluorine contents of rock-forming minerals of the Neogene granitic rocks in Kyushu, Japan. *Mining Geol. Spec. Issue*, 8, 39-48.

Nedachi, M. (1988): Behavior of halogen elements in mineralization related to magmatism, and its application to exploration. Bicentennial Gold 88, Expanded Abstract, 2, 234-237.

Nedachi, M., Enjoji, M., Yamamoto, M., Malagun, S., Taguchi, S., Shiga, Y., Higashi, S. and Manser, W. (1990): Role of halogen elements on the Panguna porphyry copper mineralization, Bougainville, Papua New Guinea. *South Pacific Study*, 11, 23-36.

Nedachi, M., Kanisawa, S. and Yamamoto, M. (1984): Chlorine and fluorine contents of the Neogene granitic rocks in Kyushu, Japan. *Mining Geol.*, 34, 437-446.

Nedachi, M. and Ueno, H. (1989): Geochemistry of the volcanic rocks around the Hishikari mine, and the role of halogen elements for the mineralization. *Rep. Sci. Kagoshima Univ.*, 25, 24-38.

Tsusue, A., Nedachi, M. and Hashimoto, K. (1981): Geochemistry of apatites in the granitic rocks of the molybdenum, tungsten, and barren provinces of Southwest Japan. *Jour. Geochem. Explor.*, 15, 285-294.

SECUENCIA CARBONIFERA DE PARGA (LLANQUIHUE, CHILE): NUEVOS ANTECEDENTES

Guillermo Alfaro y María Eugenia Cisternas
Instituto GEA, Universidad de Concepción, Casilla 4107, Concepción 3, Chile.

Introducción

La existencia de mantos de carbón en la región de Parga, Comuna de Los Muermos, Provincia de Llanquihue, Décima Región de Los Lagos (coordenadas geográficas del punto central de la zona de interés: 41°28'S y 73°49.3'W; Figura 1) se conoce al menos desde 1871. Informes datados en 1896 (1) hacen referencia a labores mineras en la costa de Parga, de las cuales aún se conservan restos de enmaderados. A principios de siglo se explotaba el carbón con máquinas de vapor, lo cual permitía una producción suficiente para justificar un puerto de mar y un ferrocarril de trocha angosta, cuyo trazado es aún visible, que unía la mina con el puerto.

Marco geológico

En el distrito de Parga se conocen afloramientos de carbón de edad terciaria a lo largo de la costa (playa Galileo), así como unos dos km hacia el interior en el valle del río Juancho (valle Ortiga) y sector de Cárcamo (Fig. 2). La secuencia sedimentaria en la región costera presenta plieges de dimensiones métricas. Un sistema de fallas de rumbo N45°W controla una tectónica de bloques que se refleja en la topografía y en la disposición de las curvas magnéticas (2).

A. Afloramientos costeros

En la costa, la secuencia portadora de mantos de carbón (N80°E/20°N) aflora en playa Galileo y se continua hacia el norte, hasta punta Puga. Consiste en una alternancia de conglomerados de cuarzo y areniscas, con intercalaciones de lutita.

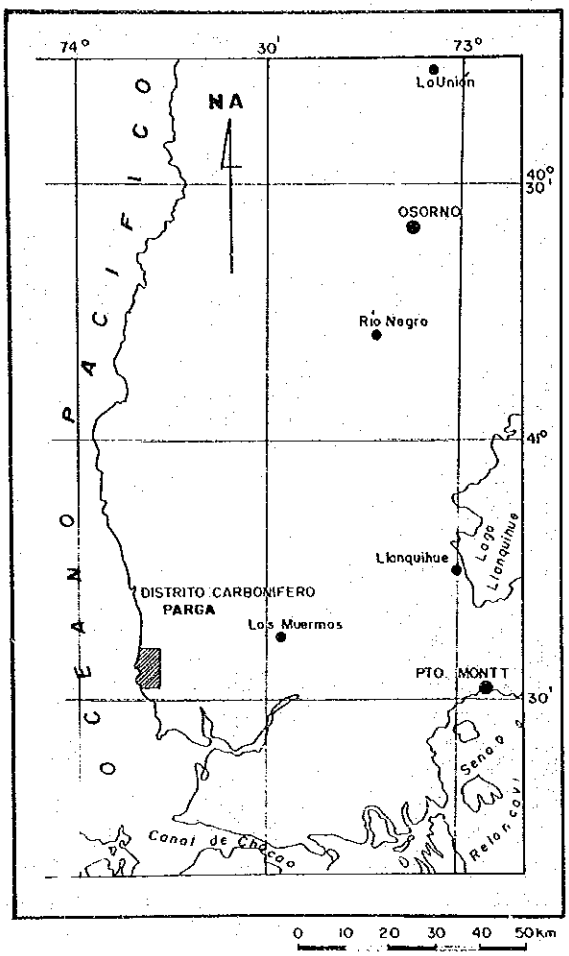

Fig. 1. Mapa de ubicación.

El espesor en afloramiento es de 140m. En esta secuencia se intercala un manto de carbón de 50 cm de potencia y algunos horizontes decimétricos de lutitas carbonosas.

De acuerdo a GEOSUR (3) la secuencia portadora de carbón de la costa, formada en un ambiente lagunar somero, se interdigita con depósitos calcáreos fosilíferos de ambiente marino, los cuales aparecen muy bien expuestos en playa Ortiga a 4 km al norte de playa Galileo.

En punta Puga, siguiendo toda la línea costera, afloran rocas traquíticas, con textura porfídica y amígdalas de hasta 15 mm, rellenas con calcedonia y óxidos de fierro. La roca presenta silicificación incipiente en los bordes de las plagioclasas (roca "almendra" de BRÜGGEN (4). No se observan relaciones de contacto con las sedimentitas, aunque la traquita parece ser posterior y cortar la secuencia.

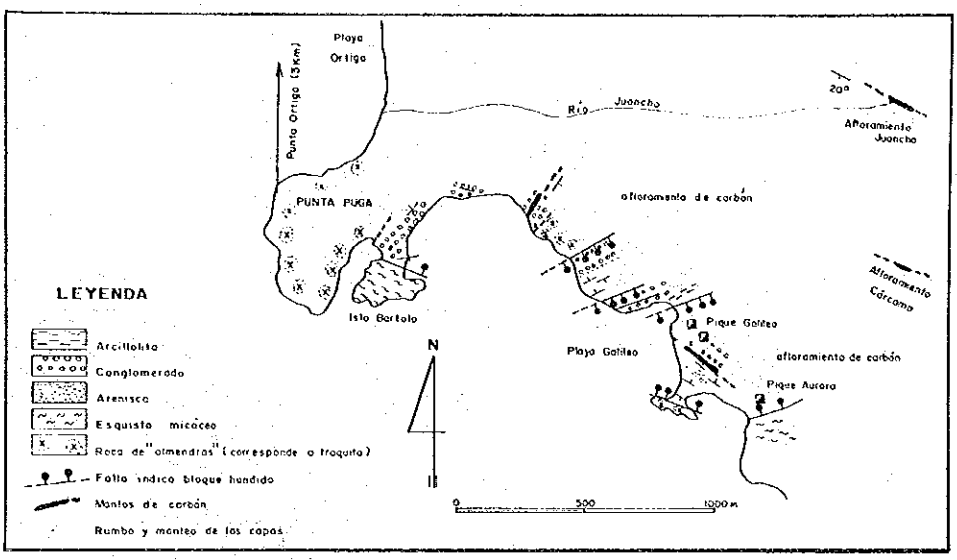

Fig. 2. Bosquejo geológico de Parga.

Al norte de punta Puga y hasta playa Ortiga aflora una sucesión de areniscas y lutitas carbonosas con intercalaciones de brechas, de hasta 60 m de potencia, con clastos decimétricos de esquisitos micáceos pertenecientes al basamento metamórfico infrayacente.

BRÜGGEN (4) correlaciona la unidad sedimentaria de la costa con el denominado Piso Concepción, en tanto que GEOSUR la incluye en la unidad informal denominada Formación Parga, de edad miocena media a superior, la cual es equivalente a la Formación Huilma definida por GARCIA (5).

B. Afloramientos del interior

Al interior del distrito Parga, en los sectores de Juancho y Cárcamo (Fig. 2) afloran limolitas grises con intercalaciones de areniscas, entre las cuales, en el río Juancho (valle Ortiga), aflora un manto de carbón de 1.8 m de potencia, cuya estructura (N65°W/20°S) es coincidente con aquella de la secuencia de playa Ortiga. El manto, escindido en dos por una intercalación arcillosa, se extiende 50 m en afloramiento, siendo imposible evaluar su continuidad por la espesa cubierta vegetal del sector. De acuerdo al modelado de la topografía se extensión podría estar controlada por fallas E-W. Menos de un km al sur, en el sector de Cárcamo hay otro afloramiento de carbón. La explotación minera histórica en el valle Ortiga parece haber estado relacionada con este horizonte carbonífero. Cubriendo la secuencia sedimentaria descrita, aparece en las partes altas un nivel de conglomerado de cuarzo, con matriz arcillosa, bien consolidado.

Características de los mantos de carbón

Las características físicas de los carbones del sector costero (playa Galileo) y el interior (afloramiento Juancho y Cárcamo) se señalan en la Tabla 1. Los afloramientos de la costa se caracterizan por la ocurrencia de un manto de carbón opaco, con bandas vítreas, meteorizado por acción del agua de mar, (rumbo N80°E/20°E; 0,5 m de potencia) y por la presencia de capas decimétricas de limolitas carbonosas, intercaladas en una secuencia predominantemente gruesa (Figura 3).

Al contrario, el carbón del interior (afloramientos Juancho y Cárcamo), está asociado a una secuencia de rocas sedimentarias finas, principalmente arcillolitas poco compactas, de color claro. El manto, de 1,8 m de potencia presenta una intercalación de arcillolita gris de 0.15 m de espesor, la cual lo divide en dos partes: el manto superior (1,5 m de potencia) consiste en carbón vítreo, con fractura concoidal y bandas centimétricas de carbón opaco; y, el manto inferior, (0.35 m de potencia) es opaco.

De acuerdo a las observaciones geológicas, el carbón de la costa (playa Galileo), parece ser más antiguo que aquel reconocido en las proximidades del río Juancho, y por extensión, al que se explotó en el valle de Ortiga, idea sostenida por BRÜGGEN (4), quien consideró eoceno al de la costa y mioceno al del interior. Sin embargo, cabe la posibilidad que ambos carbones sean de edad miocena, pudiendo representar facies diferentes de un mismo evento, o bien, el manto del interior sea algo más joven que el de la costa. Los análisis de carbón (Tabla 1) no aportan información para dilucidar esta incógnita. Una buena

Tabla 1. Características de los carbones de Parga

LOCALIDAD	Playa Galileo		Río Juancho			Cárcamo
Muestra	50588-4	FA-3	inf 50588-2	super 50588-1	común PA-1	50588-1
Humedad superficial	10,63	6,86	12,07	12,26	7,47	11,02
Humedad como recibido	15,81	23,01	16,30	11,66	16,59	11,72
Humedad total	24,76	28,29	26,40	22,49	22,82	21,45
Ceniza como recibido	19,63	5,47	11,51	25,45	19,47	24,16
Ceniza como determinado	21,97	5,87	13,09	29,01	21,04	27,15
Ceniza base seca	26,10	7,62	15,81	32,84	25,22	30,75
Azufre como recibido	0,39	nd	0,53	0,32	nd	0,49
Azufre como determinado	0,44	nd	0,60	0,37	nd	0,55
Azufre base seca	0,52	nd	0,72	0,42	nd	0,62
Poder calorífico como recibido	3756	4574	4203	3354	3714	3556
Poder calorífico como determinado	4203	4911	4780	3823	4014	3992
Poder calorífico base seca	4992	6379	5711	4328	4812	4522

aproximación puede lograrse determinando la vegetación original a través de estudios de paleopalinología, los cuales han demostrado que es posible discriminar entre carbones del Mioceno (carbones de Catamutún y Pupunahue, en la provincia de Valdivia) y carbones de Eoceno (Cuenca de Arauco).

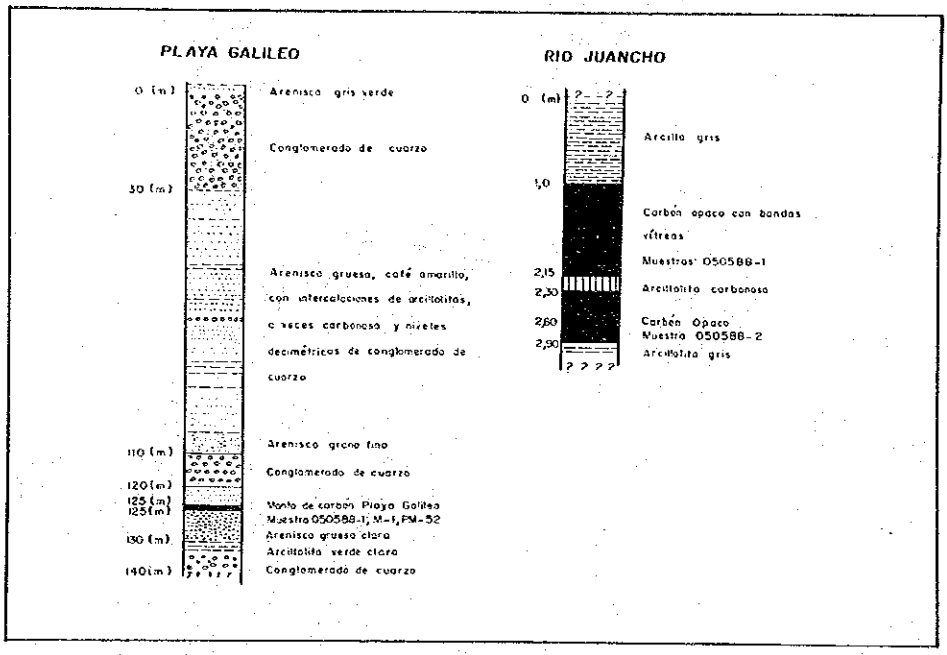

Fig. 3. Perfil estratigráfico de la secuencia carbogénica de la costa (Playa Galileo) y del interior (Río Juancho).

Agradecimientos

Se agradece a la Carbonífera San Pedro de Catamutún, quien autorizó la presente publicación. La investigación se enmarca en el Proyecto FONDECYT 89/698.

Referencias

(1) Concha y Toro, E. (1869) Memoria sobre las formaciones cuaternarias, terciarias i cretácicas (superior) de Chile. Anales Univ. de Chile, Tomo I, p. 345. Santiago.

(2) SERNAGEOMIN (1980) Carta magnética de Chile N°6 (escala 1:100'000). 1 pl. Santiago.

(3) GEOSUR Ltda. (1976) Evaluación preliminar de los recursos carboníferos de la cordillera de Sarao, Décima Región. Inf. Intendencia X Región, 122 p, 12 fig., 1 pl. Pto. Montt.

(4) Brüggen, J. (1913) Informe sobre las exploraciones geológicas de la región carbonífera del sur de Chile. Bol. Soc. Nac. Minería, 61 p., 31 pl., 12 fig. Santiago.

(5) Garcia, F. (1968) Estratigrafía del Terciario de Chile Central. in El Terciario de Chile, Zona Central. Ed. Andrés Bello, P. 25-58, Santiago.

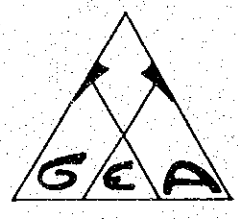

Editora Aníbal Pinto S.A. Maipú 769, Concepción, Chile